JOÃO EDUARDO GARANITO GERALDINI

DYNAMIC VIBRATION ABSORBER APPLIED TO A TELESCOPE'S CRYOCOOLER-REFRIGERATED SPECTROGRAPH

São Paulo
2024

JOÃO EDUARDO GARANITO GERALDINI

DYNAMIC VIBRATION ABSORBER APPLIED TO A TELESCOPE'S CRYOCOOLER-REFRIGERATED SPECTROGRAPH

Versão Corrigida

Dissertação apresentada à Escola Politécnica da Universidade de São Paulo para obtenção do Título de Mestre em Ciências.

Área de Concentração:

Engenharia Mecânica de Projeto e Fabricação

Orientador:

Marcílio Alves

São Paulo
2024

Este exemplar foi revisado e corrigido em relação à versão original, sob responsabilidade única do autor e com a anuência de seu orientador.

São Paulo, 26 de Junho de 2024

Assinatura do autor: 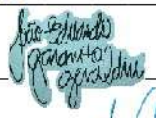

Assinatura do orientador: 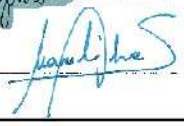

Catalogação-na-publicação

Geraldini, João Eduardo Garanito
DYNAMIC VIBRATION ABSORBER APPLIED TO A TELESCOPE'S CRYOCOOLER-REFRIGERATED SPECTROGRAPH / J. E. G. Geraldini -- versão corr. -- São Paulo, 2024.
150 p.

Dissertação (Mestrado) - Escola Politécnica da Universidade de São Paulo. Departamento de Engenharia Mecânica.

1.Spectral stability 2.Optomechanics 3.Dynamic Vibration Absorber 4.MATLAB 5.MSC Adams View I.Universidade de São Paulo. Escola Politécnica. Departamento de Engenharia Mecânica II.t.

Prof. Marcílio Alves

Prof. Rafael Celeghini

Prof. Roberto Eiki Oshiro

Dedication

To my family: my mom, Simone, aunt, Solange, and grandma, Lia. You invested so much in my education and my most sincere wish is that I'm able to retribute your kindness, selflessness, and love.

ACKNOWLEDGMENTS

Thank you to my many loyal friends and kind strangers for providing me a clear point of view I managed to find my future through, and for the endlessly entertaining small coincidences of life. Thank you, Antonio Braulio Neto, Rafael Ribeiro, Claudia Oliveira, and Thiago Amaral for supporting me when my technical knowledge reached its limit, and lighting the path ahead of me. Thank you, Prof. Marcilio Alves.

Thank you, Carl Sagan, for inspiring me to be myself.

"From this distant vantage point, the Earth might not seem of particular interest. But for us, it's different. Consider again that dot. That's here, that's home, that's us. On it everyone you love, everyone you know, everyone you ever heard of, every human being who ever was, lived out their lives. The aggregate of our joy and suffering, thousands of confident religions, ideologies, and economic doctrines, every hunter and forager, every hero and coward, every creator and destroyer of civilization, every king and peasant, every young couple in love, every mother and father, hopeful child, inventor and explorer, every teacher of morals, every corrupt politician, every "superstar," every "supreme leader," every saint and sinner in the history of our species lived there – on a mote of dust suspended in a sunbeam. (...)

Our posturings, our imagined self-importance, the delusion that we have some privileged position in the Universe, are challenged by this point of pale light. Our planet is a lonely speck in the great enveloping cosmic dark. In our obscurity, in all this vastness, there is no hint that help will come from elsewhere to save us from ourselves. (...)

It has been said that astronomy is a humbling and character-building experience. There is perhaps no better demonstration of the folly of human conceits than this distant image of our tiny world. To me, it underscores our responsibility to deal more kindly with one another, and to preserve and cherish the pale blue dot, the only home we've ever known."

-- Carl Sagan

RESUMO

Perante a abertura do Telescópio Gigante Magalhães (GMT), planejada para 2029, o Espectrógrafo Astronômico e Cosmológico Multi-objeto do GMT (GMACS) será seu instrumento mais popular onde muitas das descobertas científicas do GMT serão realizadas, mas seu design optomecânico encontra-se atualmente incompleto. A meta de estabilidade espectral do GMACS exige que, para que os dados sejam corretamente obtidos, o GMACS não se movimente mais que 11.54 mícrons (0.00001154 metro) idealmente ou 34.62 mícrons (0.00003462 metro) realisticamente por hora. O propósito dessa dissertação é desenvolver um Absorvedor Dinâmico de Vibração (DVA) para o GMACS, assim o permitindo alcançar a estabilidade espectral desejada. Um modelo matemático foi criado usando os recursos do MATLAB e um 3d, usando o SolidWorks e MSC Adams View. Os limites de estabilidade desejados não foram alcançados pelo design simples de DVA estabelecido nesse projeto; porém, essa pesquisa demonstra resultados encorajadores por ter obtido uma redução na amplitude de vibração de mais de 11 % por meio da adição do Absorvedor Dinâmico. Essa pesquisa foi realizada junto ao Grupo de Mecânica dos Sólidos e Impactos em Estruturas (GMSIE-USP) e ao escritório brasileiro do GMT (GMTBrO).

Palavras-Chave – Estabilidade espectral, Optomecânica, Absorvedores Dinâmicos de Vibração (DVA), Design, Transformadora rápida de Fourier, MATLAB, Adams View, Espaço de estados, Dinâmica multicorpos.

ABSTRACT

Upon the Giant Magellan Telescope (GMT)'s opening, currently scheduled for 2029, the GMT Multi-object Astronomical and Cosmological Spectrograph (GMACS) will be its most popular instrument where many of the scientific discoveries will be made, but it currently has no finished optomechanical design. GMACS' spectral stability goal requires that, in order for proper data to be collected, GMACS does not move more than 11.54 microns (0.00001154 meter) ideally or 34.62 microns (0.00003462 meter) realistically each hour. The purpose of this dissertation is to develop a Dynamic Vibration Absorber (DVA) for GMACS that allows it to accomplish its desired spectral stability. A mathematical model was designed employing MATLAB's resources and a 3d model, using SolidWorks and MSC Adams View. The desired stability limits were not met by the simple DVA designed in this project, but this research shows encouraging results nonetheless as an amplitude reduction of over 11 % was obtained with the Dynamic Vibration Absorber. This research was performed alongside GMSIE, the University of São Paulo Solid Mechanics and Impacts Group, and GMTBrO, the GMT's Brazil Office.

Keywords – Spectral stability, Optomechanics, Dynamic Vibration Absorber (DVA), Design, Fast Fourier Transform, MATLAB, Adams View, State space, Multibody Dynamics.

LIST OF FIGURES

LIST OF TABLES

GLOSSARY

dark energy the mysterious substance making up to 68% of the universe which scientists know nothing about besides how it affects the universe's expansion (1). 19

QSO Quasi-Stellar Object, an object that, observed from the Earth, presents all the same visible astronomical characteristics as Quasars (objects present in the centers of certain galaxies which spin at high velocities and form black holes) except with extreme luminosity (2). 19

red shift the light wave distortion as a consequence of an object's moving away from its observer (3). 19

spatial flatness the universe's now proven property of being uniformly shaped like a sheet of paper resting on a level table; a common way of defining its flatness is "if two parallel lines were to be drawn upon it, they would forever remain parallel instead of meeting at some point" (4) (5). 19

spectrograph an optical device which helps discern the chemical composition of an observed object based on the nature of the light captured from it (6). 20

CONTENTS

1 INTRODUCTION

"Of all things visible, the highest is the heaven of the fixed stars"

-- Nicolaus Copernicus

Three major developments around the year 2000 were responsible for beginning the era of the Extremely Large Telescopes (ELTs): new science, technology, and construction methods (7). The arrival of 8m class telescopes, the Lyman-break technique (a novel way of detecting otherwise invisible galaxies), the advent of Adaptive Optics, and the discovery of the positive acceleration rate of expansion of the Universe all contributed to an unprecedented increase in the caliber of optical telescopes that could be built early in the 21st century (8). Assisted by a simultaneous exponential improvement in computational power, scientists and engineers could then begin planning the construction of optical instruments dozens of times more powerful than Hubble, and with total costs deemed feasible within the capabilities of collaborating transnational institutions. Thus were born the projects for ELTs, ground-based optical telescopes with apertures of above 20 meters, which are expected to see first light between the end of the 2020 decade and the beginning of the 2030s. It should be noted that in radio astronomy, telescopes with

Figure 1: Render of European Southern Observatory's ELT (9)

diameters of up to 500 meters have existed since the beginning of the 2020 decade, but the construction employed and challenges faced by radio telescopes are vastly different from the ELTs'; the focus of this project will be entirely optical telescopes.

The engineering of ELT projects gains huge historical relevance when the astrophysical — and even some metaphysical — discoveries the scientists expect to make are observed. Based on the relation between the signal-to-noise ratio obtained from an astronomical reading and the red shift seen, and employing the known brightness and red shift records of certain QSOs, a theoretical 42 meter aperture telescope has been proven to be able to unambiguously detect the red shift drift over 20 years and 4000 hours of observing time, which would provide enough evidence for the presence of dark energy without assuming spatial flatness or any other cosmological or astrophysical constraints (10).

Gaining a more complete understanding of dark energy is only one of the possible consequences of the success of ELT projects but it is already a relevant enough reason to invest in them. The consequences of future discoveries regarding dark energy may imply that all of the current understanding of gravity needs an overhaul, or even that the true nature of it is something no one has even been able to conceive yet. These future developments might force scientists to rethink their ideas about the Big Bang, perhaps even devising a whole new scenario to explain how the universe was born (11). Or as Nobel Laureate Steven Weinberg put it, "dark energy is not only terribly important for astronomy, it's the central problem for physics. It's been the bone in our throat for a long time" (11).

In 2019, the Giant Magellan Telescope (GMT) entered its construction phase in Chile's Atacama Desert as a collaborative effort among Arizona State University, Carnegie Institution for Science, Harvard University, the Smithsonian Institution, Texas A&M University, the University of Texas at Austin, the University of Arizona, and the University of Chicago (USA), Astronomy Australia Ltd. and the Australian National University (Australia), the Korea Astronomy and Space Science Institute (South Korea), and FAPESP (Brazil). The GMT, with its 24.5 meter aperture, is one of the illustrious members of the

next generation of giant ground-based telescopes, along with the Thirty-Meter Telescope being built in Hawaii with 30 meters of aperture and the Extremely Large Telescope (Figure 1) also being built in Chile, but with an incredible 39.3 meters of aperture (12) (13) (14). The GMT is expected to be fully functional at the end of the 2020 decade, by which time it will allow astronomers to observe the sky with a resolution 10 times greater than that of the Hubble Space Telescope (12) (15). Among its tentative first tasks are to attempt to detect the presence of an Earth-mass exoplanet orbiting Sun-like stars and to study dark matter, dark energy, and the star and galaxy formation processes. Among its innovations are adaptive optics, the use of adaptable secondary mirrors that sharpen otherwise blurry points of light, and the state-of-the-art construction and assembly of seven of the world's largest single-piece mirrors — curved to a very precise shape and polished to within a wavelength of light — into a 368 m^2 light-collecting surface (15) (16) (17).

The six main instruments inside the GMT will be G-CLEF, GMACS, GMTIFS, and GMTNIRS (spectrographs), MANIFEST (a fiber optics positioner), and ComCam, which will validate the adaptive optics and natural seeing optical performance of the GMT (18).

Playing a crucial role in the development and production of optical support systems for telescopes, Opto-mechanical Engineers are tasked with overseeing the mechanical and thermal support systems for telescope optics, optical handling equipment, and diagnostic optical test instruments (19).Optomechanics is a brand new field of study which combines the extreme precision and manufacturing sophistication of optics, and the creativity and problem-solving skills of mechanics. Due to the large distances contemplated by Astronomy, small angular tweaks at the telescope site on Earth can cause significant effects on the image captured in space; thus, Optics relies as much on Optomechanics as Optomechanics on Optics. The Optomechanical engineer is also in charge of temperature, humidity, contamination, shock, stresses, costs, tolerances, and mechanical failure considerations (20) (21). The research detailed in the pages of this document lies within the realm of Optomechanics and is consequently groundbreaking in this novel field of study.

GMACS is a high throughput, general purpose multi-object spectrograph optimized for observations of very faint objects and its role within GMT will be to study "galaxy evolution, the evolution of the IGM and circumstellar matter, and resolved stellar populations" (18). Dr. Daniel Fabricant from the Harvard-Smithsonian Center for Astrophysics (CfA) is GMACS' Principal Investigator (PI) or project director, and the researchers involved are from Texas A & M and Harvard Universities, from the USA, and the University of São Paulo. Figure 2 shows an outdated GMACS design which will not correspond exactly to the final instrument but shows a basic structural skeleton that will: an Instrument Mount Frame (IMF) in the exterior, a 2.7 x 2.8 x 5.31 meter footprint, lenses made to GMACS' specifications, and mechanical mounts to hold them in place.

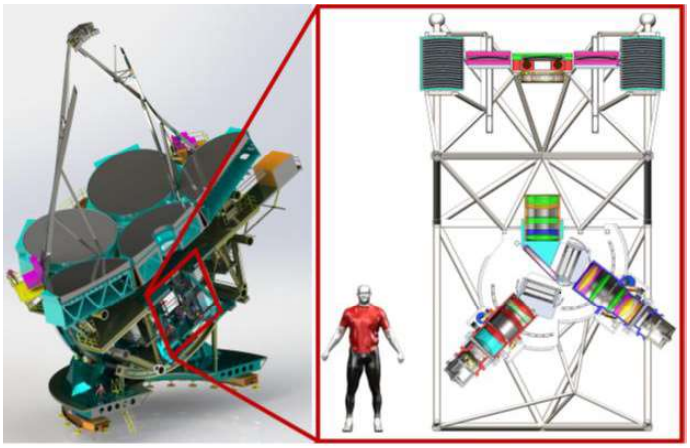

Figure 2: Render of GMT with the GMACS highlighted in red (left), an early version of what the GMACS would look like (outdated) and its scale (still applicable) compared to a human body (right) (22)

GMACS' conceptual structure has changed dramatically since the first conceptual designs were proposed in the mid-2010s, and currently there is no finalized design for it (23). As different requirements are made, specific features of the spectrograph are added or subtracted, such as specific moving mounts that had been present in previous iterations of GMACS' optical board (the dark gray surface onto which the lenses are fixed in Figure 3) that have since been substituted for immovable mounts (24). The ongoing search for a finalized design which adheres to all optical and structural requirements of the GMACS demonstrates the need for this project to succeed and provide useful, practical results.

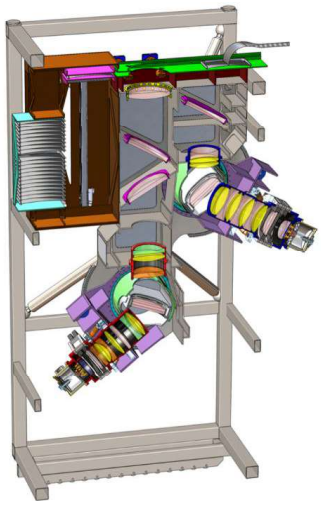

Figure 3: Recent version of GMACS (18)

Prior to this project, communication with GMT engineers and astronomers was established and an urgent need for further development in the optomechanics of the GMACS was made evident: the interface connecting the lenses to the outer structure of GMACS had yet to be designed or computationally simulated. The precise locations, compositions, and desired behaviors of the lenses had already been determined, but the structures holding them onto GMACS had not.

Cryostats and cryocoolers are two types of devices employed in optomechanics for maintenance or reduction of temperature. The main difference between the two is that cryostats work by stabilizing cryogenic temperatures already in place while cryocoolers actively reduce the surrounding temperature to reach cyogenic conditions (25). For a considerable period, CCD detectors in astronomical instruments have been effectively cooled using liquid nitrogen (LN2) cryostats. Nevertheless, with the emergence of efficient and dependable cryocoolers, this advanced technology is now supplanting LN2 cryostats in certain newly designed instruments (26). GMACS' optical instruments require a very specific, stable cryogenic temperature for proper operation. The GMT optics team has already defined that the tool that will help achieve that temperature goal is Sunpower's Cryotel® GT 16W Cryocooler (Figure 4).

Sunpower's cryocooler (Figure 5) is a 27.6 cm in length by 8.3 cm in diameter device

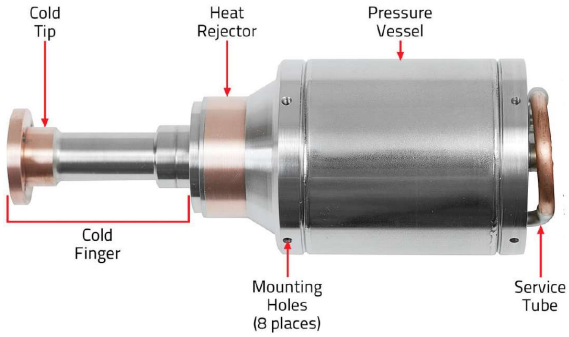

Figure 4: Sunpower's Cryotel® GT 16W Cryocooler (27)

that manages to reach cryogenic temperatures of -230 °C or 40 K through the mechanics illustrated in the step-by-step procedure shown in Figures 6 - 9 . There are two main moving parts inside of the cooler, the displacer (indicated by "1" on Figure 6) and the piston (indicated by "2" on Figure 6), which move within the hermetically enclosed, Helium-filled cryocooler interior and use the properties of the Stirling thermodynamic cycle and the Ideal Gas Law to decrease the cold tip (as pointed out in Figure 6) temperature drastically. The Stirling cycle (Figure 10) is a closed, regenerative, and reversible thermodynamic cycle with a considerable level of efficiency which is extremely challenging to be implemented — the specific point in the cycle that each Figure 6 - 9 represents is shown in the Figures next to the cryocooler. The fundamental challenge presented by the regenerator, the main heat exchanger in the Stirling cycle, is considered by notorious physicist Max Jakob to be "among the most difficult and involved that are encountered

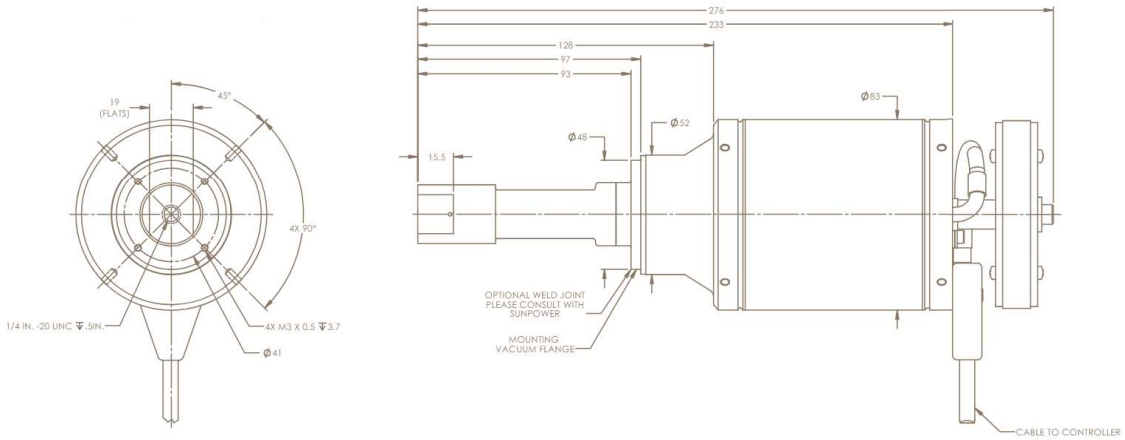

Figure 5: Sunpower's Cryotel® GT 16W Cryocooler technical drawing (27)

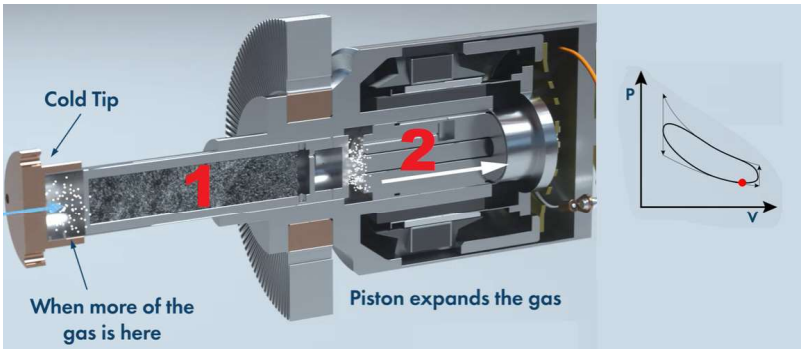

Figure 6: Sunpower's Cryotel® GT 16W Cryocooler, cold state (28)

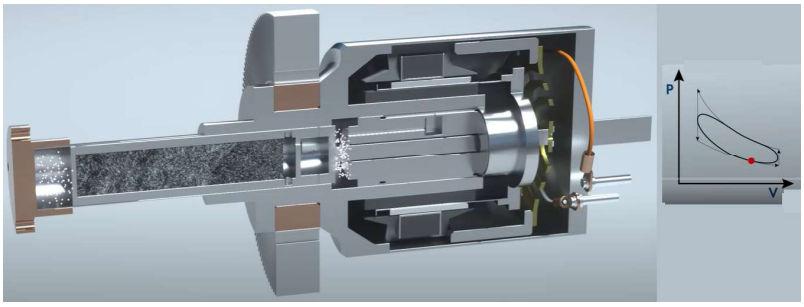

Figure 7: Sunpower's Cryotel® GT 16W Cryocooler, intermediate state (28)

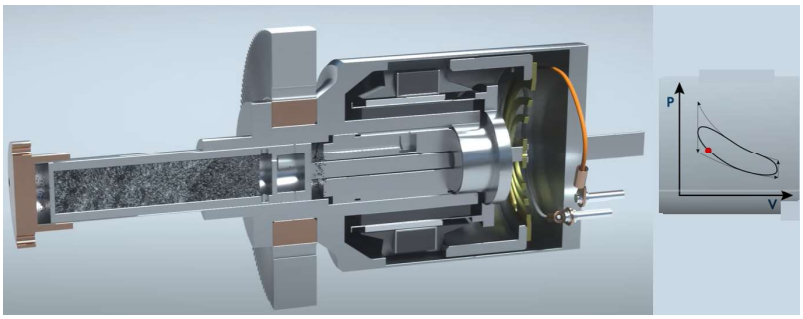

Figure 8: Sunpower's Cryotel® GT 16W Cryocooler, intermediate state (28)

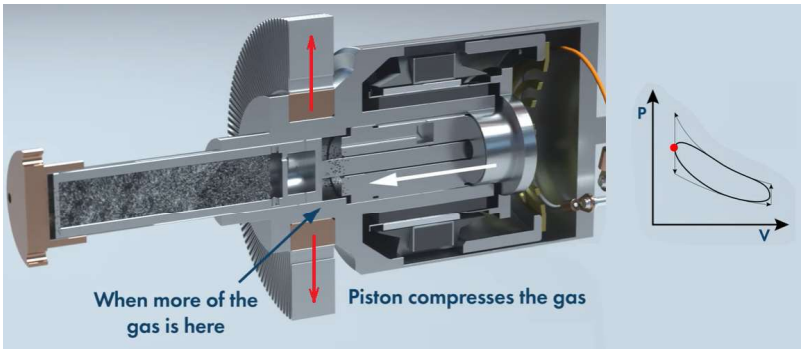

Figure 9: Sunpower's Cryotel® GT 16W Cryocooler, hot state (28)

in engineering" (29). This high level engineering is an absolute requirement of any project within Optomechanics due to the small tolerances and margins of error allowed in the field; for GMT and GMACS the stakes are even higher, considering the cryogenic temperatures that will be achieved and the monumental task of designing and building the world's largest optical telescope. The Ideal Gas Law (IGL), the most prevalent formula in the study of the behavior of gases, is the equation that attempts to approximate how various gases behave under many conditions, and is given by

$$PV = nRT$$

where P is the gas' pressure, V is the volume it occupies, n is the amount of it present (in moles), R is the ideal gas constant, and T is its temperature (30). At any point in the Stirling cycle, the gas' properties can be approximated to be following the IGL, meaning it is an adequate predictor of the dynamic gas behavior in the cryocooler.

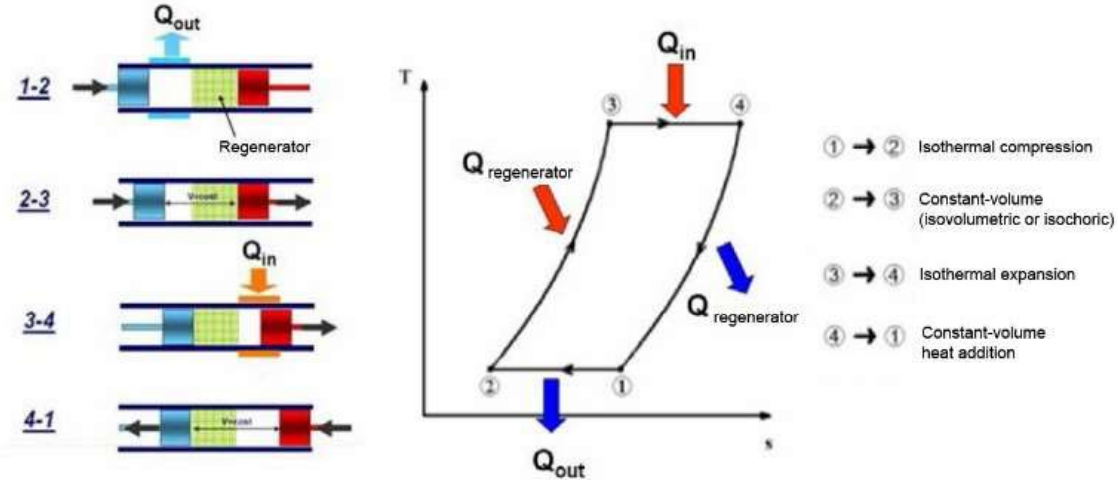

Figure 10: The Stirling cycle (31)

The cryocooler will be mounted to GMACS somewhat in a similar fashion to that showed in Figure 11, which is not a final CAD model of the mount but a good indication of what can be expected.

As the cryocooler oscilates between its cold (Figure 6) and hot (Figure 9) states,

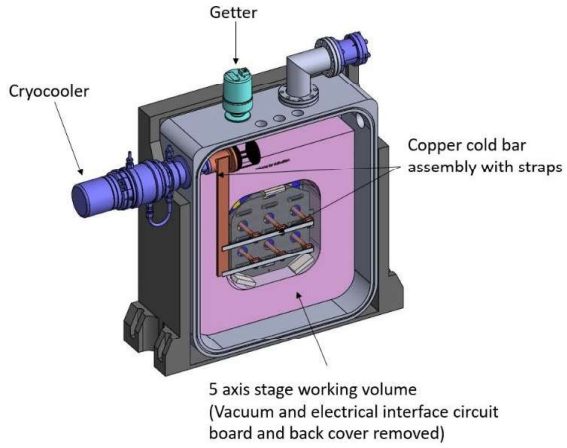

Figure 11: Cryocooler mounted to GMACS

the movement of the displacer and the piston can cause unwanted vibrations, the main component of which being in the axial direction (since that is the direction the electric current pushes the piston). One full cycle of the piston-displacer movement occurs every $\frac{1}{60}$ second, making the nominal frequency of motion 60 Hz. It is of utmost importance that the cryocooler does not cause noticeable vibrations in its surroundings because, as is the case with any optomechanical project, vibration means loss of focus in the optical instruments that were designed for very specific angles of observation — and this loss of focus leads to blurry results which render pointless the whole enterprise of building an Extremely Large Telescope.

The cryocooler placement as seen in Figure 11, if looked at from the opposite side, is that of Figure 12 (the copper screws show the connection between both images). To understand the calculation of the allowable displacement in GMACS, vibrations in axes **x** and **z** (made evident in Figure 12) will now be analyzed and scenarios will be drawn up.

1.1 Displacement along the z axis (depth of focus)

Any displacement along the **z** axis highlighted in Figure 12 propagates error in GMACS' depth of focus, causing loss of focus. It should be highlighted that the cry-

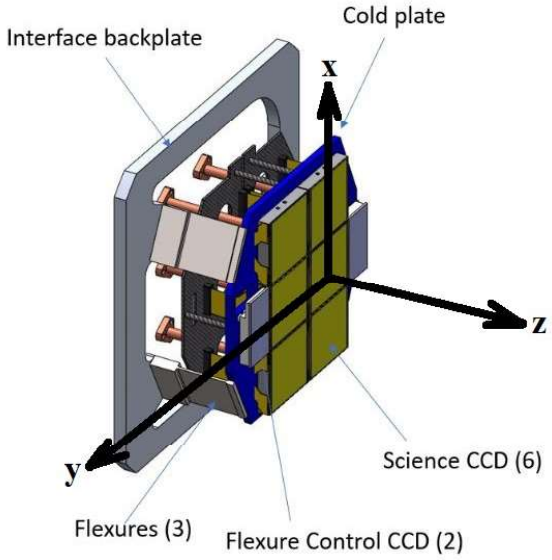

Figure 12: Cryocooler mounted to GMACS, opposite side view

ocooler's placement within GMACS is not along the z-axis, therefore considerations of z-axis effects and disturbances in depth of focus will be discussed as a point of comparison and speculation about what would happen if the cryocooler was positioned differently. The calculation of allowable depth of focus displacement is the following:

$$\delta = 2 \times (f/\#)_w \times s$$

where δ is the depth of focus of the optical instrument, a measurement of how the quality of focus changes as the sensor is moved and the object remains in the same position, $(f/\#)_w$ is an adimensional constant which in this case is equal to 2.2, and s is the pixel size of the instrument, in this case 15 μm, making

$$\delta = 66 \ \mu\text{m}$$

the maximum allowable axial amplitude of vibration the cryocooler can produce while still maintaining the same image quality (32) (33). However, it is a specification provided by the GMT engineers that the cryocooler design shall not reach that maximum value as

there are other factors that can be expected to propagate loss of image clarity, and the combination of them at their maximum potential of error could be harmful to GMACS. The allowed displacement in the cryocooler chamber will be, thus,

$$\delta = 46.6\ \mu\text{m}. \tag{1.1}$$

1.2 Displacement along the x axis (spectral stability)

Displacement along the **x** axis, however, propagates error in spectral stability, causing blurriness in obtained images. The x-axis is the direction along which the vibrations caused by the cryocooler will really be propagated in GMACS. This positioning causes a series of different consequences in how to deal with vibrations, if compared to the **z** axis displacements; these will now be reviewed.

Firstly it is of this project's interest to comprehend angular diameters or angular sizes (Figure 13). For an observer sitting anywhere on the surface of the Earth, a celestial body with diameter D will have an apparent size based on D and d, the linear distance between observer and object. That apparent size is a direct calculation of how much of the observer's field of view is occupied by the observed object and is given by the object's angular diameter A, where

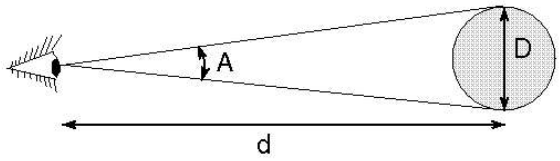

Figure 13: An illustration of angular diameters (34)

$$A = \frac{360D}{2\pi d}.$$

A can be expressed in degrees, arcminutes, and arcseconds, where

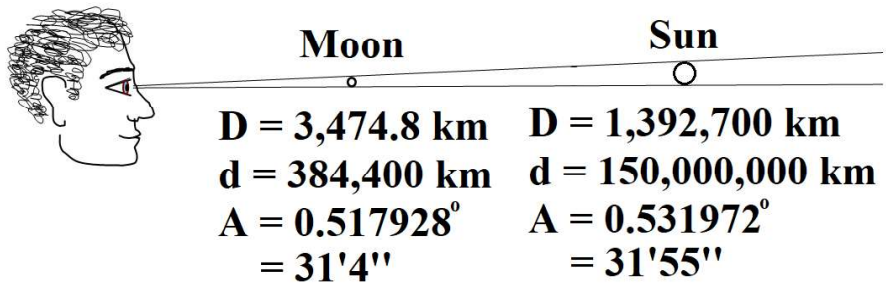

Figure 14: An illustration of the moon and the sun's angular diameters (35)

$$1 \text{ degree} = 1^\circ = 60 \text{ arcmin} = 60' = 3600 \text{ arcsec} = 3600''.$$

It is relevant to note that objects with vastly different sizes may appear to be equally large to an observer sitting on the Earth's surface if the smaller object is a lot closer to the Earth than the larger object, which is the exact phenomenon that allows the sun and the moon to look equal in size to any Earthling (Figure 14).

Some specifications provided by the GMACS optics team are summarized in Table 1.

Description of specification	**Specification**
Size of a pixel	15 x 15 μm
GMACS' resolution	0.052 "/pixel
Maximum allowable displacement, goal	0.1 resolution elements/hour
Maximum allowable displacement, requirement	0.3 resolution elements/hour
Resolution element	0.7"
Resolution element with the addition of adaptive optics	0.4"

Table 1: GMACS spectral stability requirements

In order to determine the maximum allowable x-axis displacement in this project, the following sequence of calculations based on the parameters from Table 1 are performed:

	Maximum Allowable Axial Displacement (MAAD)
Depth of focus (z-axis)	46.6 μm
Spectral stability (x-axis)	34.62 μm (requirement) 11.54 μm (goal)

Table 2: Maximum Allowable Axial Displacement (MAAD) for the cryocooler's z- and x-axis

$$\text{Maximum allowable displacement, goal} = \left(0.4'' \times 0.1\frac{\text{res el}}{\text{h}}\right) \times \frac{1}{0.052}\frac{\text{pixel}}{''} \times 15\ \mu m$$
$$= 11.54\ \mu m/h$$
$$\text{Maximum allowable displacement, req.} = \left(0.4'' \times 0.3\frac{\text{res el}}{\text{h}}\right) \times \frac{1}{0.052}\frac{\text{pixel}}{''} \times 15\ \mu m$$
$$= 34.62\ \mu m/h$$

Therefore the displacement requirements for this project are listed in Table 2.

An insight into the current state of astrophysics, astronomical discovery, and extremely large optical telescopes currently being developed has been provided and the magnitude of the GMT project has been explained. It has been highlighted that GMT is the biggest project ever supported by FAPESP (US$ 50 million, or 4% of the project's total investment, which guarantees the Brazilian nucleus within the GMT researchers 4% of the total annual operation time of the telescope) and that the Brazilian headquarters of the telescope design and engineering teams is collaborating with scientists from such institutions as Harvard — thus making the outcome of this endeavor heavily consequential towards the future of Brazilian research and research funding (36). Optomechanics and the challenges optomechanical engineers face have been discussed, as have been the pros and cons of adopting cryocoolers rather than cryostats as cryogenic temperature generators within an optical system. It has been established that a cryocooler is the most appropriate cooling solution for the project but that it does not come without its issues, since its unavoidable shaking along its main axis presents a risk to the objectives of the

telescope as a whole. Fortunately, possessing a limit to how much the cryocooler should be allowed to rock back and forth, as well as knowing that there is plenty of research nowadays concerning methods of intelligently absorbing such vibrations, can help minimize the effect of this main issue in using the cryocooler to generate the needed temperatures.

Next the main purpose of this project will be stated and a review of the foundational concepts regarding the type of motion seen in the cryocooler will be presented with the main goal of facilitating the understanding of the challenge faced by this project.

1.3 Vibrations

The general notion of a vibration is a periodic motion, or a motion that repeats itself in all its particulars after an interval of time denoted by the symbol T and called "period" (37).

Vibrations are an essential aspect of mechanical engineering, playing a vital role in the analysis, design, and performance evaluation of various structures and systems. This section provides a thorough understanding of vibrations, including their definition, main components and variables, types, their connection to field of mechanical vibrations, and their real-world applications.

Vibrations consist of several key components and variables that help describe and analyze their behavior. The primary components include the vibrating system, excitation, and response. The vibrating system comprises the structure or object that undergoes the motion. Excitation represents the force or input that causes the vibration, while the response refers to the resulting motion or behavior of the system.

The simplest type of vibration is called harmonic motion and is defined by

$$x = x_0 sin(\omega t) \tag{1.2}$$

where x is the displacement of the body in motion, x_0 is the amplitude of the harmonic motion (or its maximum displacement), t is the time variable, and ω is the angular frequency (or by how many radians the object is dislocated due to the vibration, per second), or

$$\omega = 2\pi f = \frac{2\pi}{T} \tag{1.3}$$

— where T is the aforementioned period of the vibration, measured in seconds. Figure 15 shows the displacement versus time plots for two functions, one periodic representing the motion curve of the bearing pedestal of a steam turbine and one harmonic representing the small oscillations of a simple pendulum. The latter can be described by Equation (1.2) (37).

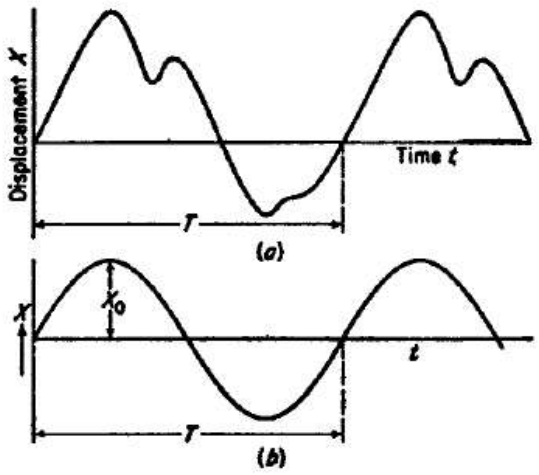

Figure 15: A periodic (a) and a harmonic (b) function, showing period T and amplitude x_0 (37)

For the purpose of this project the force that pushes the vibrating object — the piston — will be defined by the oscillating function

$$u = P_0 sin(\omega t) \tag{1.4}$$

where P_0 is the force's amplitude, or its highest value. This function's format ensures that the force input switches direction after a full oscillation cycle and also that the force has a predictable, constant amplitude that will be defined in Chapter 4.

Vibrations can be categorized into various types based on different criteria. Some common types of vibrations include:

- Free vibration: occurs when a system vibrates after being set into motion without any external force acting on it. The system oscillates at its natural frequency or frequencies, determined by its mass, stiffness, and damping characteristics;
- Forced vibration: arises when an external force or excitation is applied to a vibrating system. The excitation can be harmonic, periodic, or non-periodic, and it causes the system to respond at the excitation frequency or its harmonics;
- Damped vibration: refers to the motion of a vibrating system that gradually decreases over time due to the presence of energy dissipation mechanisms, such as damping elements. Damping reduces the amplitude of the vibration and influences the system's response;
- Resonance: happens when the frequency of the excitation matches the natural frequency of the vibrating system. It results in significantly amplified vibrations, leading to potentially destructive effects. Resonance is a critical consideration in mechanical design to prevent structural failures and ensure system stability.

Mechanical vibrations encompass the study of vibrations specifically related to mechanical systems, including structures, machines, and devices. Mechanical engineers investigate the dynamic behavior of these systems to ensure their functionality, reliability, and safety. Mechanical vibrations are interconnected with other branches of vibrations, such as civil engineering, aerospace engineering, and electrical engineering.

In the field of mechanical engineering, vibrations are analyzed using mathematical models, analytical techniques, and experimental methods. Finite element analysis (FEA),

modal analysis, and frequency response analysis are commonly employed to characterize the dynamic behavior of structures subjected to vibrations. These analyses help identify critical modes, resonances, and potential structural weaknesses, enabling engineers to design systems with improved performance and durability.

Vibrations have significant real-world implications and are of concern in various industries and applications. Some notable examples include:

- Automotive engineering: in the automotive industry, vibrations are of utmost importance for vehicle performance and passenger comfort. Engineers analyze and optimize the suspension systems, engine mounts, and tire design to minimize unwanted vibrations and noise. Excessive vibrations in vehicles can lead to discomfort, fatigue, and even mechanical failures;

- Structural engineering: vibrations pose a challenge in structural engineering, especially for large-scale buildings, bridges, and other civil infrastructure. Engineers employ advanced techniques to mitigate the effects of wind-induced vibrations, traffic-induced vibrations, and human-induced vibrations. Failure to account for vibrations can compromise structural integrity and occupant safety;

- Machinery and equipment: vibrations in rotating machinery, such as turbines, compressors, and motors, can result in decreased efficiency, increased wear and tear, and potential malfunctions. Engineers apply vibration analysis and balancing techniques to optimize performance, reduce vibrations, and prolong equipment lifespan;

- Aerospace engineering: vibrations are a crucial concern in aerospace engineering, affecting the structural integrity, stability, and performance of aircraft and spacecraft. Engineers analyze and test components and structures to ensure their ability to withstand dynamic loads and vibrations experienced during flight.

It is clear that vibrations are a key subject of mechanical engineering, useful for the study of dynamic behavior in various systems and structures. Through an understanding

of the components, types, and relationships within the broader field of vibrations, engineers can effectively analyze, design, and control vibrations in real-world applications. This knowledge plays a crucial role in enhancing system performance, reliability, and occupant comfort, while minimizing the detrimental effects of excessive vibrations.

The impact of vibrations on structures was first studied starting in the 1930s as a way to improve the protection of buildings against seismic activity (38). Subsequent discoveries and the progressive deepening of the gathered knowledge led to the highly advanced and specialized breakthroughs currently being shared within the vibration studies community, making this field of study one amongst many in engineering where, in less than a century, advancements were achieved in an exponentially accelerating pace — as seen in the timeline in Figure 16. If around ninety years ago the world was beginning to map out the behavior of a body under constant vibrational excitation, in late 2022 researchers might have just found a way to harvest electromagnetic energy from low-frequency, low

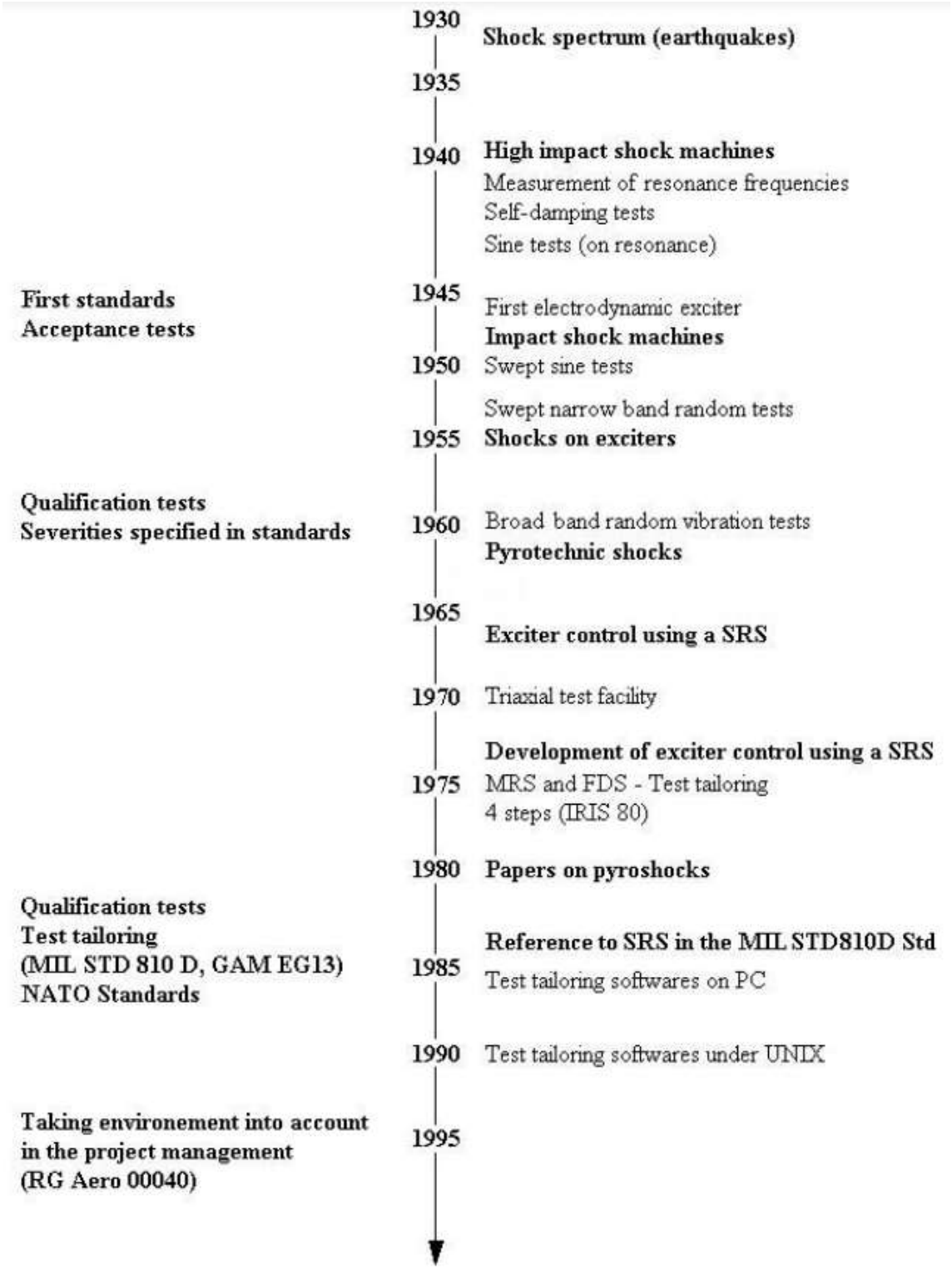

Figure 16: Timeline of major discoveries in vibration studies (38)

excitation vibrating systems using a quasi-zero stiffness harvester that exploits a novel rolling magnet technology (39). Vibrations are an ever deepening field with still a lot to be explored.

To cite a few of the most celebrated disruptors in vibration studies, a good starting point is Euler, who in 1744 made a groundbreaking contribution to the study of vibrations by deriving the wave equation for a vibrating string and developing mathematical techniques for solving various vibration problems. His work laid the foundation for subsequent studies on vibrating structures and systems (40). In 1862, Helmholtz famously wrote a seminal piece of work on the physiology of hearing and sound perception, which significantly contributed to the understanding of musical vibrations. He explored the relationship between the physical properties of sound waves and the perceptual aspects of music, introducing the concept of harmonic series and timbre. Von Helmholtz's findings continue to influence the design and construction of musical instruments and sound reproduction systems to this day (41). In "The Theory of Sound" (1877) Lord Rayleigh established a foundation for the mathematical and theoretical understanding of vibrations. He formulated the wave equation and introduced the concept of resonance, one of utmost importance in the field. Rayleigh's contributions were particularly influential in the fields of acoustics and musical instruments, leading to improved designs and sound quality (42).

Rayleigh then followed his opus which redefined music theory and acoustics with two more incredibly significant works in 1878, each of which revealed the connection between beats and the concept of phase — advancing the field of acoustics and impacting telecommunications, where frequency modulation (FM) is utilized — and consolidated the mathematical representation of complex sound fields — aiding engineers in designing structures and devices to control vibrations and minimize noise (43) (44).

Finally, Nyquist's trailblazing 1928 paper on thermal noise kicked off the study of random vibrations in electrical circuits when Nyquist managed to demonstrate that the agitation of electric charges in conductors, resulting from thermal energy, leads to noise

generation (this concept has thenceforth been named "Nyquist noise" and has guided the design of low-noise amplifiers, high-speed communication systems, and electronic devices) (45).

The outcomes of several centuries of intense research in the field of vibrations are many and diverse:

- Structural engineering: the understanding of vibrations gained from historical research allows for the design of resilient structures that can withstand dynamic loads, such as seismic vibrations or wind-induced vibrations. Breakthroughs in resonance analysis and damping techniques have facilitated the development of buildings, bridges, and offshore structures with enhanced safety and durability;

- Mechanical systems: principles of vibrations established by early pioneers have guided the design of mechanical systems to minimize unwanted vibrations, improve performance, and extend the lifespan of components. For instance, the understanding of resonance and modal analysis has allowed for the optimization of rotating machinery, automotive suspension systems, and aerospace structures (Figure 17);

- Acoustics and sound engineering: research on vibrations and wave phenomena has revolutionized the fields of acoustics and sound engineering. It has enabled the design of concert halls with optimal sound reflection and diffusion, noise-canceling technologies, and high-fidelity audio systems. The insights gained from the historical development of sound perception continue to influence audio reproduction techniques and the design of musical instruments;

- Telecommunications: understanding vibrations and wave propagation, including the concepts of frequency modulation, phase, and noise, has paved the way for the development of modern telecommunications systems. Cellular networks, satellite communication, and data transmission technologies would not exist without Vibration's innovators.

Figure 17: Spacex's Starship prototype (46)

In the domain of optics progress has also been swift: in 1621 Willebrord Snell, a professor of mathematics at Leiden University in the Netherlands, discovered a graphical procedure for determining the direction of a refracted ray from a surface given the direction of the incident ray; less than four hundred years after that, in 2009, Dr. Charles Kao was awarded the physics Nobel Prize for his work in the field of fiber optics, the technology that allows worldwide low-cost, high-capacity, low-latency telephone and internet data traffic (47) (48) (49) (50) (51).

Other notable optics researchers surely deserve a highlight in this section, too, for this project would not exist without their indirect contribution. In 1690, astronomy, physics, and mathematics juggernaut Christiaan Huygens introduced the wave theory of light, proposing that light travels in the form of waves. He explained the phenomena of reflection and refraction using his wave theory and developed the concept of secondary wavefronts (52). 14 years later, Newton conducted experiments to demonstrate the dispersion of white light into a spectrum and the reflection and refraction of light at different angles. Newton's work formed the basis of geometric optics and contributed to the understanding of phenomena such as rainbows and the formation of images through lenses (53).

In his "A Dynamical Theory of the Electromagnetic Field" (1865), Maxwell brilliantly

establishes the connection between electricity, magnetism, and light through the formulation of the now widely lauded "Maxwell's equations", which unified the understanding of these phenomena and predicted the existence of electromagnetic waves. Maxwell's work allowed for the development of modern optics and electromagnetic technologies like wireless communication and fiber optics the same way Einstein's work in "On a Heuristic Viewpoint Concerning the Production and Transformation of Light" (1905) allowed for quantum mechanics and quantum optics, which are now applied in quantum computing and cryptography (54) (55). In this paper about the photoelectric effect, Einstein proposed that light consists of discrete packets of energy, later known as photons, which forever changed how the world engineers with light.

As explained in Chapter 1, the cryocooler employed in the cooling of the GMACS will oscillate with a predictable $T = \frac{1}{60}$ s, making the equation of this harmonic motion, taken from Equations (1.2) and (1.3),

$$x = x_0 sin(120\pi t). \tag{1.5}$$

Equation (1.5) provides the displacement that will be witnessed by the piston as it oscillates. This displacement, through direct mechanical contact, will push the entire system (cryocooler) back and forth, and the cryocooler will in turn generate a small vibration in the solids touching it, and so on, generating a chain reaction of vibrations in every solid part that directly touches the piston or the components it touches.

This residual vibration is unwanted in any area of the telescope that could harm the quality of the image obtained from it. If the task to take a simple "zoomed in" photograph with a common cell phone camera is to be taken as an example, this challenge is made very clear: the more the photographer zooms into an object, the harder it is to maintain focus. The slightest hand motion can cause the image to appear blurry. Similarly, when the object is light-years away from its observer sitting inside the GMT, a minor disturbance

can ruin weeks or even months of hard work. It is, thus, the task of GMT's optomechanical engineers to ensure unwanted movement will be mitigated, and for that there are multiple different approaches of varying complexity and originating fields of study. The one that will soon be analyzed is Dynamic Vibration Absorbers, which are a good fit for vibration attenuation in this project for many reasons that will soon be explained.

1.4 Dynamic Vibration Absorbers (DVAs)

DVAs, also named Tuned Mass Dampers (TMDs), were first analyzed mathematically in the published work of MIT Mechanical Engineering Professor Emeritus Dr. Den Hartog and are famously present in projects like the Taipei World Financial Center (Figure 18), London's Millennium Bridge (Figure 19), and the Doha Sport City Tower. The way through which the displacement caused by vibration is reduced in DVAs is by adding a secondary weight to the original system and allowing it to vibrate to a frequency that cancels out the original system's vibration (37) (56) (57) (58). Figure 20 demonstrates how adding a secondary mass (red) can help minimize the displacement of the original mass (blue): when properly synchronized, like in system 2, the red component absorbs the entirety of the initial push and pull of the blue component, such that the blue spring is static throughout the entire oscillation period. For systems 1 and 3, either an incorrect value of stiffness coefficient k was selected for the red spring, or an incorrect red mass m, or both, which causes the asynchronous motion and inefficient solution to vibration. In other words, in 1 and 3 the blue mass moves vertically from the before (left) to the after (right) scenarios. In 2, which had a DVA perfectly tuned for its vibration, the blue mass does not move vertically at all.

Over the years, researchers have proposed and developed various state-of-the-art models of DVAs, each with its own unique characteristics and applications. For example, the use of viscoelastic materials in TMDs has been a significant advancement. These materials possess both elastic and viscous properties, enabling them to dissipate vibrations effectively. Researchers have explored different designs, such as using viscoelastic layers

Figure 18: The Taipei World Financial Center (59)

Figure 19: London's Millennium Bridge (60)

in sandwich structures and incorporating them into tuned liquid column dampers.

Another area of innovation is the use of semi-active and active control systems in DVAs. These systems employ sensors and actuators to continuously monitor and adjust the damping characteristics of the absorber, providing more precise and adaptive vibration mitigation.

In practice, DVAs find applications in a wide range of fields. For example, in civil engineering, they are used to reduce vibrations in tall buildings, bridges, and offshore structures exposed to wind or seismic forces. In aerospace engineering, DVAs are employed to control vibrations in aircraft wings or helicopter rotor blades. They are also used in mechanical systems, such as rotating machinery or automotive suspension systems, to minimize unwanted vibrations.

These breakthroughs in DVAs have been instrumental in improving the safety, comfort, and performance of various structures and systems. Ongoing research continues to explore innovative designs, advanced materials, and smart control strategies to further

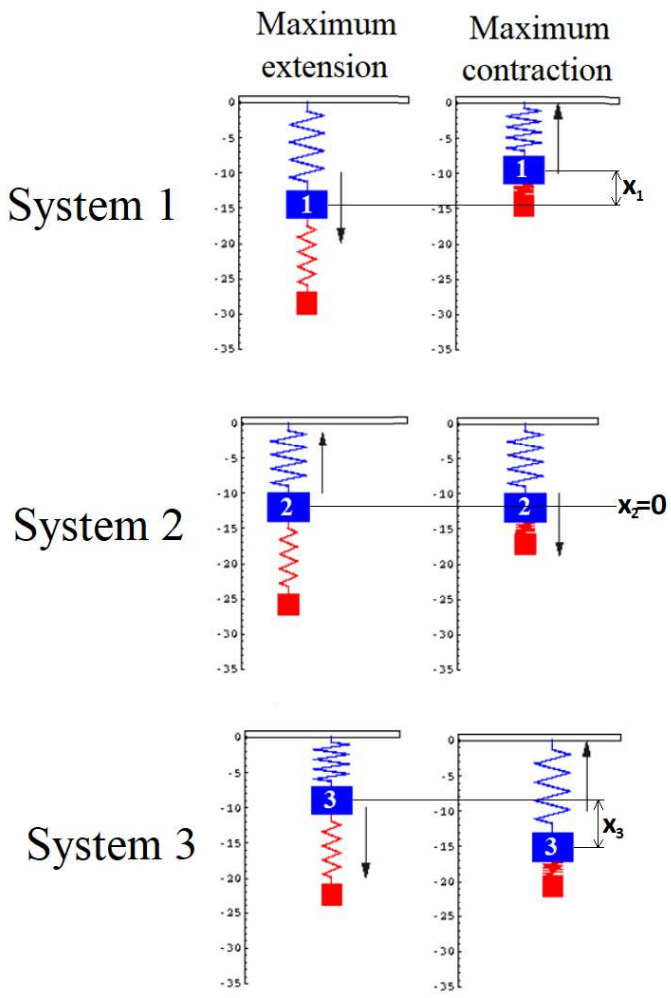

Figure 20: Three DVA systems denoted by 1, 2, and 3, being 1 and 3 non-synchronized ($x_1 \neq 0$ and $x_3 \neq 0$) and 2, perfectly synchronized ($x_2 = 0$) (61)

enhance the effectiveness and versatility of DVAs in real-world applications.

DVAs are constantly being researched and state-of-the-art technology is currently being developed. Godoy researched the application of a non-linear DVA, which can be accomplished by substituting a linear spring with a non-linear one, such as a cubic or hyperbolic spring. He also wished to explore a design inspired by Snap-Through Truss Absorbers (STTAs), a type of technology that employs the common snap-through effect (generated when an object quickly moves from one shape or orientation to another due to external forces) in a truss structure as a vibration attenuation method. At first he attempted to design a secondary mass with only one degree of freedom (d.o.f.) and which

"snaps" when moving vertically, then he upgraded it to a 2-d.o.f. system that does not snap. In Figure 21 it can be seen that the primary mass only has one degree of freedom, moving exclusively side-to-side, and is connected to the wall next to it by a spring and a damper; the secondary mass, on the other hand, can move vertically and horizontally and is connected both to the primary system and to the other wall by individual springs only. As the primary system oscillates, the secondary system is free to move in a way that absorbs some of the vibration imposed upon it. This upgraded design achieved a decrease in peak amplitude from -80 to -160dB (62).

Shen et al. studied a DVA model with a very different layout (Figure 22): the primary mass m_1 is connected to the ground by only a spring k_1 and is pushed upward by a force $F(t) = F_0 cos(\omega t)$. Connected to the top of the primary mass is a sliding element that is itself connected to a lever. The only fixed connection to the lever is in its middle, where it is grounded, and there are two sliding elements that connect the primary and the secondary system to it at each end. The secondary system is composed of the slider at the top, a spring k_2 below it, the secondary mass (constrained to only vertical movement) below the spring, and a spring k_3 and damper in parallel c below the secondary mass connected to the ground. Besides analyzing the stiffness parameters given by the ks, c, and ms in the formulation, a key point in Shen et al.'s paper is studying the ratio $\frac{r_1}{r_2}$, or how far down the lever the sliding elements should be. This very creative design accomplished an incredible 97.78% amplitude reduction ratio superior to respected DVA models proposed by M. Z. Ren and Den Hartog, which ranged between 84.65 and 92.30% (37) (63).

Acar et al. studied an adaptively passive DVA with a negative stiffness mechanism, an elegant solution to vibration that passively adjusts its own bandwidth. This design is composed of a rigid beam pivoted at one end and subjected to forced vertical vibrations at the other one through a spring k_s (Figure 23). On top of the beam there is a string-mass system that functions as this design's DVA. The mass moment of inertia of the beam about its pivoting edge is I_O, the distance between the pivoting edge and the center of

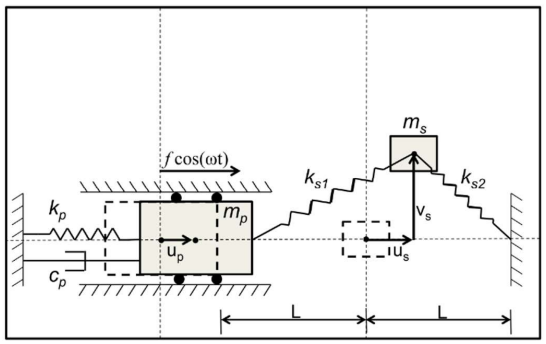

Figure 21: STTA-like model, a spring-mass system which makes use of the geometric nonlinearity contained in it to minimize vibration amplitudes (62)

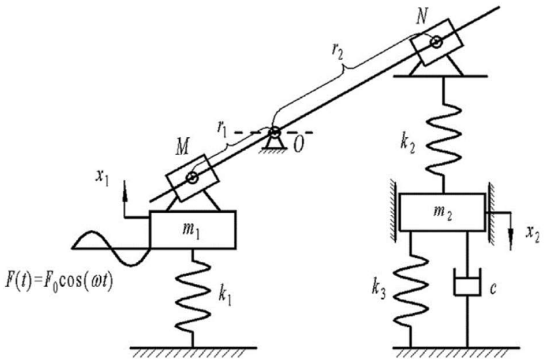

Figure 22: Lever amplifying arm, grounded element DVA (63)

mass of the secondary mass m_a is L_1, and the distance between the pivoting edge and k_s is L_2, making the basic functioning of Acar et al.'s design similar to the simplification in Figure 25 where $m_s = \frac{I_O}{{L_2}^2}$, $k'_a = k_a(\frac{L_1}{L_2})^2$, and $m'_a = m_a(\frac{L_1}{L_2})^2$. To complete this design, Acar et al. adds a negative stiffness mechanism on top of the rigid beam to aid string tension adjustment for the string-mass functioning as this design's DVA. Meaning, it can be helpful to this general vibrating system to stretch or compress the DVA's string to change its natural frequency of vibration; that being the case, a motor driver is attached to one of the edges of the DVA string which is in charge of pulling or pushing it. Attached to the motor is a mechanism which employs negative stiffness, a property that allows a spring to show larger displacement with decreasing force input rather than the usual positive stiffness norm of displacement-force direct proportionality. The designers of this DVA expertly chose to include this negative stiffness spring because, it being in series with the DVA string, which has a positive stiffness, means there is a stiffness constant resultant of the sum of the two (the negative and the positive) which adds up to zero and equates the total effort required by the motor to pull or push the DVA string to basically zero, too. This DVA design saw an average acceleration RMS reduction of 90% (64).

Barredo et al. recently proposed a nontraditional DVA (Figure 24) which makes use

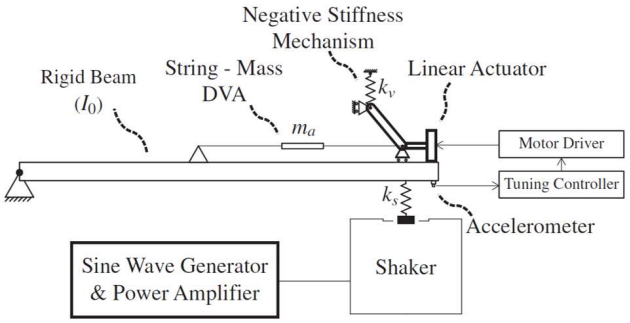

Figure 23: Negative stiffness string-mass DVA (64)

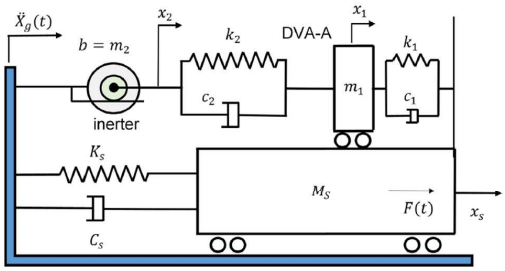

Figure 24: Inerter-based DVA (65)

of the properties of an inerter. Inerters are devices that slowly dissipate motion in the same direction that this motion was put in place, not in the opposite direction like occurs with springs. Like shown in Figure 26, when a spring is compressed, it displays resistance to the compressing motion and, if let go, will quickly return to its original shape and stretch back up — as long as no plastic deformation has happened. An inerter, composed of a rotating flywheel, a threaded shaft, and an external casing, when compressed and let go will not attempt to restore its initial state but will rather keep moving in the same direction, decelerating. Lastly, when a shock absorber is compressed, it will dissipate this energy input in the form of heat. Coupling a spring, a damper, and an inerter in a DVA allows for efficient vibration absorption as the spring's and the inerter's natural states after being compressed or stretched are opposite, thus cancelling each other out. When the spring that is compressed or stretched due to an undesired vibration in the primary system is connected to an inerter, there is good reason to believe this vibration will be attenuated. Barredo et al.'s DVA design accomplishes a 22-26% harmonic and 15-20% random vibration reduction when compared to the classic DVA — whilst also managing to attenuate broadband random excitations (65).

Yao et al. achieved a 94.92% vibration attenuation with a DVA that employs ferrofluid magnetism (Figure 27), meaning they filled a nonmagnetic chamber with a magnetic primary mass, magnets with opposite poles at the internal edges of the chamber, and magnetic ferrofluid. The whole system was, then, tested against vibrations in differ-

ent orientations and the displacement of the primary mass (or inertial mass block) was tracked. In this DVA model, the technology responsible for reducing the susceptibility of the primary mass to moving when the system undergoes unwanted vibration is the magnetic attraction the mass feels towards the magnets and the ferrofluid. It is as if a chamber containing a rock that is tied tightly to the walls with thick ropes in all directions was shaken wildly: the amount the rock would move is insignificant compared to if there were no ropes (67).

Mizuno et al. innovated as they employed high tech sensors and magnets (Figure 29), turning their DVA into a mechatronic system. Out of the list of groundbreaking DVA concepts listed above, this is perhaps the only one that fits within the category of "active" DVA, in which an algorithm is fully determining the functioning of the absorber — Acar et al.'s design uses a sensor and an actuator for reshaping the spring-mass DVA, but it serves more as assistance than the entirety of the absorption system. Mizuno et al.'s DVA containing a feedback-looping compensator controller (Figure 28) achieved an 88.89% peak displacement reduction (68).

New developments in the world of DVAs can be categorized according to their branch of technology:

- Advanced materials: breakthroughs in materials science have led to the development of new materials with improved damping properties. For instance, the utilization of

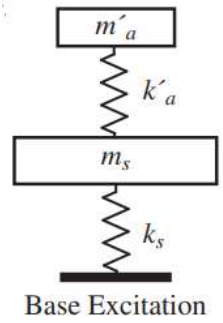

Figure 25: A simplification of Acar et al.'s design (64)

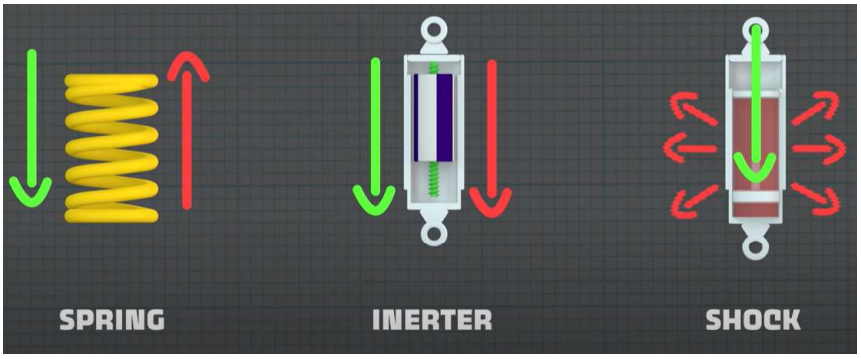

Figure 26: The inerter's response to motion; green is motion/energy input and red is motion/energy output (66)

high-performance viscoelastic materials and composites has enhanced the effectiveness and durability of DVAs in reducing vibrations;

- Miniaturization and compact designs: innovations in miniaturization techniques and compact design methodologies have enabled the integration of DVAs into smaller and lighter structures. This advancement is particularly relevant in industries such as aerospace, where weight reduction is critical;

- Smart control systems: the integration of smart control systems, such as semi-active and active control strategies, has revolutionized the performance of DVAs. These systems allow for real-time monitoring and adjustment of damping characteristics, providing adaptability and improved vibration mitigation;

- Multifunctional applications: breakthroughs in DVA design have led to the development of multifunctional devices that not only damp vibrations but also offer additional functionalities. For example, DVAs with energy harvesting capabilities have been explored, enabling the conversion of vibration energy into usable electrical power;

- Numerical modeling and optimization techniques: advancements in numerical modeling and optimization techniques have significantly improved the design and performance of DVAs. Through the use of sophisticated algorithms and simulations, engineers can accurately predict the behavior of DVAs and precisely optimize their parameters for specific applications like never before.

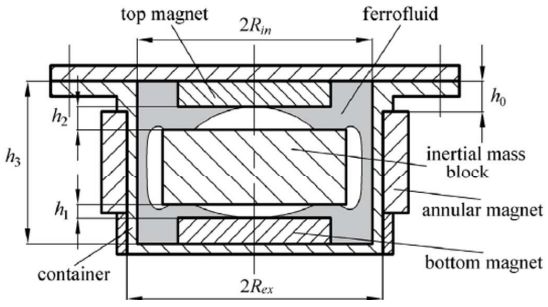

Figure 27: Ferrofluid DVA (67)

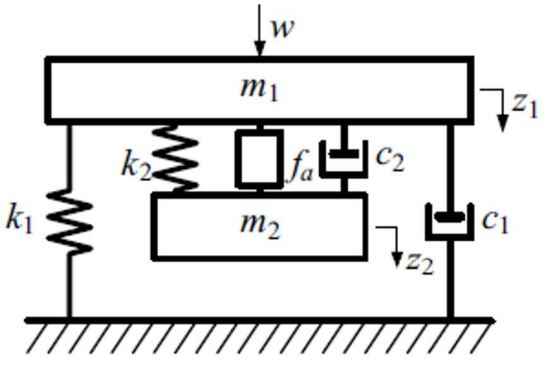

Figure 28: Active DVA (68)

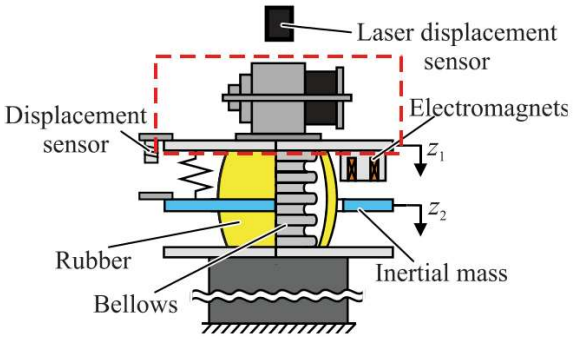

Figure 29: Schematic of Mizuno et al.'s active DVA (68)

Finally, here are a few examples of how DVAs are currently being employed:

- Skyscrapers: DVAs are integrated into tall buildings to mitigate wind-induced vibrations and enhance structural stability, ensuring occupant comfort and safety; an example of this are the aforementioned Taipei World Financial Center (Figure 18) and the Doha Sport City Tower;
- Bridges: they are utilized in bridge structures to reduce the effects of dynamic loads, such as traffic-induced vibrations or seismic events, thus minimizing structural damage and extending the lifespan of the bridge; an example of this is London's Millennium Bridge (Figure 19);
- Wind turbines: they can be installed in wind turbines to dampen tower vibrations caused by wind gusts, improving the performance and reliability of the turbine (69);
- Automotive suspension systems: they are incorporated into vehicle suspension systems to reduce vibrations and enhance ride comfort, particularly in high-performance or luxury vehicles (70);
- Rotating machinery: they find applications in various rotating machinery, such as engines or turbines, to minimize unwanted vibrations and prevent premature failure of components (71).

The fundamental concepts ranging from vibration theory to Dynamic Vibration Absorbers have been established, meaning the reader should be able to understand fully all

of the theory involved in this project. A concept that remains to be reviewed is that of the multibody dynamic analysis, the computer-aided method of simulating interactions between 3d bodies.

1.5 Multibody Dynamics (MBD) Simulation

This project will use two tools to explore the concepts listed in this chapter and attempt to map out how the forced vibration in the piston causes unwanted displacements (while also suggesting a means of attenuating these displacements):

1. A proprietary mathematical model that will be written on MATLAB — all of the reasoning behind the code is contained in the next chapter and all the codes used are in the Appendix; and
2. A Multibody Dynamics simulation, also referred to as multibody dynamic analysis, and MBD.

Multibody dynamics involves the examination of the movement of intricate mechanical systems when subjected to mechanical forces. MBD simulation software provides engineers with the means to analyze and explore the kinematic and dynamic motion of mechanical and mechatronic systems. MBD software enables the creation and analysis of virtual 3D models, allowing for the prediction and visualization of motion, as well as the assessment of coupling forces and stresses (72).

MBD is not to be mistaken with Finite Element Analysis (FEA), another widely used method of 3d model analysis in Mechanical Engineering: FEA is mostly interested in deformations and strengths, while MBD is mostly interested in motions and displacements (73). In terms of differences in methodology, FEA breaks down the bodies into nodes, the "finite elements", turning an extremely challenging series of continuous body calculations into simpler, node-by-node estimations. In general, the higher the number of nodes, the more precise the simulation is. MBD does not employ this same breaking-down-into-

nodes system; rather, it chooses to conceptualize bodies as uninterrupted solids with their respective masses and inertia and interpret the interactions among bodies through well-defined joints, grounds, forces, and dynamic elements like springs and dampers.

MBD was chosen to be the second simulation method for this project because it closely resembles the methodology of the MATLAB code, if compared to FEA — if the mathematical model in the code used for this project employed FEA, then surely a Finite Element software would have been employed as the second simulation. Choosing MBD ensures a better match in results between both simulations. The MBD software that was chosen for this project is MSC Adams View.

Now that topics ranging from the most basic concepts in vibration theory to the most advanced Dynamic Vibration Absorbers and MBD have been covered, one can move on to the next chapter, which covers the whole process of idealizing and putting in practice a DVA attached to the cryocooler, then analyzing its impact in the cooler's vibrations.

1.6 Project Fluxograms

To aid in the visualization of the tasks that will be performed from this point onward, the fluxogram in Figure 30 and the task distribution Table 3 were created.

The methodology fluxogram in Figure 31 shows in detail the rationale behind this research: firstly, a model is built based on reviewed theory, then tested for validity, then something is done with this model. This process is repeated a total 4 times, two for the mathematical model (with and without the DVA) and two for the 3d model (also, with and without the DVA).

It should be noted that this project ends up being more of a qualitative than a quantitative analysis of the cryocooler system: many determining factors are calculated based on several assumptions; thus, its main objective becomes to address the viability of adding a DVA to the system, rather than to literally calculate its optimal operating conditions.

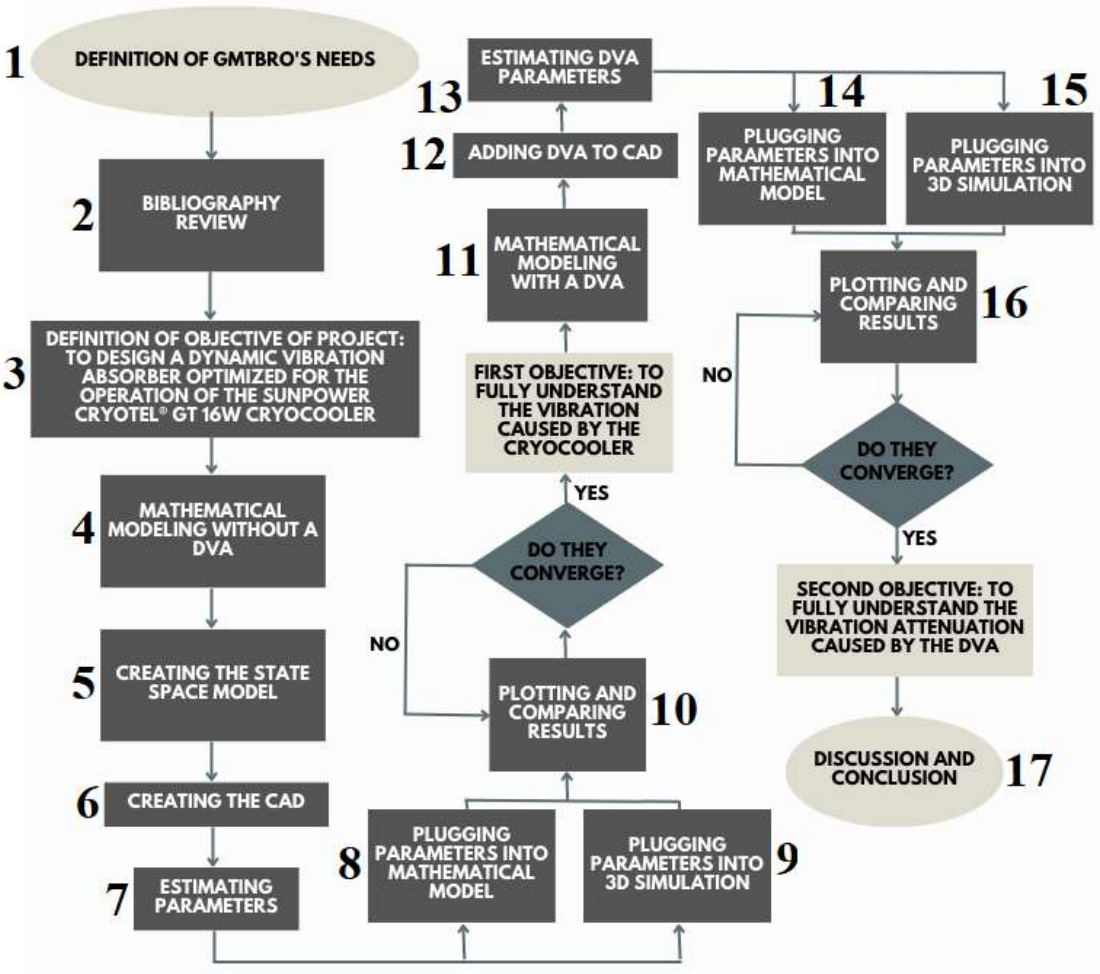

Figure 30: This project's fluxogram and task numbers; the tasks are spread throughout this document as provided in Table 3

Task number	Chapter	Task number	Chapter
1	1	10	5
2	3	11	6
3	2	12	6
4	4	13	6
5	4	14	6
6	4	15	6
7	4, 5	16	6
8	5	17	7
9	5		

Table 3: This document's task distribution per chapter (task numbers provided in the Fluxogram in Figure 30)

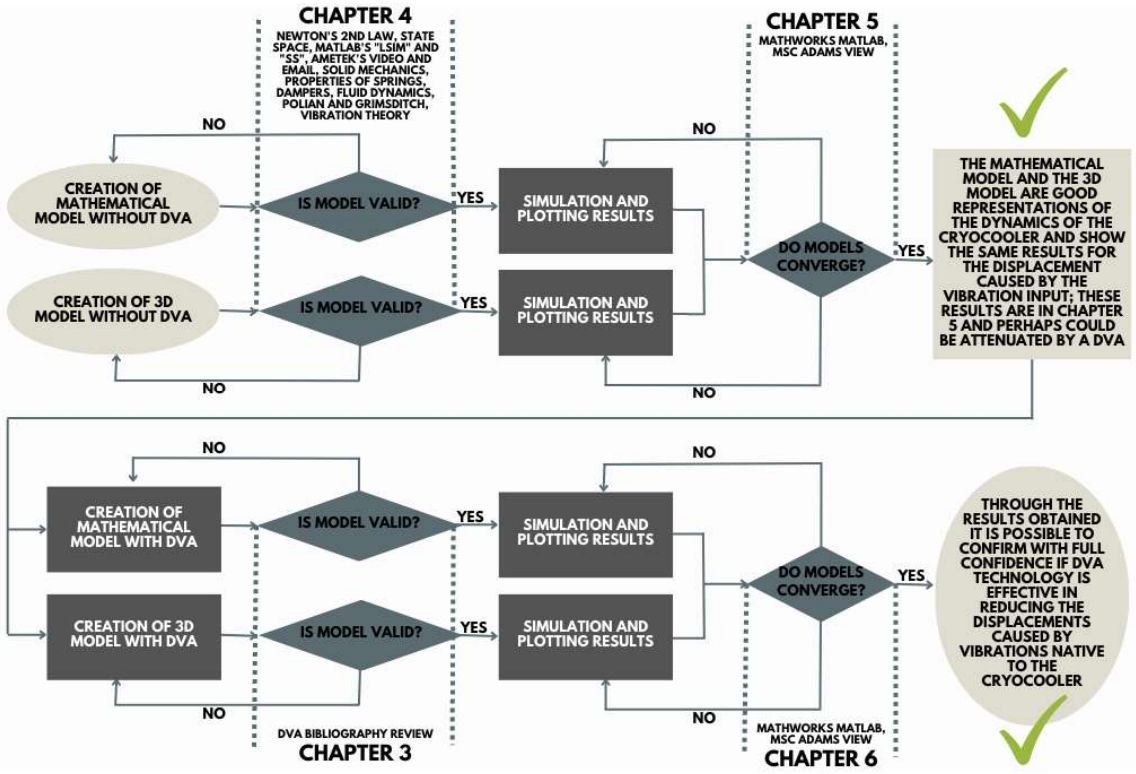

Figure 31: This project's methodology fluxogram

2 OBJECTIVE

The goal of this project is to design a Dynamic Vibration Absorber optimized for the operation of the Sunpower Cryotel® GT 16W Cryocooler.

3 CREATING TWO MODELS FOR THE CRYOCOOLER

"But remember this, Japanese boy... airplanes are not tools for war. They are not for making money. Airplanes are beautiful dreams. Engineers turn dreams into reality."

-- Hayao Miyazaki

As per the task distribution in Table 3, in this chapter will be performed:

- The mathematical modeling of the system without a DVA;
- The creation of the state-space model;
- The creation of the Computer-Aided Design (CAD), or 3d model, for the system;
- The estimation of parameters for the system.

The first task needed in the mathematical characterization of the dynamics of the cryocooler is drawing a mass-spring-damper system that properly illustrates the motions of the displacer, the piston, and the displacement caused by those two on the cooler's exterior. The representation of a valid spring-mass-damper system can be seen in Figure 32. Comparing it to Figure 6, it can be noticed that spring-damper pairs k_2 and c_2, k_3 and c_3 represent the dynamics of the Helium gas surrounding the Displacer (A) and the Piston (B). It can also be noticed that spring-damper pair k_1 and c_1 represent the physical interaction between the cryocooler and GMACS, and that the pair k_4 and c_4 represents the internal spring that absorbs the movement from the displacer.

The motions of each mass are indicated by x_A, x_B, and x_D — the choice for skipping "C" in the alphabetical ordering of variables will make itself clear in Chapter 5. The

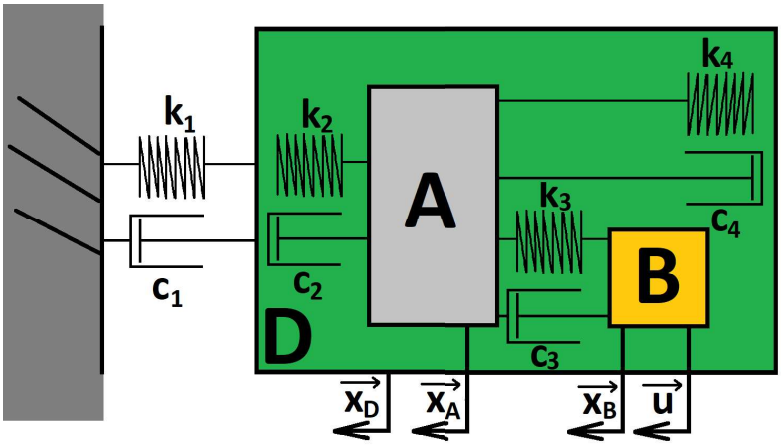

Figure 32: Free Body Diagram representing the cryocooler

direction of these displacements is illustrated in the picture as being left-pointing. Displacement x_D refers to the displacement of the entire cryocooler. Each component, A, B, and D has its own mass m_A, m_B, and m_D. Finally, force u is the external excitation imposed upon the piston.

Based on Newton's second law, $F = ma$, the following equations can be written for the three bodies A, B, and D:

$$m_A\ddot{x_A} + (c_2 + c_3 + c_4)\dot{x_A} + (k_2 + k_3 + k_4)x_A - c_3\dot{x_B} - k_3x_B$$
$$-(c_2 + c_4)\dot{x_D} - (k_2 + k_4)x_D = 0 \tag{3.1}$$
$$m_B\ddot{x_B} + c_3\dot{x_B} + k_3x_B - c_3\dot{x_A} - k_3x_A = u \tag{3.2}$$
$$m_D\ddot{x_D} - (c_2 + c_4)\dot{x_A} - (k_2 + k_4)x_A + (c_1 + c_2 + c_4)\dot{x_D}$$
$$+(k_1 + k_2 + k_4)x_D = 0. \tag{3.3}$$

where $\vec{u}$ is the force input provided by the electric current to the system. In order to properly solve for equations (3.1) - (3.3), the State Space approach is encouraged as it helps organize the multiple differential equations above (74) (75). For the state space formulation, we have

$$y_1 = x_A \quad y_2 = \dot{x_A} \quad y_3 = x_B \quad y_4 = \dot{x_B} \quad y_7 = x_D \quad y_8 = \dot{x_D}$$

(where, once again, skipping y_5 and y_6 will be explained in Chapter 5), which yields

$$\begin{aligned}
\dot{y_1} &= y_2 \\
\dot{y_2} &= -\frac{k_2+k_3+k_4}{m_A}y_1 - \frac{c_2+c_3+c_4}{m_A}y_2 + \frac{k_3}{m_A}y_3 + \frac{c_3}{m_A}y_4 + \frac{k_2+k_4}{m_A}y_7 + \frac{c_2+c_4}{m_A}y_8 \\
\dot{y_3} &= y_4 \\
\dot{y_4} &= \frac{k_3}{m_B}y_1 + \frac{c_3}{m_B}y_2 - \frac{k_3}{m_B}y_3 - \frac{c_3}{m_B}y_4 + \frac{u}{m_B} \\
\dot{y_7} &= y_8 \\
\dot{y_8} &= \frac{k_2+k_4}{m_D}y_1 + \frac{c_2+c_4}{m_D}y_2 - \frac{k_1+k_2+k_4}{m_D}y_7 - \frac{c_1+c_2+c_4}{m_D}y_8
\end{aligned}$$

or

$$\begin{bmatrix} \dot{y_1} \\ \dot{y_2} \\ \dot{y_3} \\ \dot{y_4} \\ \dot{y_7} \\ \dot{y_8} \end{bmatrix} = \begin{bmatrix} 0 & 1 & 0 & 0 & 0 & 0 \\ -\frac{k_2+k_3+k_4}{m_A} & -\frac{c_2+c_3+c_4}{m_A} & \frac{k_3}{m_A} & \frac{c_3}{m_A} & \frac{k_2+k_4}{m_A} & \frac{c_2+c_4}{m_A} \\ 0 & 0 & 0 & 1 & 0 & 0 \\ \frac{k_3}{m_B} & \frac{c_3}{m_B} & -\frac{k_3}{m_B} & -\frac{c_3}{m_B} & 0 & 0 \\ 0 & 0 & 0 & 0 & 0 & 1 \\ \frac{k_2+k_4}{m_D} & \frac{c_2+c_4}{m_D} & 0 & 0 & -\frac{k_1+k_2+k_4}{m_D} & -\frac{c_1+c_2+c_4}{m_D} \end{bmatrix} \begin{bmatrix} y_1 \\ y_2 \\ y_3 \\ y_4 \\ y_7 \\ y_8 \end{bmatrix} + \begin{bmatrix} 0 \\ 0 \\ 0 \\ \frac{1}{m_B} \\ 0 \\ 0 \end{bmatrix} u \tag{3.4}$$

.

Equation (3.4) is called the State Equation. It is accompanied by the Output Equation (3.5).

$$\begin{bmatrix} x_A \\ \dot{x_A} \\ x_B \\ \dot{x_B} \\ x_D \\ \dot{x_D} \end{bmatrix} = \begin{bmatrix} 1 & 0 & 0 & 0 & 0 & 0 \\ 0 & 1 & 0 & 0 & 0 & 0 \\ 0 & 0 & 1 & 0 & 0 & 0 \\ 0 & 0 & 0 & 1 & 0 & 0 \\ 0 & 0 & 0 & 0 & 1 & 0 \\ 0 & 0 & 0 & 0 & 0 & 1 \end{bmatrix} \begin{bmatrix} y_1 \\ y_2 \\ y_3 \\ y_4 \\ y_7 \\ y_8 \end{bmatrix} \tag{3.5}$$

The state and output equations can also be represented, respectively, as

$$\dot{x} = Ax + Bu \tag{3.6}$$

$$y = Cx + Du \tag{3.7}$$

where

$$A = \begin{bmatrix} 0 & 1 & 0 & 0 & 0 & 0 \\ -\frac{k_2+k_3+k_4}{m_A} & -\frac{c_2+c_3+c_4}{m_A} & \frac{k_3}{m_A} & \frac{c_3}{m_A} & \frac{k_2+k_4}{m_A} & \frac{c_2+c_4}{m_A} \\ 0 & 0 & 0 & 1 & 0 & 0 \\ \frac{k_3}{m_B} & \frac{c_3}{m_B} & -\frac{k_3}{m_B} & -\frac{c_3}{m_B} & 0 & 0 \\ 0 & 0 & 0 & 0 & 0 & 1 \\ \frac{k_2+k_4}{m_D} & \frac{c_2+c_4}{m_D} & 0 & 0 & -\frac{k_1+k_2+k_4}{m_D} & -\frac{c_1+c_2+c_4}{m_D} \end{bmatrix}, \tag{3.8}$$

$$B = \begin{bmatrix} 0 \\ 0 \\ 0 \\ \frac{1}{m_B} \\ 0 \\ 0 \end{bmatrix}, \tag{3.9}$$

$$C = \begin{bmatrix} 1 & 0 & 0 & 0 & 0 & 0 \\ 0 & 1 & 0 & 0 & 0 & 0 \\ 0 & 0 & 1 & 0 & 0 & 0 \\ 0 & 0 & 0 & 1 & 0 & 0 \\ 0 & 0 & 0 & 0 & 1 & 0 \\ 0 & 0 & 0 & 0 & 0 & 1 \end{bmatrix}, \text{ and} \tag{3.10}$$

$$D = 0. \tag{3.11}$$

Using MATLAB's State Space **ss** and Simulated Time Response **lsim** functions it is possible to obtain the displacements of masses A, B, and D at each time instance. The main issue to be addressed, thus, becomes detailing which are the realistic values that can be approximated for c_1, c_2, c_3, c_4, k_1, k_2, k_3, k_4, and m_A, m_B, and m_D. Once these are properly approximated, the mathematical model given by Equations 3.6 - 3.11 will have been fully validated and the graphs plotted will correctly show the relationship between the amplitude of displacement of each mass A, B, and D, and the forced vibration being imposed onto mass B. Furthermore, once these parameters are defined, a multibody dynamic analysis software will prove right the spring-mass-damper dynamics found analytically through the MATLAB code.

Some of the assumptions made in the modeling of this system were:

1. All solids are homogeneously dense
2. The elastic behaviors of springs k_1 and k_4 can be described linearly
3. All elements being studied present some calculable stiffness and a damping coefficient
4. k_1 can be approximated by Equation 3.20
5. k_4 is an axially loaded, initially flat spiral spring such as the one in Figure 36

In order to be able to properly determine realistic values for the currently unknown variables in Equations (3.6) - (3.11), they will now be broken up into three categories (mass approximations m, coefficients of stiffness aproximations k, and damping coefficients c) and studied in depth.

A proper analysis of these parameters would be impossible without a CAD model of the cryocooler. An official model unfortunately is not available since its geometry is a private property of Sunpower Inc.; however, an approximate CAD can be drawn having as an inspiration the proportions from the video uploaded to YouTube by Sunpower exposing the device's cross-section, and the cryocooler's official datasheet, which provides its total length (27) (28) (76). By calculating simple rules-of-three, the model shown in Figure 33 was drawn in SolidWorks maintaining the same color scheme from Figure 32 for ease of understanding; here it stands out how the approximated CAD presents proportions very similar to the official ones of Figure 6.

In Figure 33:

- A is the displacer;
- B is the piston
- D is the outer shell;
- W is the wall;

- The red spring has mass m_4, stiffness coefficient k_4, and damping coefficient c_4; and
- The orange flange has mass m_1, stiffness coefficient k_1, and damping coefficient c_1.

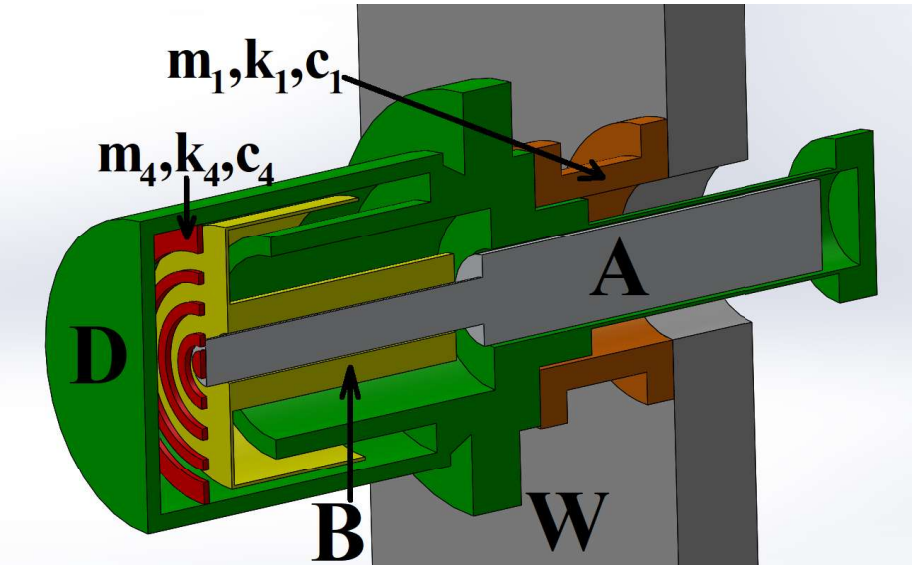

Figure 33: An approximated CAD model for the cryocooler attached to GMACS' wall

It should be noted that the addition of the flange to the CAD was a structural necessity in order to guarantee the correct placing of the cryocooler within GMACS. It is neither in the mathematical nor in the 3d model (it is simply characterized as having a stiffness constant k_1 and damping coefficient c_1) because its dynamic effect on the motion of the other bodies A, B, and D is negligible. The geometry of the flange in this project is speculative and only serves to properly fix the cryocooler to GMACS' wall.

3.1 Estimation of masses

According to a Sunpower/Ametek representative, the cryocooler's outer shell is made out of grade 304 Stainless Steel; for the purpose of this project, and due to lack of further knowledge of material choice for the cryocooler's manufacturing process, the rest of the cryocooler will be assumed to be made of the same material (76) (77). From SolidWorks:

$$m_A = 759.49 \text{ g} \tag{3.12}$$

$$m_B = 566.14 \text{ g} \tag{3.13}$$

$$m_D = 4,802.53 \text{ g} \tag{3.14}$$

3.2 Estimation of stiffness constants

3.2.1 About k_1 and k_4 (spring stiffnesses)

If the springs are modeled as simple rods, as represented in Figure 34, then Equations (3.15) - (3.18) follow (78) (79):

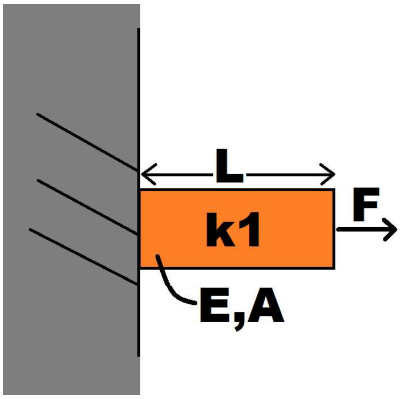

Figure 34: Spring k1 modeled as a rod

$$F = kx \tag{3.15}$$

$$\sigma = E\varepsilon \tag{3.16}$$

Where

$$\sigma = \frac{F}{A} \tag{3.17}$$

$$\varepsilon = \frac{x}{L} \tag{3.18}$$

Here it is assumed that the area and length of the solid being modeled like a rod will be negligibly deformed. Thus:

$$\frac{kx}{A} = E\frac{x}{L}$$
$$\therefore k = E\frac{A}{L}. \tag{3.19}$$

Knowing the material properties E (Young's modulus of the material of the spring), A (cross-sectional area of the rod representing the spring), and L (length of the rod representing the spring), then, a realistic value can be found for k_1 and k_4.

3.2.1.1 k_1

The flange, highlighted in Figure 35, can be simplified as a block with stiffness coefficient k_1. Applying Equation (3.19) to the flange and disregarding the thicker sections with radius r_{big}:

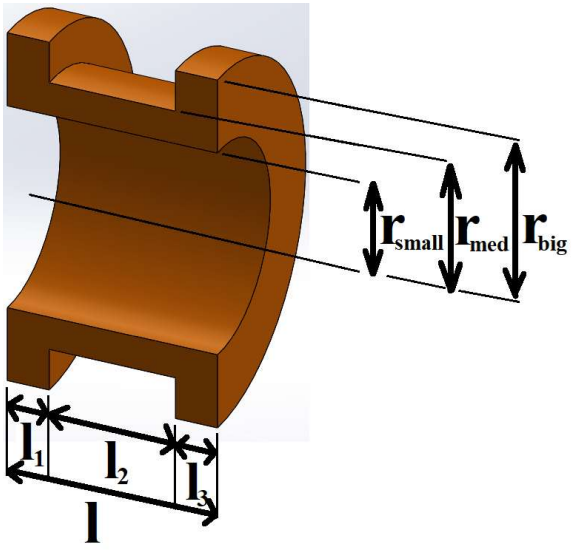

Figure 35: CAD of flange, cross section

$$k_1 = E\frac{\pi({r_{med}}^2 - {r_{small}}^2)}{l} \tag{3.20}$$

where r_{big}, r_{med}, and r_{small}, l_1, l_2, and l_3 are defined as in Figure 35 and Equations 3.21 - 3.27.

$$r_{small} = 24.00 \text{ mm} \tag{3.21}$$

$$r_{med} = 31.82 \text{ mm} \tag{3.22}$$

$$r_{big} = 41.82 \text{ mm} \tag{3.23}$$

$$l_1 = 10 \text{ mm} \tag{3.24}$$

$$l_2 = 19.42 \text{ mm} \tag{3.25}$$

$$l_3 = 10 \text{ mm} \tag{3.26}$$

$$l = 39.42 \text{ mm} \tag{3.27}$$

Young's Modulus E of Stainless Steel 304 is 190 GPa; thus, Equation 3.20 becomes

$$k_1 = 190,000\frac{\pi(31.82^2 - 24^2)}{39.42} = 6.61 \times 10^6 \text{ N/mm} \tag{3.28}$$

3.2.1.2 k_4

As can be seen in Figures 6 and 9, this spring is an axially loaded, initially flat spiral spring whose stiffness coefficient will be approximated by the common helical spring stiffness equation,

$$k = \frac{d^4 G}{8D^3 N_a}$$

where d is the wire diameter, G is the shear modulus of elasticity, D is the mean spring diameter, and N_a is the number of active coils as shown in Figure 36 (80).

d, D, and N_a can be obtained from the Cryocooler model provided by Sunpower (28):

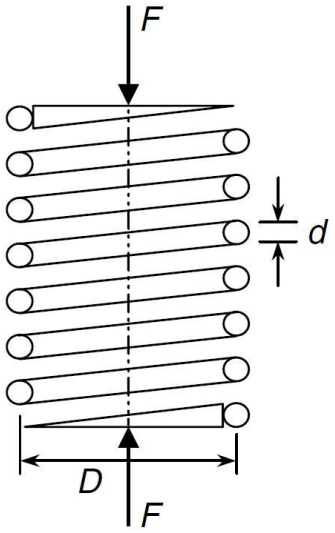

Figure 36: A helical spring (80)

$$d = 3.1 \text{ mm}$$

$$D = 42.64 \text{ mm}$$

$$N_a = 4$$

and it is known that (81) (82) (83)

$$G = 77.2 \text{ GPa}$$

$$\therefore k_4 = \frac{3.1^4 \times 77200}{8 \times 42.64^3 \times 4} = 2.87 \text{ N/mm} \tag{3.29}$$

While for the purpose of the mathematical model and the multibody dynamic analysis a helical model such as the one in Figure 36 will be used, for the calculation of damping coefficients in Section 3.3 a CAD of the flat spring from the video published by Sunpower was drawn in order for an approximation of the spring's mass to be attainable (28). The flat spring CAD can be seen in Figure 37, where the part's properties such as number

of coils, diameter, and thickness were all estimated using the 3d rendered simulation Sunpower made available online (28).

When running the multibody dynamic analysis on MSC Adams View, the software's "helical spring" tool will be employed to simulate the dynamics of the spring with constants k_4 and c_4, rather than using the model in Figure 37. This choice was due to the software providing specialized tools for elements like springs, dampers, actuators, and such, that do not function as well if one tries to CAD those elements by hand. The fact that the helical spring simplification was also applied to the mathematical model, as described above, also helps validate this choice.

Figure 37: Flat spring's CAD

3.2.2 About $k2$ and $k3$ (fluid stiffnesses)

When analyzing the dynamics of a system, any system parts that hold a compressible fluid will behave like a spring and can be considered as such (84). Just as the spring stiffness constant k describes the resistance to deformation, for a hydraulic actuator such as the cryocooler's piston, the opposition to motion is represented by the hydraulic stiffness C_H:

$$C_H = \frac{E_\upsilon A^2}{V}. \tag{3.30}$$

Here E_υ is the fluid's bulk modulus, A is the piston's cross-sectional area, and V is the volume of fluid being expanded and contracted (78) (85) (84).

The chambers containing Helium gas, which will be approximated in the spring-mass-damper system as possessing stiffness constants k_2 and k_3, are shown in Figure 38; for the purpose of this project,

$$C_{H_{k_2}} \sim k_2 \tag{3.31}$$

$$C_{H_{k_3}} \sim k_3. \tag{3.32}$$

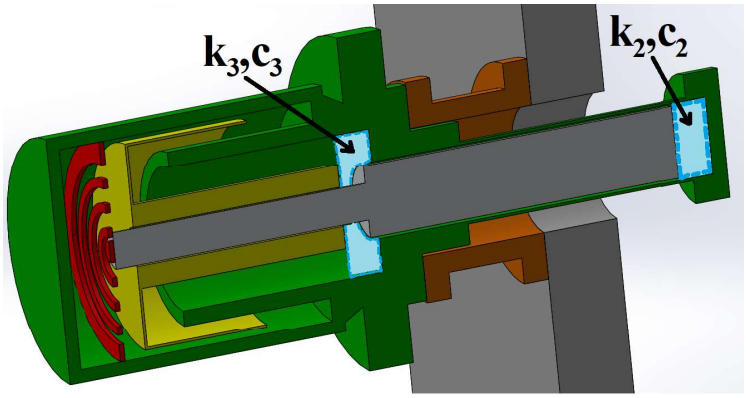

Figure 38: Cryocooler CAD Highlighting the helium-filled chambers with stiffness coefficients k_2 and k_3

Knowing

$$E_\upsilon = \frac{dp}{d\rho/\rho}$$

and applying the results obtained from A. Polian and M. Grimsditch's experiments with Helium gas in 1986 (Figure 39), it can be confidently claimed that

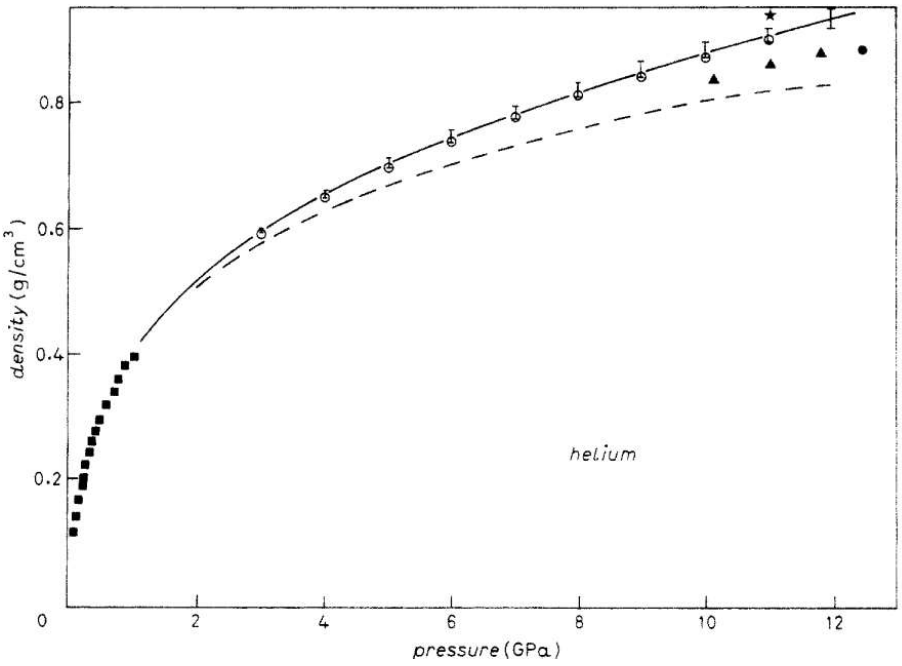

Figure 39: A. Polian and M. Grimsditch's results correlating pressure and density of helium gas at room temperature; here, the experimental values are represented by the black squares (86)

$$E_v = \frac{1.2 \text{ GPa}}{\frac{0.3 \text{ g/cm}^3}{0.1 \text{ g/cm}^3}} = 0.4 \text{ GPa} \tag{3.33}$$

is a sufficiently accurate approximation of the bulk modulus of Helium gas for the conditions of the cryocooler's operation (85) (86).

From the CAD model designed and shown in Figure 38 it can be calculated that the cross-sectional areas of the chambers where helium contracts and expands, as shown in Figures 40 and 41, are

$$A_{k_2} = \pi\left(\frac{2r_{k_2}}{2}\right)^2 = \pi\left(\frac{30}{2}\right)^2 = 706.86 \text{ mm}^2 \tag{3.34}$$

$$A'_{k_3} = \pi\left(\frac{2r'_{k_3}}{2}\right)^2 = \pi\left(\frac{30}{2}\right)^2 = 706.86 \text{ mm}^2 \tag{3.35}$$

$$A''_{k_3} = \pi\left(\frac{2r''_{k_3}}{2}\right)^2 = \pi\left(\frac{43}{2}\right)^2 = 1,452.20 \text{ mm}^2; \tag{3.36}$$

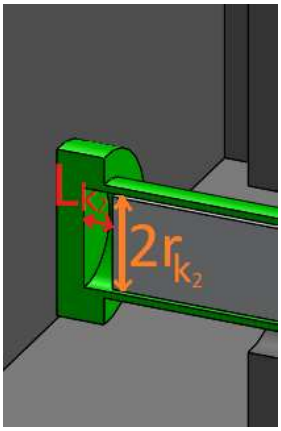

Figure 40: k_2 with its dimensions

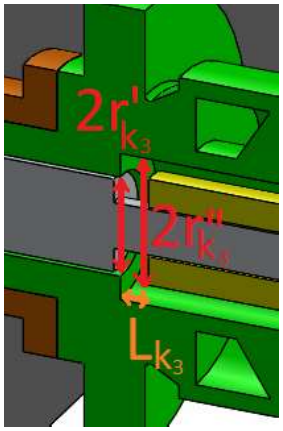

Figure 41: k_3 with its dimensions

since the chamber being approximated as having a spring constant k_3 has two radii and two cross-sectional areas, given by Equations 3.33 and 3.34 as A'_{k_3} and A''_{k_3}, then the effective area that will be used is

$$A_{k_3} = \frac{A'_{k_3} + A''_{k_3}}{2} = 1,079.53 \text{ mm}^2. \tag{3.37}$$

Obtaining the maximum length L of each chamber, using Sunpower's video as a reference, and dividing them by 2 to find their average values: (28)

$$L_{k_2} = \frac{25.46}{2} \text{ mm} = 12.73 \text{ mm} \tag{3.38}$$

$$L_{k_3} = \frac{15.43}{2} \text{ mm} = 7.72 \text{ mm}. \tag{3.39}$$

Combining Equations (3.30), (3.31), (3.32), (3.33), (3.34), (3.37), (3.38), and (3.39):

$$k_2 = \frac{400 \times 706.86^2}{706.86 \times 12.73} = 5.56 \times 10^3 \text{ N/mm} \tag{3.40}$$

$$k_3 = \frac{400 \times 1,079.53^2}{1,079.53 \times 7.72} = 14.00 \times 10^3 \text{ N/mm} \tag{3.41}$$

3.3 Estimation of damping constants

When there is no dissipation of energy due to friction or other forms of resistance during oscillation, the vibration is referred to as undamped vibration; if there is any energy loss, it is called damped vibration (87). When just enough energy is dissipated to allow it to stop oscillating as quickly as possible, the system is called critically damped. These three types of damping can be seen in Figure 42.

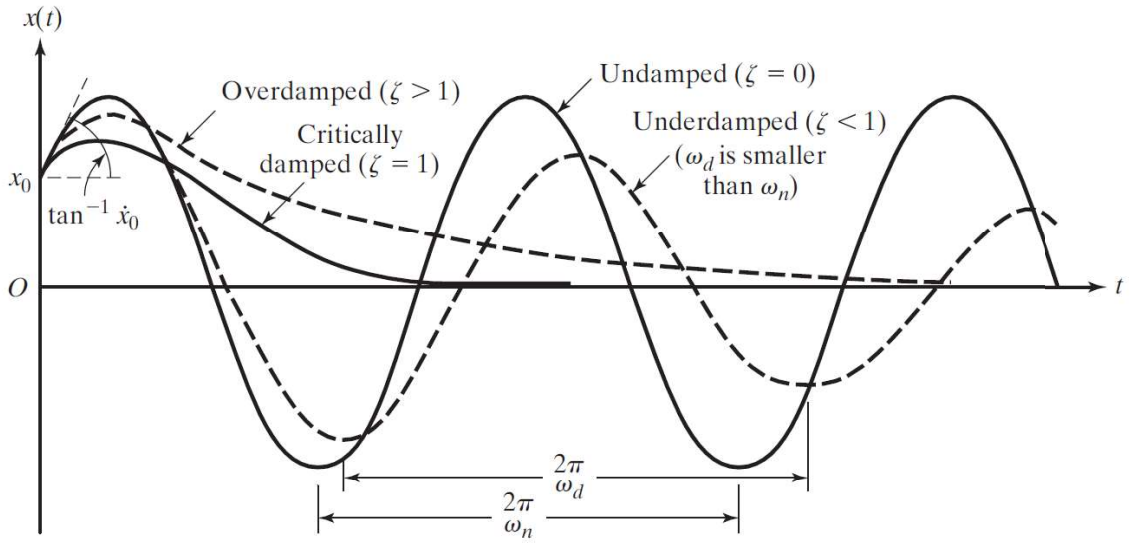

Figure 42: Comparison of motions with different types of damping (87)

The damping ratio of a structure subjected to harmonic motion is defined as

$$\zeta = \frac{c}{c_c}$$

where c_c is the system's critical damping coefficient and c is the system's damping coefficient, and where the system's critical damping coefficient represents the required numerical value of c to cease the oscillation as quickly as possible (87). The damping ratio describes how close to that critical damping an oscillating system is, $\zeta = 1$ meaning the system is critically damped, $\zeta < 1$ under, and $\zeta > 1$ overdamped.

It is known that

$$c_c = 2\sqrt{km}$$

where k is the value obtained in Section 3.2 and m_1 and m_4 are the masses of the respective bodies, making

$$c_1 = 2\zeta\sqrt{k_1 m_1} \tag{3.42}$$

$$c_4 = 2\zeta\sqrt{k_4 m_4} \tag{3.43}$$

for the steel damping elements.

According to Mevada and Patel, the damping ratio of an oscillating steel beam or plate is 0.0069 or 0.69% (88). Masses m_1 and m_4 (where m_4 refers to the mass of the reference spring from Figure 37) are given by SolidWorks, as

$$m_1 = 802.81 \text{ g}$$

$$m_4 = 51.94 \text{ g}$$

Equations (3.42) and (3.43) thus become, for an initial $\zeta = 0.0069$:

$$c_1 = 2 \times 0.0069 \times \sqrt{6.61 \times 10^9 \text{ N/m} \times 802.81 \text{ g}} = 31,789.68\sqrt{\text{Ng/m}} = 31,789.68 \text{ Ns/m} \tag{3.44}$$

$$c_4 = 2 \times 0.0069 \times \sqrt{2.87 \times 10^3 \text{ N/m} \times 51.94 \text{ g}} = 5.33\sqrt{\text{Ng/m}} = 5.33 \text{ Ns/m} \tag{3.45}$$

For the fluid damping elements,

$$c = \frac{\mu A}{L}$$

where μ is the fluid's viscosity, or its resistance to deformation, A is the cross-sectional area of the chamber holding the fluid (A_{k_2} and A_{k_3} from Section 3.2.2) and L is the chamber length (L_{k_2} and L_{k_3} from Section 3.2.2) (87). Here it is worth mentioning that μ does definitely vary according to temperature and is not a stable numerical value, but will be considered so for the purpose of this project due to lack of found evidence of a quantifiable correlation between Helium's viscosity and temperature.

Therefore,

$$\mu_{\text{He}} = 1.96 \times 10^{-5} \text{ Pa s} \tag{3.46}$$

$$c_2 = \frac{1.96 \times 10^{-5} \times 706.86 \times 10^{-6}}{12.73 \times 10^{-3}} = 2.72 \times 10^{-7} \text{ Ns/m} \tag{3.47}$$

$$c_3 = \frac{1.96 \times 10^{-5} \times 1,079.53 \times 10^{-6}}{7.72 \times 10^{-3}} = 2.74 \times 10^{-6} \text{ Ns/m} \tag{3.48}$$

are the damping coefficients for the fluid damping elements c_2 and c_3 (89).

All of the previously unknown variables, m_A, m_B, m_D, k_1, k_2, k_3, k_4, c_1, c_2, c_3, and c_4, have now been determined and can be applied to the linear system in Equations (3.6) - (3.11), which will now provide results that display realistically the dynamics of the cryocooler.

4 SIMULATIONS AND ANALYSES

This chapter, following the task distribution from Table 3, will promote:

- The final parameter estimations for the DVA-less system, which will allow the mathematical and 3d simulation to run properly and be good predictors for the behavior of the cryocooler;
- The plugging in of all the parameters found into both simulations, allowing the acquisition of the displacement results for the cryocooler using two different methods;
- The confection of the plots for each and the juxtaposition of them, allowing a comparison between them.

From Equations (3.12), (3.13), (3.14), (3.28), (3.29), (3.40), (3.41), (3.44), (3.45), (3.47), and (3.48) the parameters obtained can be gathered in Table 4.

Parameter	**Estimation**
m_A	0.75949 kg
m_B	0.56614 kg
m_D	4.80253 kg
k_1	6.61×10^9 N/m
k_2	5.56×10^6 N/m
k_3	14.00×10^6 N/m
k_4	2.87×10^3 N/m
c_1	31,789.68 Ns/m
c_2	2.72×10^{-7} Ns/m
c_3	2.74×10^{-6} Ns/m
c_4	5.33 Ns/m

Table 4: Parameters used for the simulations

It is now of this project's interest to specify that the magnitude of the force $\vec{u}$ being applied to piston, or mass B in Figure 33, is defined by Equation (1.4):

$$u = P_0 sin(\omega t).$$

It is given by Sunpower/Ametek that the cryocooler's operational vibration frequency, the frequency of oscillation of the piston, is (27)

$$f = 60 \text{ Hz},$$

meaning the angular frequency is

$$\omega = 2\pi f = 376.99 \text{ rad/s}. \tag{4.1}$$

The last two variables needed in order to run the MATLAB code are P_0, the force factor, measured in Newtons (N), and x_0, the initial positions and speeds matrix for masses A, B, and D.

Figures 43 and 44 show the total distance travelled by the piston, which is a value needed to calculate the piston's initial position, x_{B_0}. Since $x'_{B_0} = 245.3$ mm and $x''_{B_0} = 258.6$ mm, then

$$x_{B_0} = \frac{258.6 - 245.3}{2} \times 10^{-3} \text{ m} = 6.65 \times 10^{-3} \text{ m}. \tag{4.2}$$

Being P_0 the only remaining unknown and recognizing that a realistic estimate for the force pushing the piston periodically has no straightforward means of being obtained, numerical values ranging from 10 to 10^6 N are tested using Equations (3.6) - (3.11) and

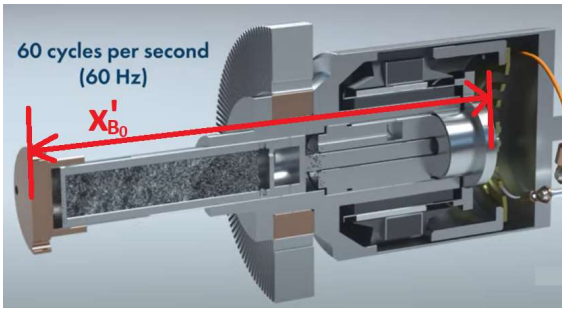

Figure 43: Minimum piston-cold tip distance

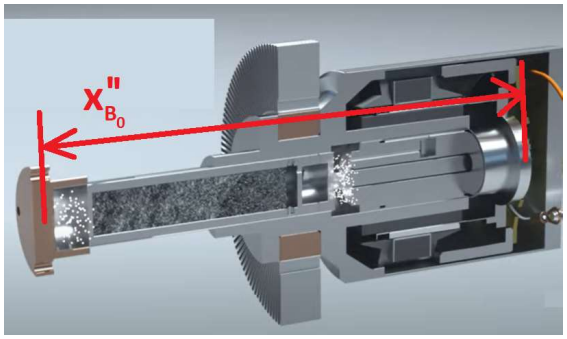

Figure 44: Maximum piston-cold tip distance

the MATLAB code developed in Chapter 3.

Figure 45 shows that the displacement curves of masses A and B start showing a more discernible sinusoid-like profile somewhere between $P_0 = 10,000$ and $P_0 = 100,000$ Newtons, making this a range of interest of this project because it makes the amplitude and frequency of motion analyses more visually clear. If the arithmetic average of these two force values is to be used as the P_0 for this project, then

$$P_0 = \frac{100,000 - 10,000}{2} = 45,000 \text{ N}.$$

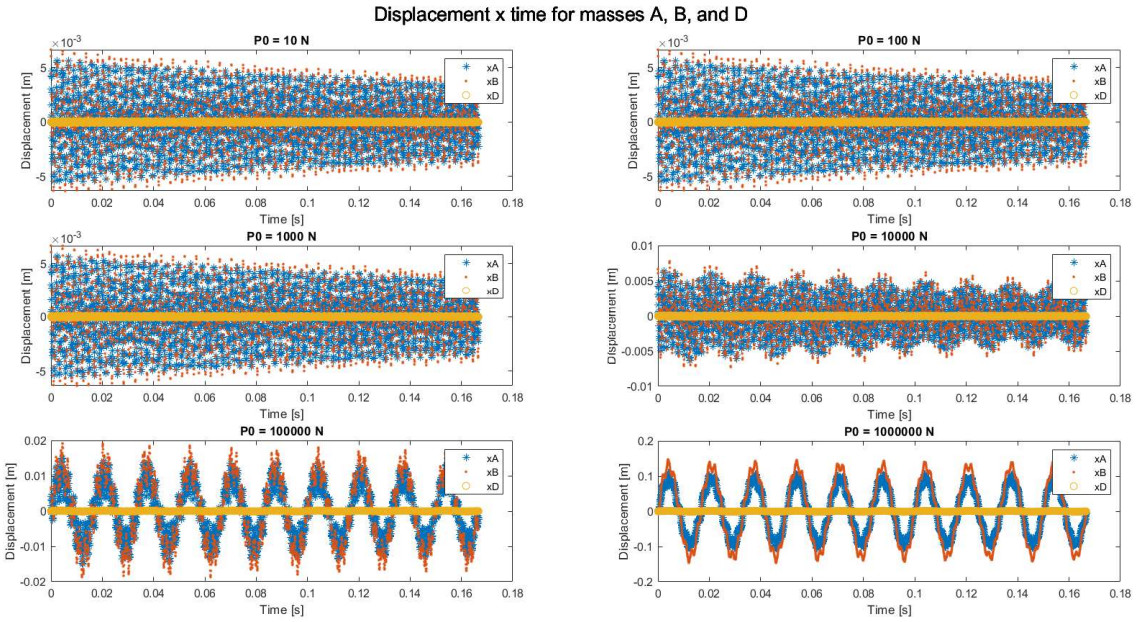

Figure 45: Displacement x time results for varying values of P_0

It is now possible to begin the multibody dynamic analysis, or Multibody Dynamics (MBD) simulation. According to Rao, springs and dampers behave similarly when placed in parallel to one another (87):

$$k_{eq} = k_1 + k_2 + k_3 + ... + k_n$$

$$c_{eq} = c_1 + c_2 + c_3 + ... + c_n$$

for n dampers and springs.

Therefore, in order to allow for a symmetrical placing of the spring-damper element given by stiffness constant k_3 and damping coefficient c_3, the single spring k_3 from the Free Body Diagram in Figure 32 will be broken up into two springs (with their respective two dampers) with half of the damping and stiffness constants. Or,

$$k_3' = 0.5k_3$$

$$k_3'' = 0.5k_3$$

$$c_3' = 0.5k_3$$

$$c_3'' = 0.5k_3,$$

resulting in the ready-for-analysis setup shown in Figure 46, with two springs with constants k_3', k_3'', c_3', and c_3''. The same exact process followed for k, c pair k_1 and c_1, where now

$$k_1' = 0.5k_1$$

$$k_1'' = 0.5k_1$$

$$c_1' = 0.5k_1$$

$$c_1'' = 0.5k_1.$$

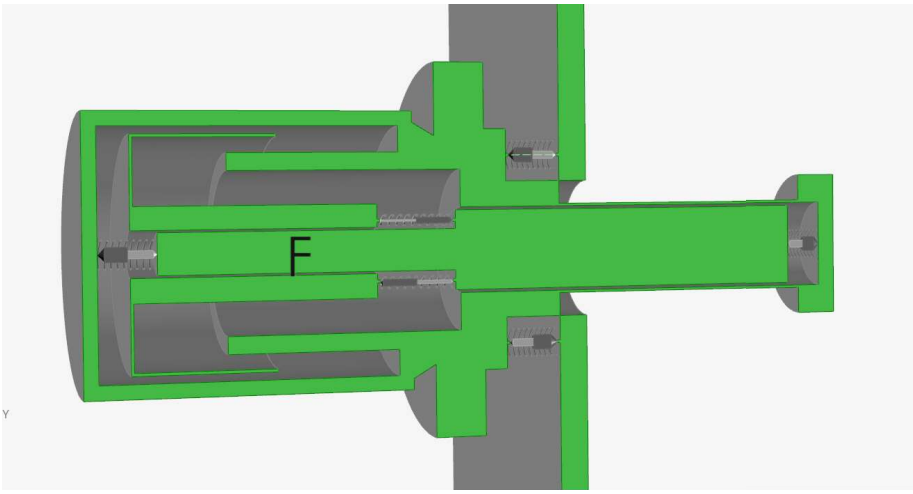

Figure 46: Cross-section layout of cryocooler mounted to GMACS' wall used in MBD

The MBD was, then, set up on MSC Adams View (Figure 47) following the configurations summarized in Table 5. The force input comparison between MATLAB and Adams View is found in Figure 48.

The results obtained from the analysis are in Figures 49 - 51 superimposed with the MATLAB results.

In order to provide a fair, accurate comparison of the MATLAB and Adams curves that disregard the noise in the results, the Fast Fourier Transform function **fft** from MATLAB was employed. The Fourier Transform is a mathematical tool that helps define any function as a combination of sinusoids, thus making its characteristics (namely amplitude and frequency) more evident and operations with it, possible. The big issue with computing Fourier Transforms was that, while Gauss analyzed the critical factorization step as

Ground element and rigid groups	
Ground element	Wall
Rigid group	None
Joints	
Outer shell and displacer	Translational
Displacer and piston	Translational
Wall and outer shell	Translational
Force	
Part	Piston
Function	$45000 * sin(376.99 * \text{time})$
Springs-dampers	
k_1'	$3.31E+06$ N/mm
c_1'	15.9 Ns/mm
k_1''	$3.31E+06$ N/mm
c_1''	15.9 Ns/mm
k_2	$5.56E+03$ N/mm
c_2	$2.72E-10$ Ns/mm
k_3'	$7.00E+03$ N/mm
c_3'	$1.37E-9$ Ns/mm
k_3''	$7.00E+03$ N/mm
c_3''	$1.37E-9$ Ns/mm
k_4	2.87 N/mm
c_4	0.005 Ns/mm
Simulation control	
End time	0.167 s
Step size	$6.1E-05$ s

Table 5: Configurations for the MBD analysis

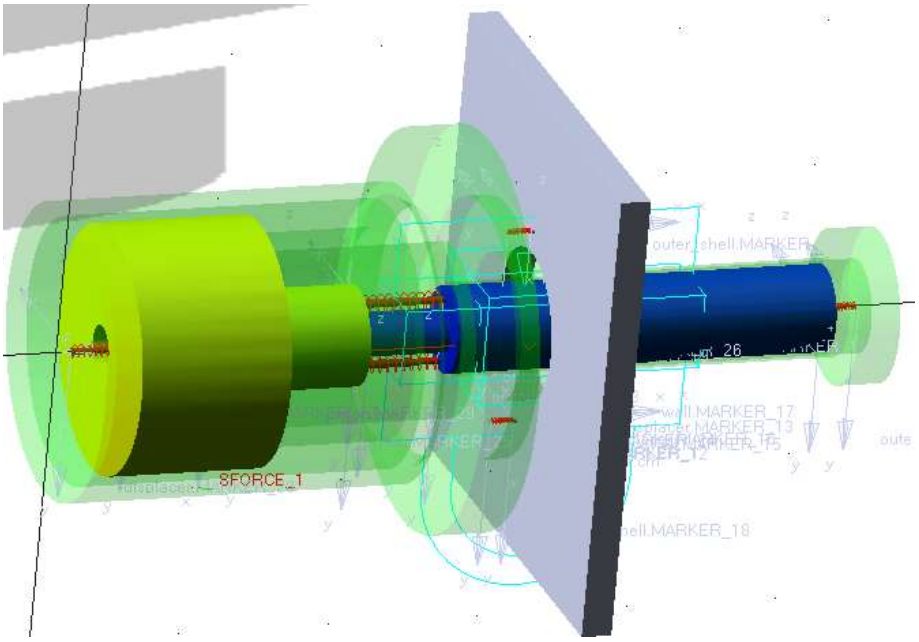

Figure 47: Setup of cryocooler system as seen in Adams View; note the outer shell is transparent to allow the visualization of the displacer (blue), piston (yellow), and springs (red)

early as 1805, FT calculations were very time consuming until Cooley and Tukey began the discussion around FFTs in the 1960s. And it was not until the 1990s that a real gain in processing speed was made possible in FFT algorithms (90) (91).

A summary of the MATLAB vs. Adams results brought about by the FFT MATLAB algorithm is presented in Table 6, where A_M corresponds to a body's MATLAB-predicted amplitude and A_A, to its Adams-simulated amplitude, and f_M and f_A, the MATLAB and Adams results regarding sinusoidal frequencies. It should be noted that the results converge as expected, meaning the 3d simulation and the mathematical model are both excellent predictors of the behavior of the cryocooler and how it affects the depth of field of the GMACS.

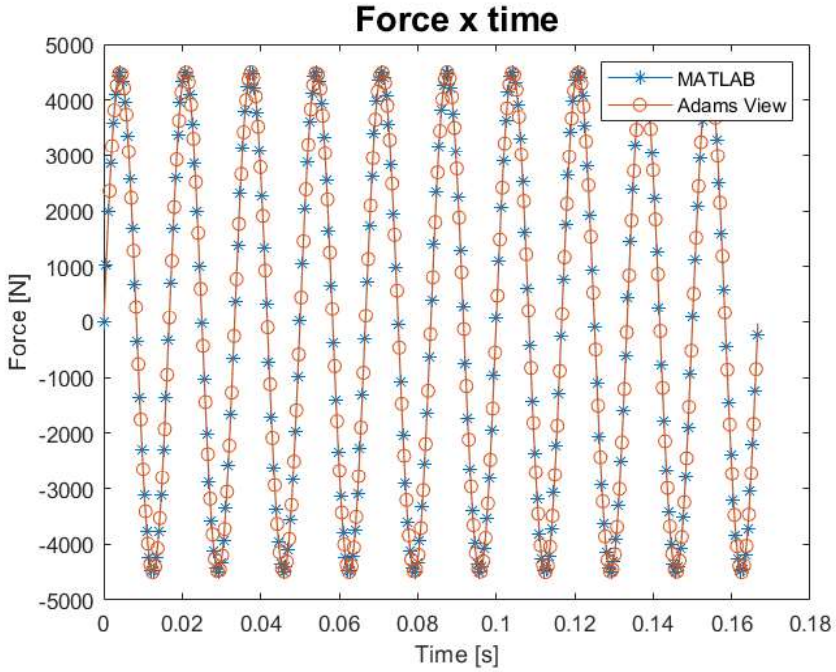

Figure 48: Force curve: MATLAB vs. Adams View

Body	Description of result	Result	Result
A	Amplitude ratio ($\frac{A_M}{A_A}$)	0.99931	$A_M \sim A_A$
	Frequency ratio ($\frac{f_M}{f_A}$)	0.99974	$f_M \sim f_A$
B	Amplitude ratio	0.99934	$A_M \sim A_A$
	Frequency ratio	0.99974	$f_M \sim f_A$
D	Amplitude ratio	0.99936	$A_M \sim A_A$
	Frequency ratio	0.99974	$f_M \sim f_A$

Table 6: MATLAB vs. Adams results, no DVA

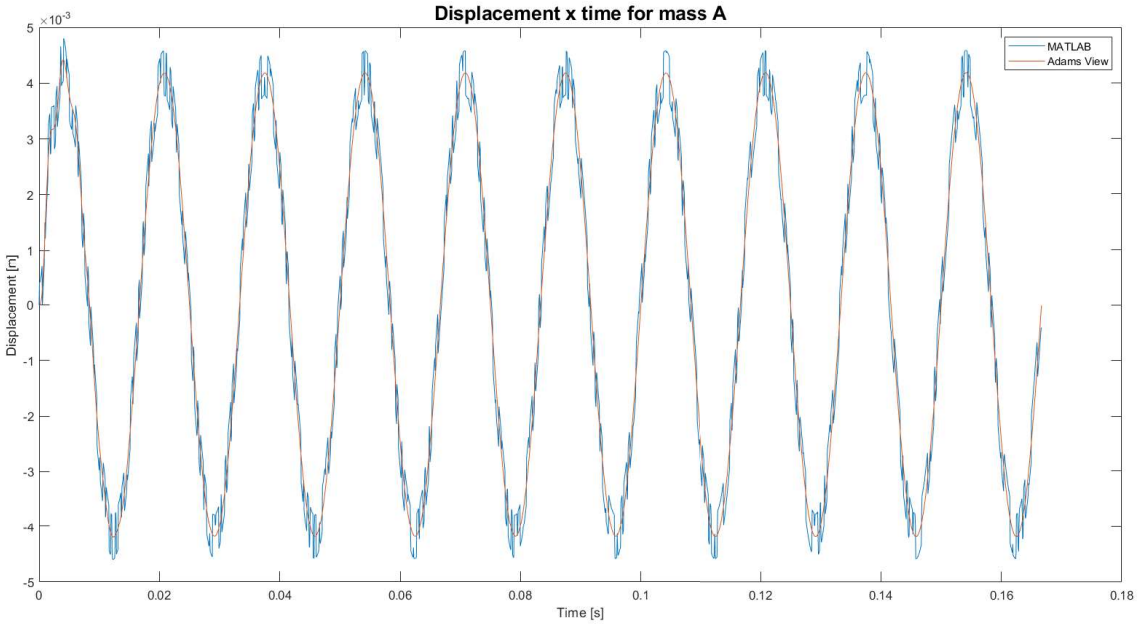

Figure 49: Displacement of mass A with no DVA, MATLAB vs. Adams View

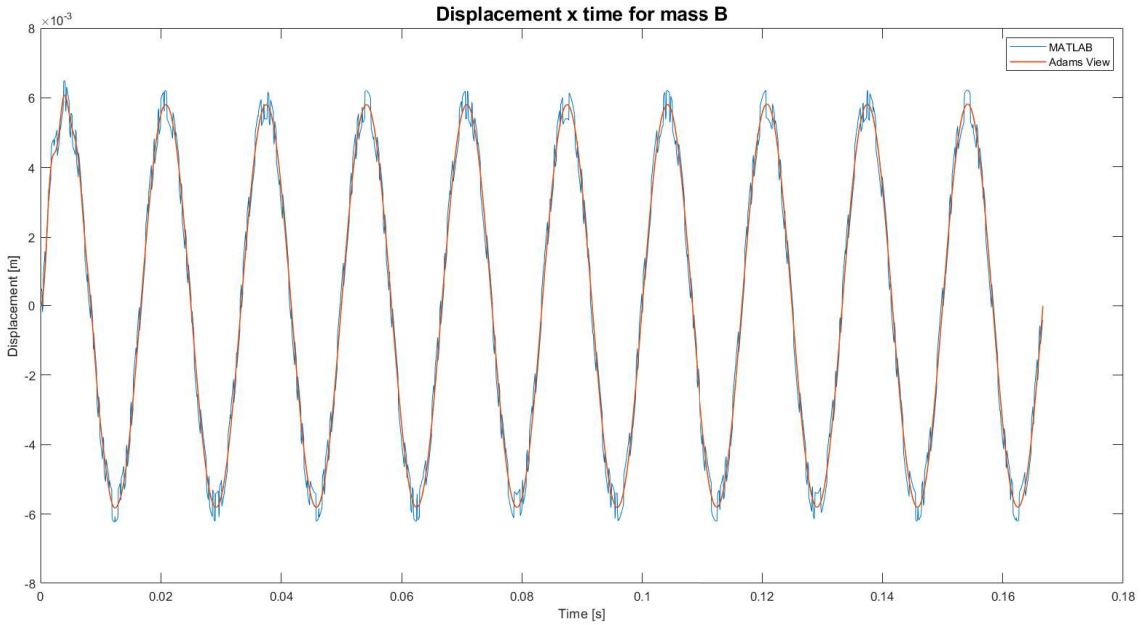

Figure 50: Displacement of mass B with no DVA, MATLAB vs. Adams View

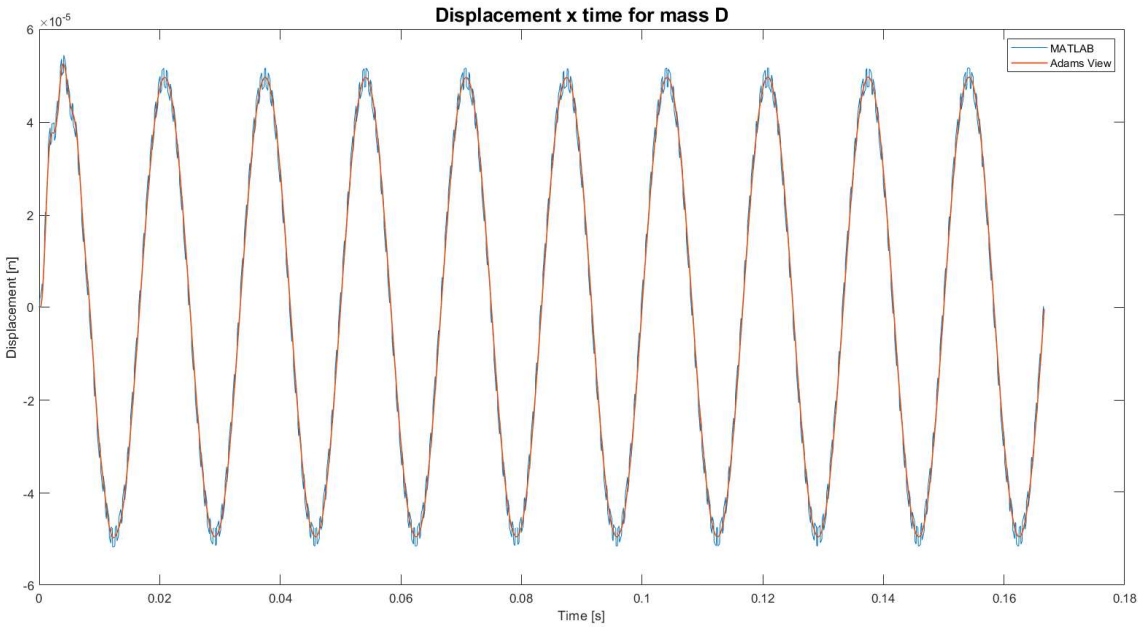

Figure 51: Displacement of mass D with no DVA, MATLAB vs. Adams View

divergence as well.

Whether the displacement seen in the MATLAB and Adams simulations for the DVA-less system is small or large, corroborating or not the necessity to develop a vibration absorber, is a topic that will be addressed in Chapter 6.

In this chapter both simulation methods were fully validated and the first real notion of how much vibration the cryocooler imposes on GMACS was obtained. Now all the elements required for the last section of the project, the minimization of these calculated vibrations through a DVA, have been put in place; the next chapter will be the culmination of the project, thus: it will show the design and simulations of a DVA in the cryocooler system.

5 DESIGNING AN OPTIMAL DVA

To conclude this project, the system shown in Figure 52 will be designed and, much like the process that was followed to obtain the parameters for the DVA-less system, approximations will be made taking in account material properties and general laws. Optimal DVA parameters have been suggested by Den Hartog and will be taken in account when examining the dynamics of this new setup (37). As per Table 3, the specific goals that will be achieved in this section are:

- The new mathematical model of the cryocooler system, this time with the addition of a simple DVA (mass "C" in Figure 52);
- The simultaneous addition of a DVA to the 3d model;
- The estimation of c_5, k_5, and m_C, the parameters for the DVA itself;

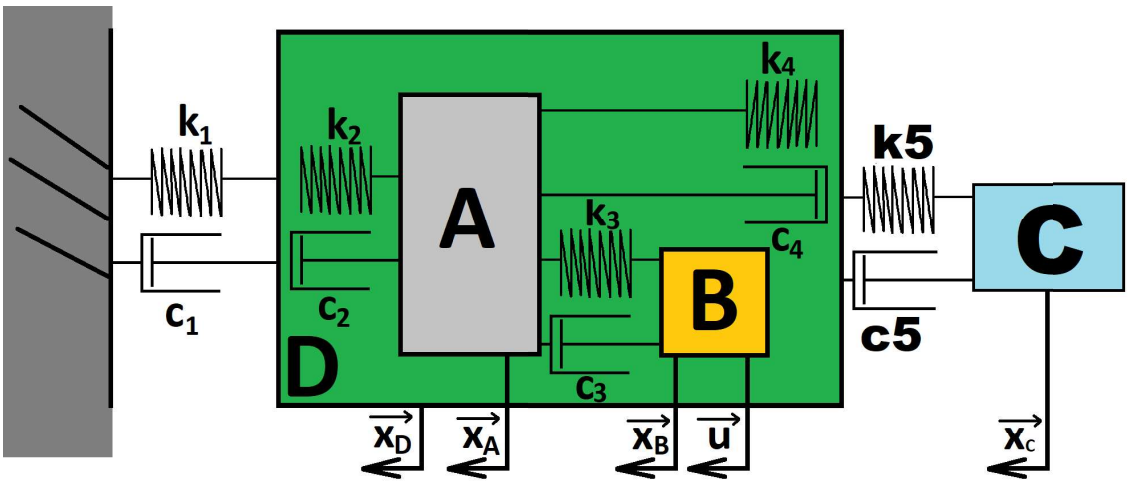

Figure 52: Free Body Diagram representing the cryocooler with the added DVA

- The plugging in of these parameters to both simulations; and finally,
- The acquisitions of results from both methods, elaboration of plots based on them, and a quick comparison of the two methods' results and of the results with and without the DVA.

In Figure 52 the spring-damper pair k_5 and c_5, together with mass C, form the Passive Balancer complex. x_C represents the motion of mass C.

The following equations can be written for the four bodies A, B, C, and D:

$$m_A\ddot{x_A} + (c_2 + c_3 + c_4)\dot{x_A} + (k_2 + k_3 + k_4)x_A - c_3\dot{x_B} - k_3x_B - (c_2 + c_4)\dot{x_D} - (k_2 + k_4)x_D = 0 \tag{5.1}$$

$$m_B\ddot{x_B} + c_3\dot{x_B} + k_3x_B - c_3\dot{x_A} - k_3x_A = u \tag{5.2}$$

$$m_C\ddot{x_C} + c_5\dot{x_C} + k_5x_C - c_5\dot{x_D} - k_5x_D = 0 \tag{5.3}$$

$$m_D\ddot{x_D} - (c_2 + c_4)\dot{x_A} - (k_2 + k_4)x_A + (c_1 + c_2 + c_4 + c_5)\dot{x_D} + (k_1 + k_2 + k_4 + k_5)x_D = 0. \tag{5.4}$$

Applying the State Space approach to Equations (5.1) - (5.4):

$$y_1 = x_A \qquad y_2 = \dot{x_A} \qquad y_3 = x_B \qquad y_4 = \dot{x_B}$$

$$y_5 = x_C \qquad y_6 = \dot{x_C} \qquad y_7 = x_D \qquad y_8 = \dot{x_D}$$

$$\dot{y_1} = y_2$$

$$\dot{y_2} = -\frac{k_2+k_3+k_4}{m_A}y_1 - \frac{c_2+c_3+c_4}{m_A}y_2 + \frac{k_3}{m_A}y_3 + \frac{c_3}{m_A}y_4 + \frac{k_2+k_4}{m_A}y_7 + \frac{c_2+c_4}{m_A}y_8$$

$$\dot{y_3} = y_4$$

$$\dot{y_4} = \frac{k_3}{m_B}y_1 + \frac{c_3}{m_B}y_2 - \frac{k_3}{m_B}y_3 - \frac{c_3}{m_B}y_4 + \frac{u}{m_B}$$

$$\dot{y_5} = y_6$$

$$\dot{y_6} = \frac{k_5}{m_C}y_7 + \frac{c_5}{m_C}y_8 - \frac{k_5}{m_C}y_5 - \frac{c_5}{m_C}y_6$$

$$\dot{y_7} = y_8$$

$$\dot{y_8} = \frac{k_2+k_4}{m_D}y_1 + \frac{c_2+c_4}{m_D}y_2 - \frac{k_1+k_2+k_4+k_5}{m_D}y_7 - \frac{c_1+c_2+c_4+c_5}{m_D}y_8$$

Yielding the State and Output equations

$$\begin{bmatrix} \dot{y_1} \\ \dot{y_2} \\ \dot{y_3} \\ \dot{y_4} \\ \dot{y_5} \\ \dot{y_6} \\ \dot{y_7} \\ \dot{y_8} \end{bmatrix} = \begin{bmatrix} 0 & 1 & 0 & 0 & 0 & 0 & 0 & 0 \\ -\frac{k_2+k_3+k_4}{m_A} & -\frac{c_2+c_3+c_4}{m_A} & \frac{k_3}{m_A} & \frac{c_3}{m_A} & 0 & 0 & \frac{k_2+k_4}{m_A} & \frac{c_2+c_4}{m_A} \\ 0 & 0 & 0 & 1 & 0 & 0 & 0 & 0 \\ \frac{k_3}{m_B} & \frac{c_3}{m_B} & -\frac{k_3}{m_B} & -\frac{c_3}{m_B} & 0 & 0 & 0 & 0 \\ 0 & 0 & 0 & 0 & 0 & 1 & 0 & 0 \\ 0 & 0 & 0 & 0 & -\frac{k_5}{m_C} & -\frac{c_5}{m_C} & \frac{k_5}{m_C} & \frac{c_5}{m_C} \\ 0 & 0 & 0 & 0 & 0 & 0 & 0 & 1 \\ \frac{k_2+k_4}{m_D} & \frac{c_2+c_4}{m_D} & 0 & 0 & 0 & 0 & -\frac{k_1+k_2+k_4+k_5}{m_D} & -\frac{c_1+c_2+c_4+c_5}{m_D} \end{bmatrix} \begin{bmatrix} y_1 \\ y_2 \\ y_3 \\ y_4 \\ y_5 \\ y_6 \\ y_7 \\ y_8 \end{bmatrix}$$

$$+ \begin{bmatrix} 0 \\ 0 \\ 0 \\ \frac{1}{m_B} \\ 0 \\ 0 \\ 0 \\ 0 \end{bmatrix} \text{u}$$

and

$$\begin{bmatrix} x_A \\ \dot{x_A} \\ x_B \\ \dot{x_B} \\ x_C \\ \dot{x_C} \\ x_D \\ \dot{x_D} \end{bmatrix} = \begin{bmatrix} 1 & 0 & 0 & 0 & 0 & 0 & 0 & 0 \\ 0 & 1 & 0 & 0 & 0 & 0 & 0 & 0 \\ 0 & 0 & 1 & 0 & 0 & 0 & 0 & 0 \\ 0 & 0 & 0 & 1 & 0 & 0 & 0 & 0 \\ 0 & 0 & 0 & 0 & 1 & 0 & 0 & 0 \\ 0 & 0 & 0 & 0 & 0 & 1 & 0 & 0 \\ 0 & 0 & 0 & 0 & 0 & 0 & 1 & 0 \\ 0 & 0 & 0 & 0 & 0 & 0 & 0 & 1 \end{bmatrix} \begin{bmatrix} y_1 \\ y_2 \\ y_3 \\ y_4 \\ y_5 \\ y_6 \\ y_7 \\ y_8 \end{bmatrix}$$

,

or

$$\dot{x} = Ax + Bu \tag{5.5}$$

$$y = Cx + Du \tag{5.6}$$

where

$$A = \begin{bmatrix} 0 & 1 & 0 & 0 & 0 & 0 & 0 & 0 \\ -\frac{k_2+k_3+k_4}{m_A} & -\frac{c_2+c_3+c_4}{m_A} & \frac{k_3}{m_A} & \frac{c_3}{m_A} & 0 & 0 & \frac{k_2+k_4}{m_A} & \frac{c_2+c_4}{m_A} \\ 0 & 0 & 0 & 1 & 0 & 0 & 0 & 0 \\ \frac{k_3}{m_B} & \frac{c_3}{m_B} & -\frac{k_3}{m_B} & -\frac{c_3}{m_B} & 0 & 0 & 0 & 0 \\ 0 & 0 & 0 & 0 & 0 & 1 & 0 & 0 \\ 0 & 0 & 0 & 0 & -\frac{k_5}{m_C} & -\frac{c_5}{m_C} & \frac{k_5}{m_C} & \frac{c_5}{m_C} \\ 0 & 0 & 0 & 0 & 0 & 0 & 0 & 1 \\ \frac{k_2+k_4}{m_D} & \frac{c_2+c_4}{m_D} & 0 & 0 & 0 & 0 & -\frac{k_1+k_2+k_4+k_5}{m_D} & -\frac{c_1+c_2+c_4+c_5}{m_D} \end{bmatrix}, \tag{5.7}$$

$$B = \begin{bmatrix} 0 \\ 0 \\ 0 \\ \frac{1}{m_B} \\ 0 \\ 0 \\ 0 \\ 0 \end{bmatrix}, \tag{5.8}$$

$$C = \begin{bmatrix} 1 & 0 & 0 & 0 & 0 & 0 & 0 & 0 \\ 0 & 1 & 0 & 0 & 0 & 0 & 0 & 0 \\ 0 & 0 & 1 & 0 & 0 & 0 & 0 & 0 \\ 0 & 0 & 0 & 1 & 0 & 0 & 0 & 0 \\ 0 & 0 & 0 & 0 & 1 & 0 & 0 & 0 \\ 0 & 0 & 0 & 0 & 0 & 1 & 0 & 0 \\ 0 & 0 & 0 & 0 & 0 & 0 & 1 & 0 \\ 0 & 0 & 0 & 0 & 0 & 0 & 0 & 1 \end{bmatrix}, \text{ and} \tag{5.9}$$

$$D = 0. \tag{5.10}$$

The behavior of the system without the DVA is already known and has been studied previously, but now a new mass, spring, and damper have to be taken in account. Optimal relations relating m_C, c_5, and k_5 to the other parameters are given by Den Hartog in "Mechanical Vibrations" and by Kordi and Alamatian in their DVA study (37) (92).

According to Farid Kordi and Javad Alamatian from the Islamic Azad University, the optimal parameters for a simple DVA are

$$k_2 = \frac{k_1\mu(1-\mu)}{(1+\mu)^2} \tag{5.11}$$

$$\zeta = \frac{\sqrt{\mu}}{1-\mu} \tag{5.12}$$

where k_2 is the stiffness constant of the spring directly connected to the secondary mass (in the case of this project, k_5), k_1 is the stiffness constant connecting a grounded element to the primary mass (in this project, k_1), and

$$\mu = \frac{m_C}{m_D}$$
$$\zeta = \frac{c}{c_c}$$
$$c_c = 2\sqrt{km},$$

making

$$k_5 = \frac{k_1\mu(1-\mu)}{(1+\mu)^2} \tag{5.13}$$

$$c_5 = 2\frac{\sqrt{\mu}}{1-\mu}\sqrt{k_5 m_C}. \tag{5.14}$$

In order to determine the final missing parameter, m_C, a number of iterations will be ran to analyze the practical effect that changing μ has on the displacement of the mass of interest, the outer shell m_D. This section will focus on minimizing x_D, thus all analyses including the new DVA mass C will focus on understanding the DVA's effect on the displacement of D.

Iterating μ provides the plots in Figures 53 and 54. Since it is now of this project's interest to know which μ provides the lowest amplitude of motion for body D, naturally the prime method for calculating these displacement values will be the same Fast Fourier Transform used to compare the amplitudes and frequencies in Section 4. Running **fft**

on MATLAB for each of the curves in Figures 53 and 54 provides the results in Figure 55 — where the μ that provides the lowest amplitude of motion is highlighted. Figure 56 contrasts the displacement curve for the outer shell when μ provides the maximum amplitude of motion and when it provides minimum amplitude of motion.

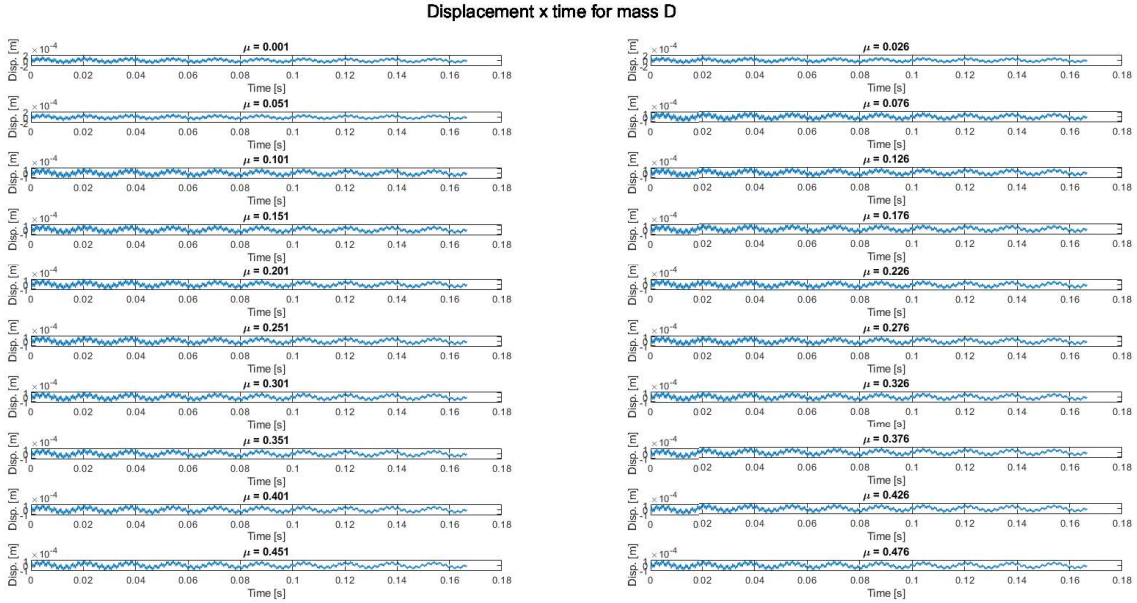

Figure 53: Displacement of mass D when μ varies between 0.001 and 0.476

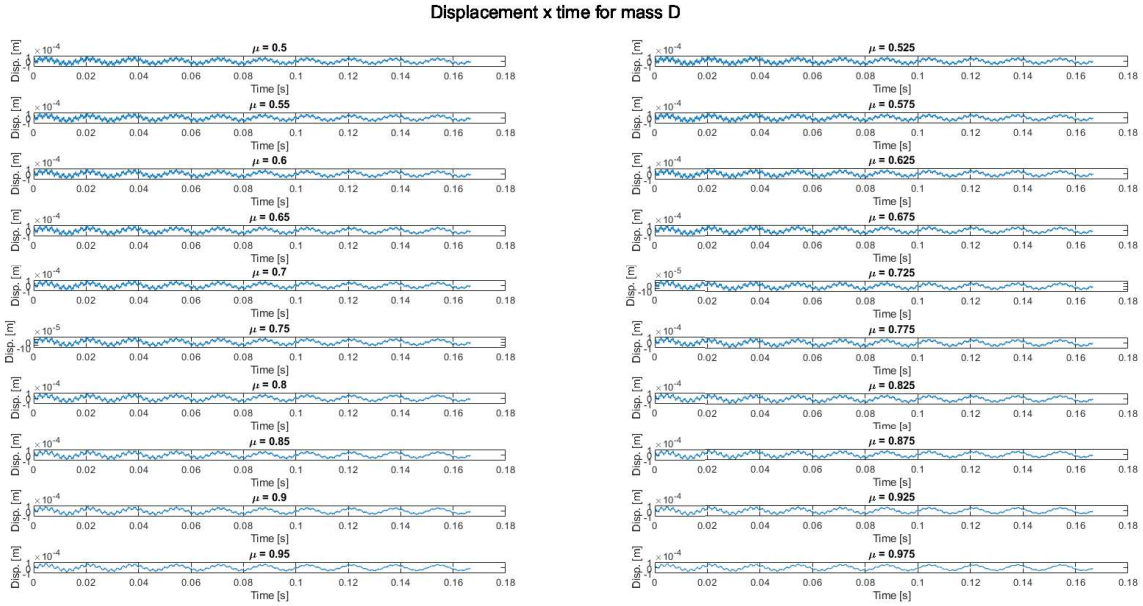

Figure 54: Displacement of mass D when μ varies between 0.500 and 0.975

The optimal μ according to FFT is 0.326. The displacement of x_D is plotted without

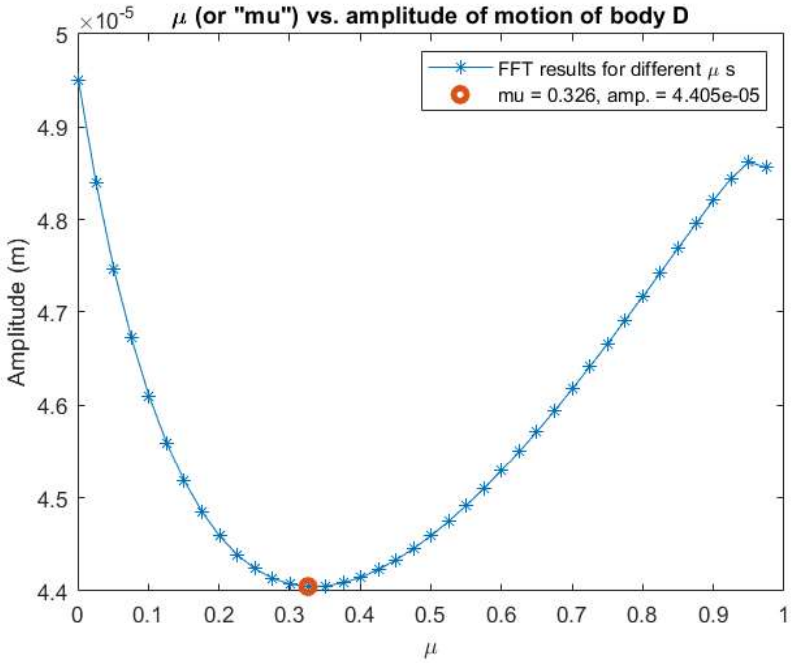

Figure 55: μ vs. amplitude for the tested values of μ

the addition of the DVA, then with a DVA with $\mu = 0.326$ in Figure 57.

The μ, amplitude pair that minimizes displacement is, hence,

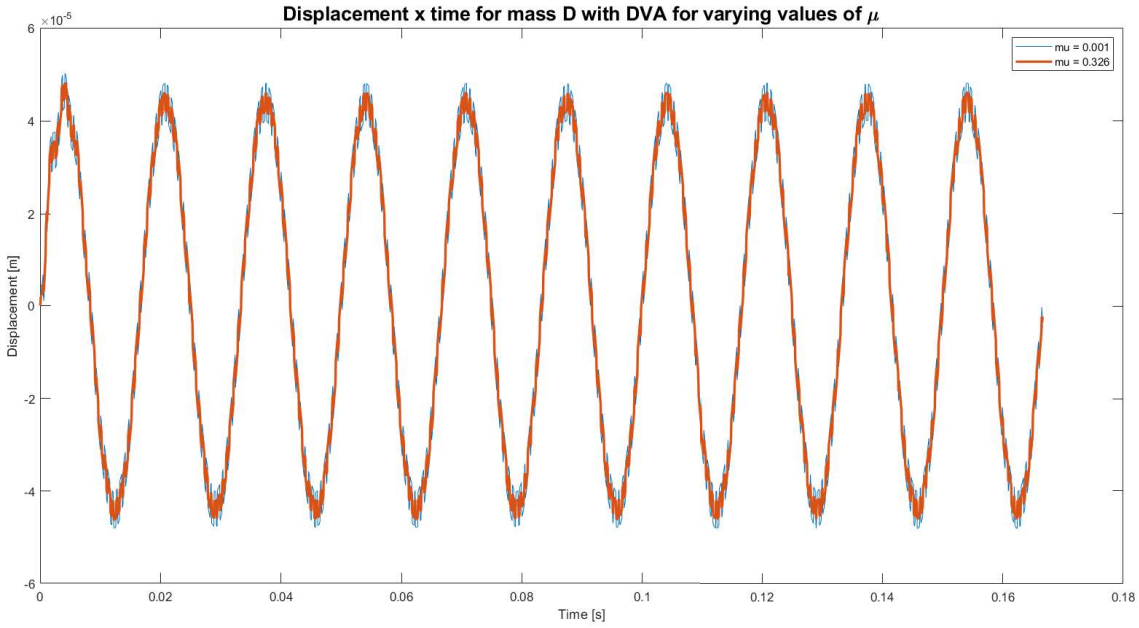

Figure 56: Displacement of mass D when amplitude is maximum ($\mu = 0.001$) and minimum ($\mu = 0.326$)

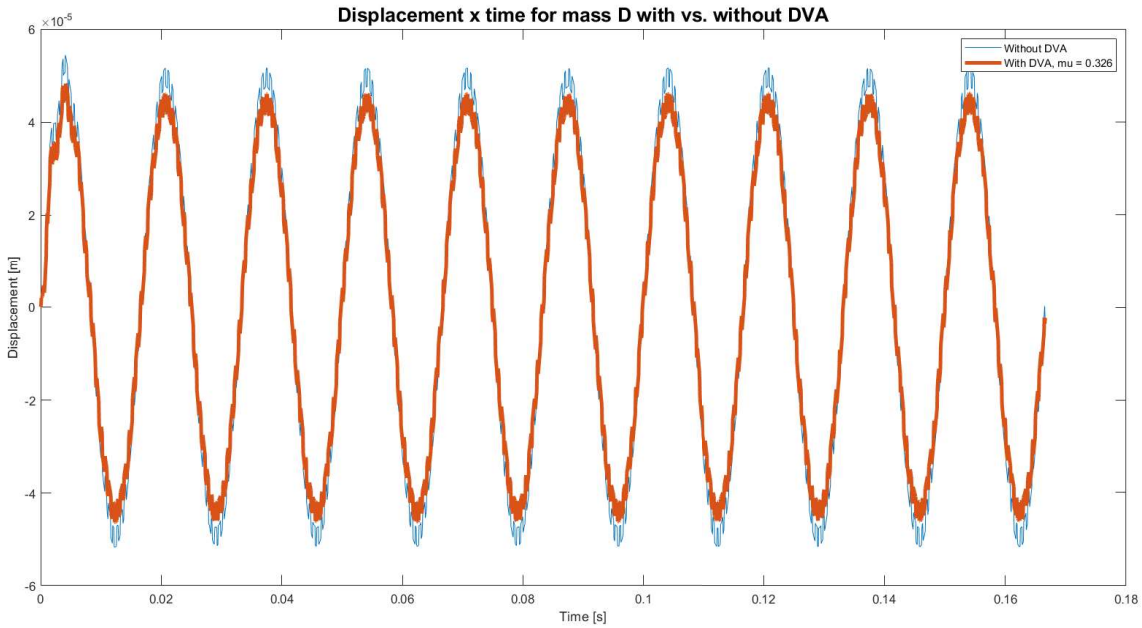

Figure 57: Displacement of mass D obtained through MATLAB simulation without the DVA vs. with the DVA

$$\mu = 0.326$$

$$Amplitude = 4.40 \times 10^{-5} \text{ m}.$$

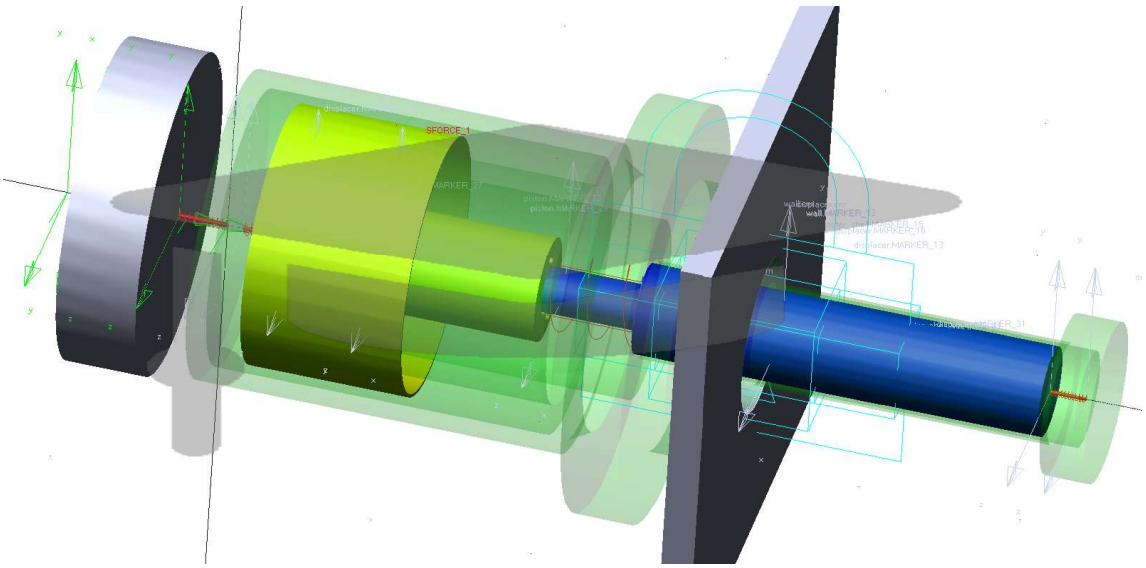

Figure 58: Adams View setup with the DVA

Joints	
DVA and outer shell	Translational
Springs-dampers	
k_5	$1.16E+08$ N/mm
c_5	$2.28E+01$ Ns/mm

Table 7: Additional configurations for the MBD analysis with DVA

Now, finally, all three parameters that will be used in this section to run the analyses on MATLAB and Adams View can be calculated:

$$m_C = 0.326 \times 4.80253 = 1.56 \text{ kg} \tag{5.15}$$

$$k_5 = \frac{6.61 \times 10^9 \times 0.326(1-0.326)}{(1+0.326)^2} = 8.26 \times 10^8 \text{ N/m} \tag{5.16}$$

$$c_5 = 2\frac{\sqrt{0.326}}{1-0.326}\sqrt{8.26 \times 10^8 \times 1.56} = 6.08 \times 10^4 \text{ Ns/m}. \tag{5.17}$$

Now the last task remaining in this project is to simulate the DVA in the 3d model using Adams View. The Adams setup including the DVA is seen in Figure 58; besides the simulation settings in Table 5, the configurations in Table 7 were added. Figures 59,

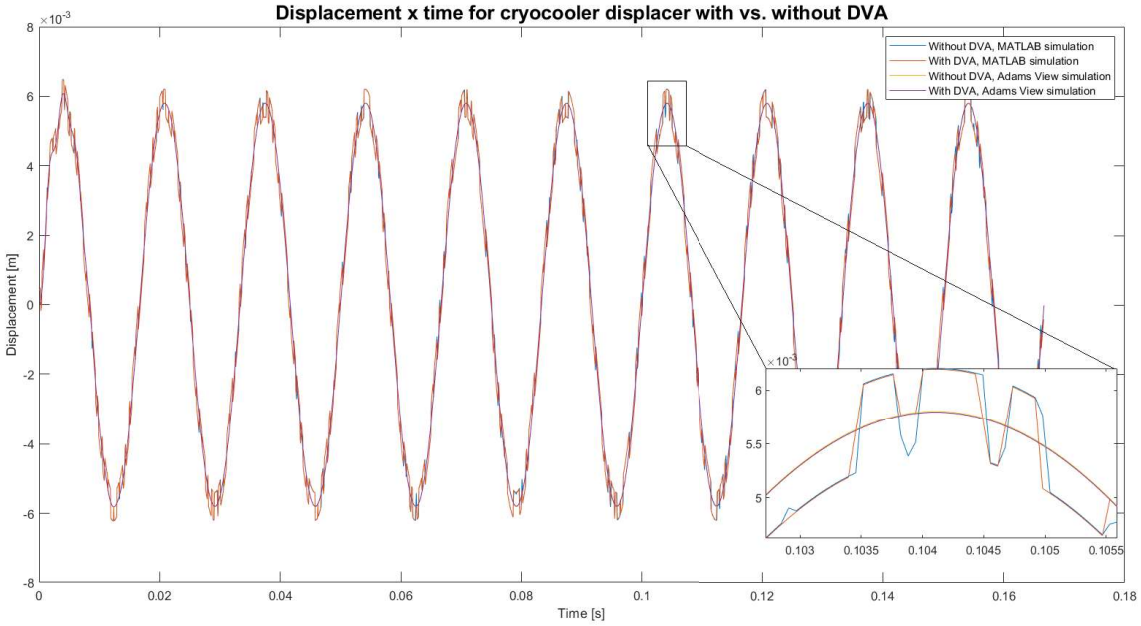

Figure 59: The displacement of the cryocooler's displacer as simulated in MATLAB and Adams View, with and without the designed DVA

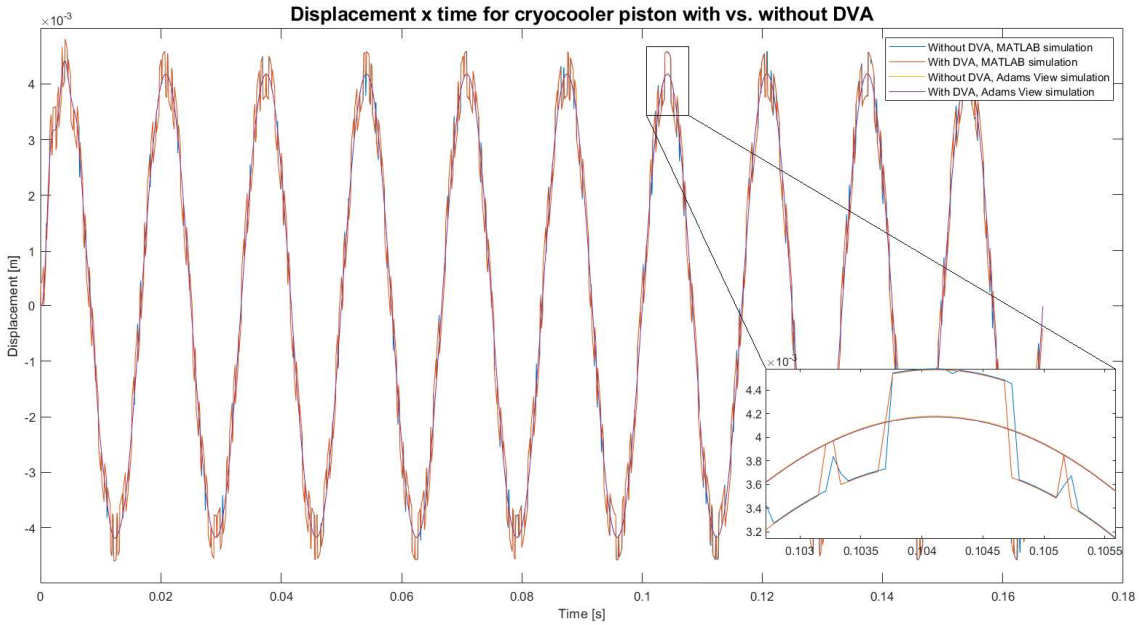

Figure 60: The displacement of the cryocooler's piston as simulated in MATLAB and Adams View, with and without the designed DVA

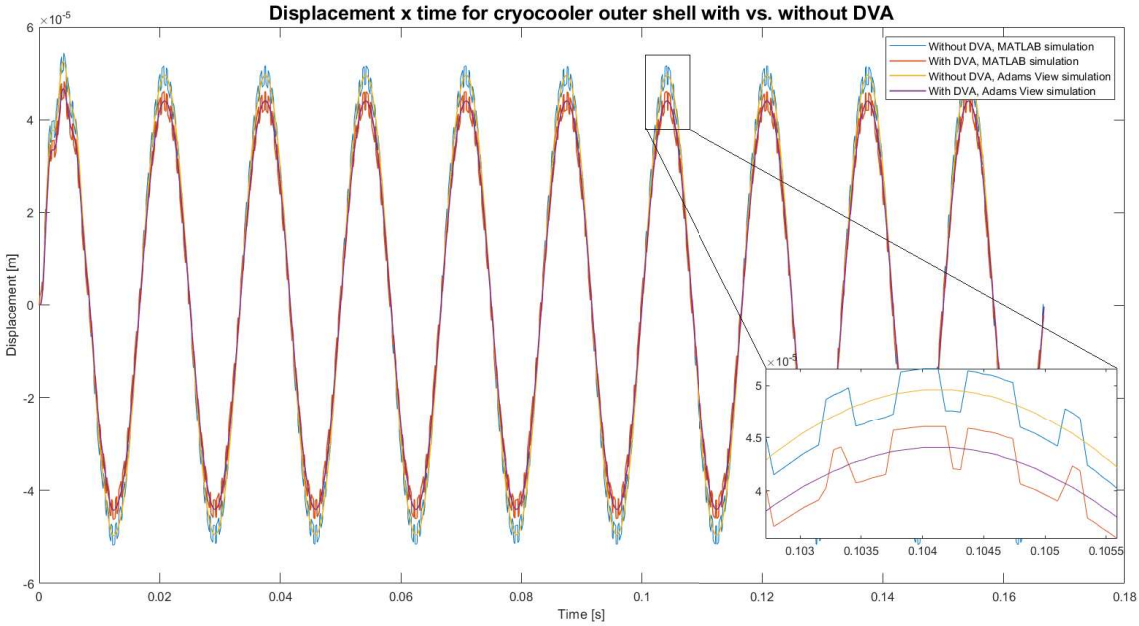

Figure 61: The displacement of the cryocooler's outer shell as simulated in MATLAB and Adams View, with and without the designed DVA

60, and 61 can be considered the most important plots in this project, as they summarize all of the main results obtained in this project and all the work performed in Chapters 3-5. They illustrate the displacements of the three moving bodies of interest in the cryocooler

system with and without the presence of the Dynamic Vibration Absorber, and obtained through the MultiBody Dynamic and the mathematical analyses. Finally, Table 8 presents the results obtained from all the analyses in this Section, and will be discussed in depth in Section 6. It should be noted that the amplitude reduction designed in this project had body D, the outer shell of the cryocooler, as its main focus, hence why the results in Table 8 are significantly better for the outer shell.

Body	Description of result	Result
A	DVA amplitude reduction, MATLAB simulation	0.13%
	DVA amplitude reduction, Adams View simulation	0.17%
B	DVA amplitude reduction, MATLAB simulation	0.09%
	DVA amplitude reduction, Adams View simulation	0.15%
D	DVA amplitude reduction, MATLAB simulation	11.12%
	DVA amplitude reduction, Adams View simulation	11.16%

Table 8: Reduction of amplitude of vibration of the cryocooler with vs. without the DVA: results table

Lastly, to analyze if Ametek chose a nominal frequency of vibration for the cryocooler that minimizes the displacement of the outer shell and maximizes spectral stability, a spectral analysis was plotted in Figure 62. It can be seen that there is an increasing

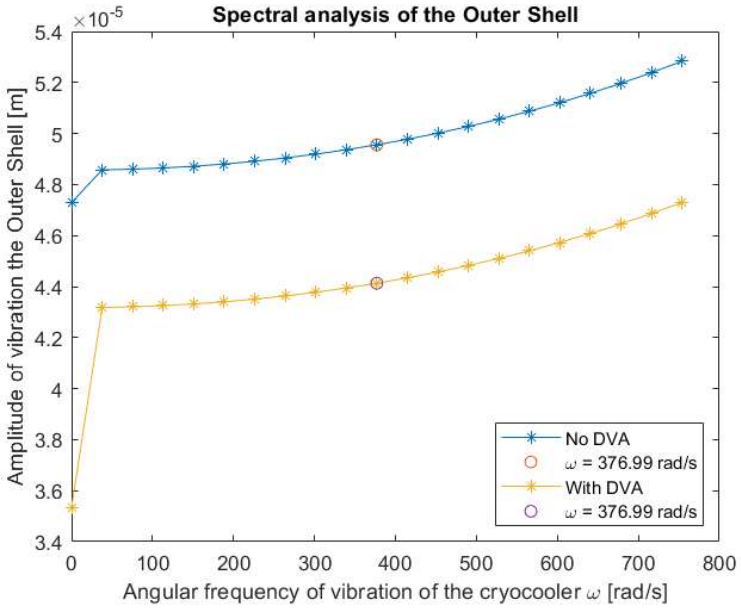

Figure 62: The frequency of vibration of the cryocooler versus the amplitude of motion of the outer shell (obtained through FFT)

trend in both the DVA and the no DVA curve, meaning any frequency lower than the nominal $\omega = 376.99$ rad/s would have been preferable for the purpose of improving spectral stability. However, ω is a project constant which cannot be modified.

In this chapter the last few tasks within the planned methodology were completed: the mathematical simulation and the MBD simulation, which had both been validated in Chapter 4, were repeated but considering the addition of the DVA, or mass "C" — which was designed based on researched evidence aimed at optimizing parameters for an ideal DVA. Figure 61 and Table 8 prove that there is noticeable reduction in the amplitude of vibration in the simulations; the next chapter will focus on deciphering whether this reduction is enough to ensure the desired standard of quality of astronomical observations for GMACS.

6 DISCUSSION AND CONCLUSIONS

"One man's 'magic' is another man's engineering. 'Supernatural' is a null word."

-- Robert Heinlein

All of the methodology of this project has been conducted and now enough data has been obtained for results to be analyzed and conclusions to be drawn, wrapping up this project and this document.

In Chapter 4 the Fast Fourier Transform was employed to find the amplitude of the displacement obtained through the MATLAB code (mathematical model) and through Adams View (3d model). Table 2 established the Maximum Allowable Axial Displacement (MAAD) for GMACS in two different orientations, being the x-axis orientation the actual positioning used in GMACS and the z-axis orientation being presented only as a study case. These values are compiled in Table 9.

		Body	2× **Amplitude** (μm)	**MAAD** (μm)
No DVA	MATLAB	Displacer	8,352.22	46.6 μm (depth of focus)
		Piston	11,597.08	
		Outer shell	99.12	
	Adams View	Displacer	8,357.98	34.62 μm (spectral stability, requirement)
		Piston	11,604.78	
		Outer shell	99.18	
With DVA	MATLAB	Displacer	8,341.36	
		Piston	11,586.42	
		Outer shell	88.10	
	Adams View	Displacer	8,343.76	11.54 μm (spectral stability, goal)
		Piston	11,586.94	
		Outer shell	88.12	

Table 9: Displacement results vs. Maximum Allowable Axial Displacement

It is noticeable by comparing the MATLAB and Adams View curves in Fig. 61 that they present different profiles, the analytical results being a lot more sinuous. While the

difference is small enough to have been considered negligible for the purpose of this project, it is worth mentioning that these differences are believed to be due to the difference in methodology when acquiring both sets of results: Adams View is a commercial, ready-for-use software which possesses a lot more built-in constraints than the proprietary, written-from-scratch MATLAB code. A major assumption that was made — and undoubtedly assisted in propagating error — was that the cryocooler system can be described as a mass-spring-damper system. Besides, the properties of the resistance to motion presented by the Helium chambers were considered to be unaffected by the change of temperature.

Though not within the scope of this project, the assembly of the DVA to the cryocooler can be assumed to occur via soldering in real life, so that the high frequency motions can be comfortably supported.

In this project the amplitude of interest is that of the outer shell, x_D, because the outer shell is the component of the cryocooler that is in direct contact with GMACS' wall and has the potential to rock it back and forth as it vibrates. In Table 9 the amplitude results are not provided directly but the value of two times these amplitudes is considered; the explanation for this is that the GMACS optics team expressed during the preparation of this project that the peak-to-peak amplitude of vibration is actually the parameter restricted by MAAD, not the simple sinusoid amplitude. In the real-world application of the cryocooler, the backwards motion (directed away from the GMACS wall to which the cooler is attached) is as undesirable as the forward motion, since both are displacements of the optical system from its original position at $t = 0$. Therefore, the peak-to-peak amplitude, which is equal to twice the size of the amplitude calculated through the Fast Fourier Transform, is the parameter that should be compared to MAAD, as is showed in Table 9.

To properly analyze if the peak-to-peak amplitude of motion of the outer shell has met the MAAD restrictions, the results will be broken into segments related to the axes of motion. Figure 63 shows a summary of the results for the outer shell.

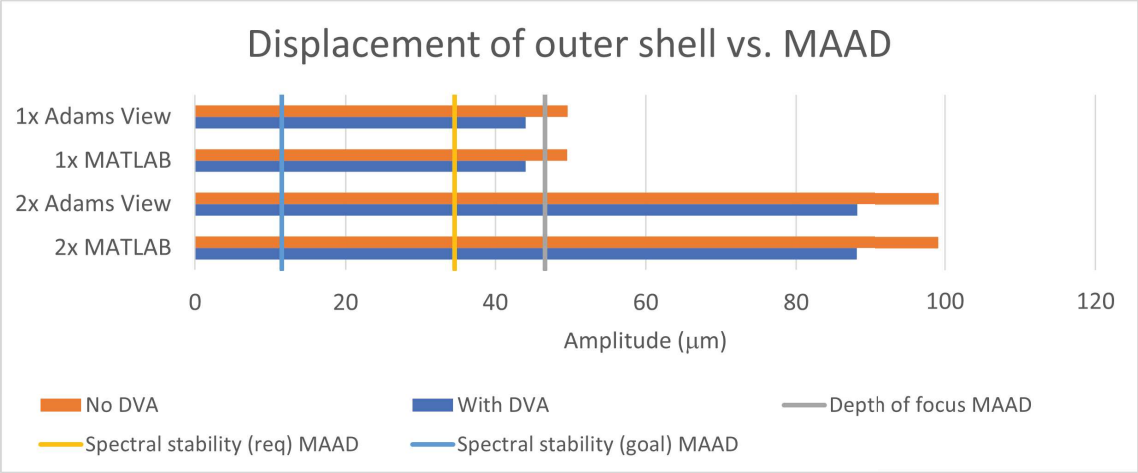

Figure 63: Displacement of the outer shell vs. MAAD

6.1 Along the z-axis

The z-axis was presented in Chapter 1 as a case study to be analyzed as a point of comparison with the real-world x-axis cryocooler displacements. As seen in Figure 63, the consequences of positioning the cryocooler to vibrate along the z-axis would indeed cause significant difference in the vibration analysis of this project.

The peak-to-peak amplitude of the outer shell without a DVA is in the 99.12 - 99.18 μm range, being reduced to the 88.10 - 88.12 μm range when the DVA is added. Since the depth of focus MAAD is a mere 46.6 μm, this reduction does not allow the DVA to be used to clear the limit established; however, were the direct amplitude to be considered, an interesting phenomenon occurs: the addition of the DVA manages to clear the MAAD by a margin of 5.47 %. This is but a speculative scenario, but it is encouraging for future research nonetheless. Should this research keep going past the presentation of this dissertation, ways to lower the dependence of this vibration study on the peak-to-peak amplitude and increase the correlation to the direct amplitude could well improve the efficacy of the already established DVA design. The orientation of the cryocooler could also be discussed, since the depth of focus MAAD is more permissive than the spectral stability MAAD. As the research concerning vibration attenuation for the GMACS stands today, the DVA designed in this project would sufficiently absorb vibration that is not

peak-to-peak and is oriented along the z-axis. Any effort to accommodate these changes in orientation and placement would be of high value to GMT's engineering.

6.2 Along the x-axis

As has been stated before, the actual positioning of the cryocooler within GMACS is that of Figures 11 and 12, in the x-axis, and the MAAD of interest of this project is related to spectral stability. That makes the goal (best case scenario) of the engineers and optics team of GMT to reach a maximum 11.54 μm in the vibration amplitude of the outer shell, with a more lenient 34.62 μm limit set as an absolute requirement. The result obtained with no DVA is a peak-to-valley amplitude range of 99.12 - 99.18 μm, which is well above both the requirement and the goal. The addition of the DVA does decrease the peak-to-valley amplitude to 88.10 - 88.12 μm, but that is not enough to clear the MAAD.

Were the direct amplitude of motion to be considered rather than the peak-to-peak amplitude, the requirement would almost be reached, since the addition of the DVA drops the direct amplitude of the outer shell to the 44.05 - 44.06 μm range, 27.24 % away from the 34.62 μm requirement.

These results suggest that this research in vibration attenuation for the Sunpower Cryotel® GT 16W Cryocooler ought to continue as there are still more sophisticated DVA technologies which were not within the scope of this project to apply but will certainly will bring the peak-to-peak outer shell vibrations closer to the requirement and goal MAAD. Furthermore, means for reducing the effect of the backwards motion of the cryocooler in the spectral stability should also be looked into further, since it would be preferable to work with the direct amplitude of motion as opposed to the peak-to-peak amplitude.

The objective set in Chapter 2 was met. In this project the principles of vibration were studied, then the specific case of vibrations caused by the cryocooler within the GMACS structure of the Giant Magellan Telescope was analyzed, and a methodology for designing a Dynamic Vibration Absorber was set up. This proposed methodology combined two

different technologies, 3d and mathematical modeling, which were both validated and presented converging results, proving the methodology accurate. The addition of a simple DVA proved successful as it reduced the amplitude of motion of the cryocooler's outer shell over 11%, even if the limits for allowable vibration by the GMT engineering and optics teams were not reached yet.

There is still much room for improvement in the DVA design. This project was an introduction to solving an issue that is currently faced by the GMT researchers but can also be useful for a plethora of engineers with concerns about vibration absorption.

REFERENCES

1 NASA. Dark energy, dark matter. Disponível em: ⟨https://science.nasa.gov/astrophysics/focus-areas/what-is-dark-energy⟩.

2 PETERSON, B. quasar. Encyclopedia Britannica, 2022. Disponível em: ⟨https://www.britannica.com/science/quasar\#ref1095692⟩.

3 CROCKETT, C. What do redshifts tell astronomers? 2001. Disponível em: ⟨https://earthsky.org/astronomy-essentials/what-is-a-redshift/⟩.

4 CAIN, F. How do we know the universe is flat? discovering the topology of the universe. 2017. Disponível em: ⟨https://phys.org/news/2017-06-universe-flat-topology.html⟩.

5 WOLCHOVER, N. What shape is the universe? a new study suggests we've got it all wrong. Quanta Magazine, 2019. Disponível em: ⟨https://www.quantamagazine.org/what-shape-is-the-universe-closed-or-flat-20191104/⟩.

6 JABR, F. How does a spectrograph work? [infographic]. Scientific American, December 2012. Disponível em: ⟨https://www.scientificamerican.com/article/ancient-stars-how-does-spectrograph-work/⟩.

7 CARLBERG, R. G. An overview of extremely large telescopes projects. Cambridge University Press, May 2006. Disponível em: ⟨https://doi.org/10.1017/S1743921306000238⟩.

8 STEIDEL, C. et al. Spectroscopic confirmation of a population of normal star-forming galaxies at redshifts $z > 3$. v. 462, n. 1, February 1996. Disponível em: ⟨https://doi.org/10.1086/310029⟩.

9 ESO. *News and Multimedia*. Disponível em: ⟨https://elt.eso.org/media/⟩.

10 LISKE, J. et al. Cosmic dynamics in the era of extremely large telescopes. Monthly Notices of the Royal Astronomical Society, v. 386, p. 1192–1218, May 2008. Disponível em: ⟨https://doi.org/10.1111/j.1365-2966.2008.13090.x⟩.

11 DARK Energy: Just Breaking the Surface. Hobby-Eberly Telescope Dark Energy Experiment. Disponível em: ⟨https://hetdex.org/dark_energy.html⟩.

12 GMT. *The Giant Magellan Telescope*. Disponível em: ⟨https://www.gmto.org/overview/⟩.

13 TMT. *Thirty Meter Telescope: Astronomy's Next-Generation Observatory*. Disponível em: ⟨tmt.org⟩.

14 ELT. *Telescope Overview*. Disponível em: ⟨https://elt.eso.org/telescope/⟩.

15 CARTER, J. One of the world's largest telescopes is underway. get to know the giant magellan telescope. Forbes, October 2019. Disponível em: ⟨https://www.forbes.com/sites/jamiecartereurope/2019/10/30/the-worlds-largest-telescope-is-underway-all-you-need-to-know-about-the-giant-magellan-\\telescope/?sh=4fcf4ad65d6a⟩.

16 HARVARD-CFA. The giant magellan telescope will revolutionize our view and understanding of the universe. SciTech Daily, January 2021. Disponível em: ⟨https://scitechdaily.com/the-giant-magellan-telescope-will-revolutionize-our-view-and-understanding-of-the-universe/⟩.

17 GMT. *GMT Science Book*. 2018. Disponível em: ⟨https://www.gmto.org/wp-content/uploads/GMTScienceBook2018.pdf⟩.

18 GMT. *Science Instruments*. Disponível em: ⟨https://www.gmto.org/resources/⟩.

19 GMT. *Engineering the Giant Magellan Telescope*. Disponível em: ⟨https://www.gmto.org/wp-content/uploads/GMT_Engineering.pdf⟩.

20 MARQUARDT, F.; GIRVIN, S. M. Optomechanics. American Physical Society, May 2009. Disponível em: ⟨https://physics.aps.org/articles/v2/40?referer=rss⟩.

21 JR., P. Y. Optomechanical design in five easy lessons. February 2004. Disponível em: ⟨https://spie.org/news/optomechanical-design-in-five-easy-lessons⟩.

22 PROCHASKA, T. et al. Optomechanical design concept for the giant magellan telescope multiobject astronomical and cosmological spectrograph (gmacs). August 2016. Disponível em: ⟨https://doi.org/10.1117/12.2233530⟩.

23 RIBEIRO, R. Video call. 2021.

24 NETO, A. B. Video call. 2021.

25 TYNAN, K. C. What is a cryocooler? About Mechanics, 2022. Disponível em: ⟨https://www.aboutmechanics.com/what-is-a-cryocooler.htm\#:~:text=A\\%20cryostat\\%20is\\%20used\\%20to,environmental\\%20conditions\\%20that\\%20already\\%20exist.⟩

26 SCOWEN, P.; MAUSKOP, P.; BUTLER, N. Gmacs cooling system trade. June 2019.

27 SUNPOWER. *Sunpower Cryotel® GT 16W Cryocooler Datasheet*. [S.l.]. Disponível em: ⟨https://www.sunpowerinc.com/-/media/project/ameteksxa/sunpower/ameteksunpower/productdocuments/cryotel-gt-datasheet.pdf?la=en&revision=b056b237-621c-4163-ae2d-8a0cb40f6887&hash=B2412117AB0816B4C2BC227AC82D0545⟩.

28 SUNPOWER. *How Does a Sunpower Stirling Cryocooler Work? Sunpower Free-Piston Stirling Cryocooler Animation*. 2020. Disponível em: ⟨https://www.youtube.com/watch?v=ZSJFPb8030g⟩.

29 JAKOB, M. *Heat Transfer II*. 2. ed. [S.l.]: John Wiley Sons Inc., 1957. ISBN 047143857X.

30 MORAN, M. J. et al. *Fundamentals of Engineering Thermodynamics*. 7. ed. [S.l.]: John Wiley Sons Inc., 2011. ISBN 13 978-0470-49590-2.

31 MENNITI, D. et al. The concentrated solar power system with stirling technology in a micro-grid: The simulation model. In: . 2014 International Symposium on Power Electronics, Electrical Drives, Automation and Motion (SPEEDAM 2014), 2014. Disponível em: ⟨https://ieeexplore.ieee.org/document/6872095⟩.

32 HOLLOWS, G.; JAMES, N. Depth of field and depth of focus. Edmund Optics. Disponível em: ⟨https://www.edmundoptics.com/knowledge-center/application-notes/imaging/depth-of-field-and-depth-of-focus/⟩.

33 RIBEIRO, R. Video call. 2023.

34 DETERMINING Planet Properties. AstronomyNotes.com. Disponível em: ⟨https://www.astronomynotes.com/solarsys/s2.htm⟩.

35 ALMEIDA, G. de. *Porque razão é que o Sol e a Lua nos parecem do mesmo tamanho no céu?* SulInformacao, 2016. Disponível em: ⟨https://www.sulinformacao.pt/2016/04/porque-razao-e-que-o-sol-e-a-lua-nos-parecem-do-mesmo-tamanho-no-ceu/⟩.

36 SéTIMO e último espelho do Telescópio Gigante Magalhães começa a ser produzido. FAPESP, 2023. Disponível em: ⟨https://agencia.fapesp.br/setimo-e-ultimo-espelho-do-telescopio-gigante-magalhaes-comeca-a-ser-produzido/50028⟩.

37 HARTOG, J. P. D. *Mechanical Vibrations*. [S.l.]: DOVER PUBLICATIONS, INC., 1985. ISBN 0-486-64785-4.

38 LALANNE, C. Vibration tests: a brief historical background. Sinusoidal Vibration, v. 1, 2009. Disponível em: ⟨https://onlinelibrary.wiley.com/doi/pdf/10.1002/9780470611906.oth1⟩.

39 WANG, W. et al. Energy harvesting from ultra-low-frequency vibrations through a quasi-zero stiffness electromagnetic energy harvester. Journal of Vibration Engineering Technologies, 2022. Disponível em: ⟨https://doi.org/10.1007/s42417-022-00753-z⟩.

40 EULER, L. Methodus inveniendi lineas curvas maximi minimive proprietate gaudentes. Lausanne Geneva: Marcum-Michaelem Bousquet, v. 1744, p. 1–322. Disponível em: ⟨https://link.springer.com/book/9783764314248,year=⟩.

41 HELMHOLTZ, H. L. F. *On the Sensations of Tone as a Physiological Basis for the Theory of Music*. 3. ed. Cambridge University Press, 2009. ISBN 9780511701801. Disponível em: ⟨https://doi.org/10.1017/CBO9780511701801⟩.

42 STRUTT, J. W. *The Theory of Sound*. Cambridge University Press, 1877. v. 2. ISBN 9781139058094. Disponível em: ⟨https://doi.org/10.1017/CBO9781139058094⟩.

43 STRUTT, J. W. *The Explanation of Certain Acoustical Phenomena*. Nature, 1878. v. 18. 319-321 p. Disponível em: ⟨https://doi.org/10.1038/018319a0⟩.

44 STRUTT, J. W. *The theory of sound, Volume 2*. Macmillan, 1878. v. 2. Disponível em: ⟨https://soundandscience.de/node/556⟩.

45 NYQUIST, H. Thermal agitation of electric charge in conductors. American Physical Society, v. 32, 1928. Disponível em: ⟨https://doi.org/10.1103/PhysRev.32.110⟩.

46 WENDEL, J. Spacex ceo elon musk explains why we need a 'whole new architecture' for space travel. Space.com, 2020. Disponível em: ⟨https://www.space.com/elon-musk-spacex-starship-new-spaceflight-architecture.html⟩.

47 FOWLES, G. R. *Introduction to Modern Optics*. 2. ed. [S.l.]: DOVER PUBLICATIONS, INC., 1989. ISBN 9780486659572.

48 WILLIAMS, C. The £300m cable that will save traders milliseconds. The Telegraph, 2011. Disponível em: ⟨https://web.archive.org/web/20110911194258/http://www.telegraph.co.uk/finance/newsbysector/mediatechnologyandtelecoms/8753784/The-300m-cable-that-will-save-traders-milliseconds.html⟩.

49 GREGERSEN, E. Charles kao. Encyclopaedia Britannica, 2022. Disponível em: ⟨https://www.britannica.com/biography/Charles-Kao⟩.

50 FIBER Optics. Encyclopaedia Britannica. Disponível em: ⟨https://www.britannica.com/science/fiber-optics⟩.

51 THOMPSON, B. J. Optics. Encyclopaedia Britannica. Disponível em: ⟨https://www.britannica.com/science/optics⟩.

52 HUYGENS, C. *Traite de la lumiere*. Chez Pierre vander Aa, marchand libraire, A Leide, 1690. Disponível em: ⟨https://doi.org/10.5479/sil.294285.39088000545160⟩.

53 NEWTON, I. *Opticks: or, A treatise of the reflections, refractions, inflexions and colours of light*. Printed for Sam. Smith, and Benj. Walford, 1704. Disponível em: ⟨https://doi.org/10.5479/sil.302475.39088000644674⟩.

54 MAXWELL, J. C. A dynamical theory of the electromagnetic field. Royal Society, v. 155, 1865. ISSN 0261-0523. Disponível em: ⟨https://doi.org/10.1098/rstl.1865.0008⟩.

55 EINSTEIN, A. On a heuristic viewpoint concerning the production and transformation of light. Annalen der Physik, v. 17, p. 132–148, 1905. Disponível em: ⟨https://doi.org/10.1002/andp.19053220607⟩.

56 KOURAKIS, I. *Structural systems and tuned mass dampers of super-tall buildings : case study of Taipei 101*. Tese (Doutorado), 2007. Disponível em: ⟨https://dspace.mit.edu/handle/1721.1/38947⟩.

57 NEWLAND, D. E. Vibration of the london millennium bridge: Cause and cure. International Journal of Acoustics and Vibration, v. 8, p. 9–14, 2003. Disponível em: ⟨https://doi.org/10.20855/ijav.2003.8.1124⟩.

58 NAWROTZKI, P. Tuned-mass systems for the dynamic upgrade of buildings and other structures. In: . Eleventh East Asia-Pacific Conference on Structural Engineering Construction, 2008. Disponível em: ⟨http://citeseerx.ist.psu.edu/viewdoc/download?doi=10.1.1.574.3485&rep=rep1&type=pdf⟩.

59 TAIPEI Financial Center Corporation. Council on Tall Buildings and Urban Habitat. Disponível em: ⟨https://www.skyscrapercenter.com/company/542⟩.

60 LONDON Millennium Footbridge. WalkLondon.com. Disponível em: ⟨https://www.walklondon.com/london-attractions/millennium-footbridge.htm⟩.

61 RUSSELL, D. A. The dynamic vibration absorber. Pennsylvania State University, 2011. Disponível em: ⟨https://www.acs.psu.edu/drussell/Demos/absorber/DynamicAbsorber.html⟩.

62 GODOY, W. R. A. de. *PROJETO, ANÁLISE E OTIMIZAÇÃO DE UM ABSORVEDOR DINÂMICO DE VIBRAÇÕES NÃO LINEAR*. Tese (Doutorado), 2017. Disponível em: ⟨http://doi.org/10.11606/T.18.2017.tde-06112017-140840⟩.

63 SHEN, Y. et al. Parameters optimization for a novel dynamic vibration absorber. Mechanical Systems and Signal Processing, v. 133, 2019. Disponível em: ⟨https://doi.org/10.1016/j.ymssp.2019.106282⟩.

64 ACAR, M. A.; YILMAZ, C. Design of an adaptive–passive dynamic vibration absorber composed of a string–mass system equipped with negative stiffness tension adjusting mechanism. Journal of Sound and Vibration, v. 332, p. 231–245, 2013. Disponível em: ⟨http://dx.doi.org/10.1016/j.jsv.2012.09.007⟩.

65 BARREDO, E. et al. A novel high-performance passive non-traditional inerter-based dynamic vibration absorber. Journal of Sound and Vibration, v. 485, 2020. Disponível em: ⟨https://doi.org/10.1016/j.jsv.2020.115583⟩.

66 DONUT. *Why F1 Banned This Genius Device*. 2021. Disponível em: ⟨https://www.youtube.com/watch?v=t58qjcNwEbo&t=297s&ab_channel=Donut⟩.

67 YAO, J. et al. Damping performance of a novel ferrofluid dynamic vibration absorber. Journal of Fluids and Structures, v. 90, p. 190–204, 2019. Disponível em: ⟨https://doi.org/10.1016/j.jfluidstructs.2019.06.009⟩.

68 MIZUNO, T. et al. Suppression of vibration induced by reciprocal motion of displacer in cryopump with an active dynamic vibration absorber. IFAC PapersOnLine, v. 52-15, p. 531–536, 2019. Disponível em: ⟨https://doi.org/10.1016/j.ifacol.2019.11.730⟩.

69 LIMA, D. M. de; LóPEZ-YáNEZ, P. A.; PEREIRA, M. A. Vibration control device for steel tubular towers of horizontal axis wind turbines. Lat. Am. j. solids struct., v. 16, 2019. Disponível em: ⟨https://doi.org/10.1590/1679-78255436⟩.

70 BRöTZ MANUEL REXER, N. P. N.; PELZ, P. F. Fluid dynamic vibration absorber for vehicle suspension system. *Vehicle System Dynamics*, Taylor Francis, v. 0, n. 0, p. 1–20, 2023. Disponível em: ⟨https://doi.org/10.1080/00423114.2023.2223325⟩.

71 BAYAT, M. et al. Dynamic vibration absorber with negative stiffness for rotor system. Hindawi Publishing Corporation, v. 2016, 2016. Disponível em: ⟨https://doi.org/10.1155/2016/5231704⟩.

72 MOTION AND MULTIBODY DYNAMICS SIMULATION SOFTWARE. Dassault Systemes Simulia. Disponível em: ⟨https://www.3ds.com/products-services/simulia/products/multibody-system-simulation/⟩.

73 REVIEW, A. Multibody simulation. ABB, 7 2021. Disponível em: ⟨https://new.abb.com/news/detail/80786/multibody-simulation\#:~:text=Often\\%20confused\\%20with\\%20the\\%20finite,deals\\%20with\\%20deformation\\%20and\\%20strength.⟩

74 OGATA, K. *Modern Control Engineering*. 5. ed. [S.l.]: Prentice Hall, 2010. ISBN 978-0136156734.

75 LACERDA, M. J. *Sistemas Lineares - Resposta de sistema na forma de espaço de estados usando comando lsim do Matlab*. 2020. Disponível em: ⟨https://www.youtube.com/watch?v=4co2jef1ZWE⟩.

76 FRALICK, C. E-mail exchange with ametek sales engineer. 2022.

77 BEER, F. P. et al. *Mechanics of Materials*. 6. ed. [S.l.]: McGraw Hill, 2012. ISBN 978-0-07-338028-5.

78 BEER, F. P. et al. *Mechanics of Materials*. 6. ed. [S.l.]: McGraw Hill, 2012. ISBN 978-0-07-338028-5.

79 HERTZBERG, R. W.; VINCI, R. P.; HERTZBERG, J. L. *Deformation and Fracture Mechanics of Engineering Materials*. 5. ed. [S.l.]: John Wiley and Sons, Inc., 2013. ISBN 978-0-470-52780-1.

80 BROWN, J. T. H. *Mark's calculations for machine design*. [S.l.]: McGraw Hill, 2005. ISBN 0-07-146691-6.

81 BEER, F. P. et al. *Mechanics of Materials*. 6. ed. [S.l.]: McGraw Hill, 2012. ISBN 978-0-07-338028-5.

82 MECHCONTENT. *Torsional stiffness: Definition, Equation, Units, of shaft with Pdf*. Disponível em: ⟨https://mechcontent.com/torsional-stiffness/\#:~:text=stiffness\\%20of\\%20shaft\\%3A-,What\\%20is\\%20torsional\\%20stiffness\\%3F,Torsional\\%20stiffness\\%20\\%3D\\%20T⟩.

83 TOKAISPRING. *Torsion Springs*. Disponível em: ⟨https://www.tokaibane.com/en/spring-design/torsion-springs-formulas⟩.

84 FLUIDPOWERJOURNAL. *Understanding Hydraulic Stiffness of a System*. 2018. Disponível em: ⟨https://fluidpowerjournal.com/understanding-hydraulic-stiffness-system/\#:~:text=The\\%20stiffness\\%20of\\%20a\\%20hydraulic,its\\%20bulk\\%20modulus\\%20of\\%20elasticity⟩.

85 GERHART, P. M.; GERHART, A. L.; HOCHSTEIN, J. I. *Munson, Young and Okiishi's Fundamentals of Fluid Mechanics*. 8. ed. [S.l.]: John Wiley and Sons, Inc., 2016. ISBN 978-1-119-08070-1.

86 POLIAN, A.; GRIMSDITCH, M. Elastic properties and density of helium up to 20 gpa. IOP Publishing Ltd, v. 2, n. 11, 1986. Disponível em: ⟨https://iopscience.iop.org/article/10.1209/0295-5075/2/11/006/pdf⟩.

87 RAO, S. *Vibrações Mecânicas*. 4. ed. [S.l.]: Pearson Prentice Hall, 2009. ISBN 978-85-7605-200-5.

88 MEVADA, H.; PATEL, D. Experimental determination of structural damping of different materials. Procedia Engineering, v. 144, p. 110–115, 2016. Disponível em: ⟨https://doi.org/10.1016/j.proeng.2016.05.013⟩.

89 BEER, F. P. et al. *Mechanics of Materials*. 6. ed. [S.l.]: McGraw Hill, 2012. ISBN 978-0-07-338028-5.

90 THEFOURIERTRANSFORM.COM. *Introduction to the Fourier Transform*. Disponível em: ⟨https://www.thefouriertransform.com/\#introduction⟩.

91 WOLFRAMMATHWORLD. *Fast Fourier Transform*. Disponível em: ⟨https://mathworld.wolfram.com/FastFourierTransform.html⟩.

92 KORDI, F.; ALAMATIAN, J. Analytical method for designing the tuned mass damper based on the complex stiffness theory. Iranian Journal of Science and Technology, https://doi.org/10.1007/s40996-018-0222-0, 2019.

APPENDIX A – APPENDIX

A.1 State space code without the DVA

The following code plots Figures 48-51.


```
clear all;
close all;
clc;
%pkg load control;

%%%%%%%%%%%%%%%%%%%%%%%%%%%%%%% SI %%%%%%%%%%%%%%%%%%%%%%%%%%%%%%%%%%%%%%%%%%%%%%%%%
% K = [N/m]                                                                        %
% C = [Ns/m]                                                                       %
% m = [kg]                                                                         %
% F = [N]                                                                         %
% omega = [rad/s]                                                                  %
% x = [m]                                                                          %
%%%%%%%%%%%%%%%%%%%%%%%%%%%%%%%%%%%%%%%%%%%%%%%%%%%%%%%%%%%%%%%%%%%%%%%%%%%%%%%%%%%%

%% Given

k1 = 9.26*10^(8); k2 = 11.11*10^(6); k3 = 27.99*10^(6); k4 = 2.87*10^(3); % [N/m]
c1 = 11898.47; % [Ns/m]
c2 = 5.44*10^(-7); % [Ns/m]
c3 = 1.83*10^(-6); % [Ns/m]
c4 = 5.33; % [Ns/m]
mA = 0.75949; mB = 0.56614; mD = 4.80253; % [g]
xB0 = 6.65*10^(-3); % [m]

% Time

t_final = 0.1666666666666;
t_iteration = 6.1e-5; % 1.9e-06;
t = 0:t_iteration:t_final;

% For C
%mC = 5; k5 = 1000; c5 = 10;

%%
%%%%%%%%%%%%%%%%%%%%%%%%%%%%%%%%%%%%%%%%%%%%%%%%%%%%%%%%%%%%%%%%%%%%%%%%%%%%%%%
%%%%%%%%%%%%%%%%%%%%%%%%%%%% ADAMS VIEW %%%%%%%%%%%%%%%%%%%%%%%%%%%%%%%%%%%%%%%%%%
%%%%%%%%%%%%%%%%%%%%%%%%%%%%%%%%%%%%%%%%%%%%%%%%%%%%%%%%%%%%%%%%%%%%%%%%%%%%%%%

t_inspire = readtable('adams_time.xlsx');
t_inspire = t_inspire(2:end,1);
t_inspire = table2array(t_inspire);
t_inspire = string(t_inspire);
t_inspire = str2double(t_inspire);

xA2_noC_inspire = readtable('adams_displacer_novo.xlsx');
xA2_noC_inspire = xA2_noC_inspire(2:end,end);
xA2_noC_inspire = table2array(xA2_noC_inspire);
xA2_noC_inspire = string(xA2_noC_inspire);
xA2_noC_inspire = str2double(xA2_noC_inspire);
```

```
xA2_noC_inspire = 10^(-3).*xA2_noC_inspire;

% xA2_noC_inspire_corr = corr_factor_A*xA2_noC_inspire;

xB2_noC_inspire = readtable('adams_piston_novo.xlsx');
xB2_noC_inspire = xB2_noC_inspire(2:end,end);
xB2_noC_inspire = table2array(xB2_noC_inspire);
xB2_noC_inspire = string(xB2_noC_inspire);
xB2_noC_inspire = str2double(xB2_noC_inspire);
xB2_noC_inspire = 10^(-3).*xB2_noC_inspire;

% xB2_noC_inspire_corr = corr_factor_B*xB2_noC_inspire;

% 'adams_outershell_0.75k3_tentative3.xlsx'
xD2_noC_inspire = readtable('adams_outershell_0.75k3_tentative3.xlsx');
xD2_noC_inspire = xD2_noC_inspire(2:end,end);
xD2_noC_inspire = table2array(xD2_noC_inspire);
xD2_noC_inspire = string(xD2_noC_inspire);
xD2_noC_inspire = str2double(xD2_noC_inspire);
xD2_noC_inspire = 10^(-3).*xD2_noC_inspire;

% xD2_noC_inspire_corr_2 = corr_factor_D*xD2_noC_inspire;

% 'adams_outershell_0.75k3_tentative3.xlsx'
xD2_inspire = readtable('adams_outershell_dva_novo.xlsx');
xD2_inspire = xD2_inspire(2:end,end);
xD2_inspire = table2array(xD2_inspire);
xD2_inspire = string(xD2_inspire);
xD2_inspire = str2double(xD2_inspire);
xD2_inspire = 10^(-3).*xD2_inspire;

% xD2_noC_inspire_corr_2 = corr_factor_D*xD2_noC_inspire;

% teste = readtable('adams_outershell.xlsx');
% teste = teste(2:end,end);
% teste = table2array(teste);
% teste = string(teste);
% teste = str2double(teste);
% teste = 10^(-3).*teste;
%
% teste_corr = corr_factor_D*teste;

t_inspire_AB = t_inspire - t_final*(1.5/10);
t_inspire_D = t_inspire - t_final*(1.75/10);

force_inspire = readtable('adams_force.xlsx');
force_inspire = force_inspire(2:end,1);
force_inspire = table2array(force_inspire);
force_inspire = string(force_inspire);
```

```
force_inspire = str2double(force_inspire);

%% %%%%%%%%%%%%%%%%%%%% STRAIGHTFORWARD FEA %%%%%%%%%%%%%%%%%%%%%%%%%%%%%%

A_noC = [0 1 0 0 0 0;...
    -(k2+k3+k4)/mA -(c2+c3+c4)/mA k3/mA c3/mA (k2+k4)/mA (c2+c4)/mA; ...
    0 0 0 1 0 0;...
    k3/mB c3/mB -k3/mB -c3/mB 0 0;...
    0 0 0 0 0 1;...
    (k2+k4)/mD (c2+c4)/mD 0 0 -(k1+k2+k4)/mD -(c1+c2+c4)/mD];

% A_noC = [0 1 0 0 0 0;...
%     -(k2+k3-k4)/mA -(c2+c3-c4)/mA k3/mA c3/mA (k2-k4)/mA (c2-c4)/mA;...
%     0 0 0 1 0 0;...
%     k3/mB c3/mB -k3/mB -c3/mB 0 0;...
%     0 0 0 0 0 1;...
%     (k2-k4)/mD (c2-c4)/mD 0 0 -(k1+k2-k4)/mD -(c1+c2-c4)/mD];

B_noC = [0;0;0;1/mB;0;0];

C_noC = eye(6);

D_noC = 0;

% Sys

sys = ss(A_noC,B_noC,C_noC,D_noC);

% Initial condition

x0_noC = [0;0;xB0;0;0;0];

% %%%%%%%%%%%%%% Plotting displacements for one specific omega %%%%%%%%%%%%%%%%%%

P0 = 45000; % [N]
omega_spec = 376.99; % [rad/s]

% External excitation
%for n = 1:6

%omega_spec = 200*(n-1);
%P0 = 10^n;
u2_noC = P0*sin(omega_spec*t);
%u = 0*t;

% Simulating a linear system
[y2_noC,t,x2_noC] = lsim(sys,u2_noC,t,x0_noC);

% Plotting results
```

```
%y_positions = zeros(length(y),length(B)/2);
y2_positions_noC = [y2_noC(:,1) y2_noC(:,3) y2_noC(:,5)];
xA2_noC = y2_noC(:,1); xB2_noC = y2_noC(:,3); xD2_noC = y2_noC(:,5);
testeA = x2_noC(:,1); testeB = x2_noC(:,3); testeD = x2_noC(:,5);

%% Fast Fourier Transform

%%%%%%%%%%%%%%%%%%%%%%%%%%%%%%%% mA %%%%%%%%%%%%%%%%%%%%%%%%%%%%%%%%%%%%%%%%

dt_sign = t_iteration;
nt_sign = length(t);
y_A = xA2_noC;
% Fourier transformation
y_fft_A = y_A - mean(y_A);
nfft = 2^nextpow2(nt_sign)*2;
FFT_A = fft(y_fft_A,nfft)/nt_sign;
FFT_A = 2*abs(FFT_A(1:nfft/2+1));
fs=1/dt_sign;
f = fs/2*linspace(0,1,nfft/2+1);
% find maximum amplitude and frequency
[pks_A,locs_A] = findpeaks(FFT_A,f);
[pks_max_A,idx_pks_max_A] = max(pks_A);
locs_max_A = locs_A(idx_pks_max_A);
% results
f_fft_A = locs_max_A;
a_fft_A = pks_max_A;

% figure(7)
% plot(t,y)

%%%%%%%%%%%%%%%%%%%%%%%%%%%% mA INSPIRE %%%%%%%%%%%%%%%%%%%%%%%%%%%%%%%%%%%%

dt_sign_inspire = t_inspire(end)/length(t_inspire);
nt_sign_inspire = length(t_inspire);
y_A_inspire = xA2_noC_inspire;
% Fourier transformation
y_fft_A_inspire = y_A_inspire - mean(y_A_inspire);
nfft_inspire = 2^nextpow2(nt_sign_inspire)*2;
FFT_A_inspire = fft(y_fft_A_inspire,nfft_inspire)/nt_sign_inspire;
FFT_A_inspire = 2*abs(FFT_A_inspire(1:nfft_inspire/2+1));
fs_inspire=1/dt_sign_inspire;
f_inspire = fs_inspire/2*linspace(0,1,nfft_inspire/2+1);
% find maximum amplitude and frequency
[pks_A_inspire,locs_A_inspire] = findpeaks(FFT_A_inspire,f_inspire);
[pks_max_A_inspire,idx_pks_max_A_inspire] = max(pks_A_inspire);
locs_max_A_inspire = locs_A_inspire(idx_pks_max_A_inspire);
% results
f_fft_A_inspire = locs_max_A_inspire;
a_fft_A_inspire = pks_max_A_inspire;
```

```
disp(['A_mA_MATLAB/A_mA_INSPIRE = ',num2str(a_fft_A/a_fft_A_inspire)])
disp(['f_mA_MATLAB/f_mA_INSPIRE = ',num2str(f_fft_A/f_fft_A_inspire)])

%%%%%%%%%%%%%%%%%%%%%%%%%%%%%%%% mB %%%%%%%%%%%%%%%%%%%%%%%%%%%%%%%%%%%%%%%%

y_B = xB2_noC;
% Fourier transformation
y_fft_B = y_B - mean(y_B);
FFT_B = fft(y_fft_B,nfft)/nt_sign;
FFT_B = 2*abs(FFT_B(1:nfft/2+1));
% find maximum amplitude and frequency
[pks_B,locs_B] = findpeaks(FFT_B,f);
[pks_max_B,idx_pks_max_B] = max(pks_B);
locs_max_B = locs_B(idx_pks_max_B);
% results
f_fft_B = locs_max_B;
a_fft_B = pks_max_B;

%%%%%%%%%%%%%%%%%%%%%%%%%%%%%%%% mB INSPIRE %%%%%%%%%%%%%%%%%%%%%%%%%%%%%%%%%%%%

y_B_inspire = xB2_noC_inspire;
% Fourier transformation
y_fft_B_inspire = y_B_inspire - mean(y_B_inspire);
FFT_B_inspire = fft(y_fft_B_inspire,nfft_inspire)/nt_sign_inspire;
FFT_B_inspire = 2*abs(FFT_B_inspire(1:nfft_inspire/2+1));
% find maximum amplitude and frequency
[pks_B_inspire,locs_B_inspire] = findpeaks(FFT_B_inspire,f_inspire);
[pks_max_B_inspire,idx_pks_max_B_inspire] = max(pks_B_inspire);
locs_max_B_inspire = locs_B_inspire(idx_pks_max_B_inspire);
% results
f_fft_B_inspire = locs_max_B_inspire;
a_fft_B_inspire = pks_max_B_inspire;

disp(['A_mB_MATLAB/A_mB_INSPIRE = ',num2str(a_fft_B/a_fft_B_inspire)])
disp(['f_mB_MATLAB/f_mB_INSPIRE = ',num2str(f_fft_B/f_fft_B_inspire)])

%%%%%%%%%%%%%%%%%%%%%%%%%%%%%%%% mD %%%%%%%%%%%%%%%%%%%%%%%%%%%%%%%%%%%%%%%%

y_D = xD2_noC;
% Fourier transformation
y_fft_D = y_D - mean(y_D);
FFT_D = fft(y_fft_D,nfft)/nt_sign;
FFT_D = 2*abs(FFT_D(1:nfft/2+1));
% find maximum amplitude and frequency
[pks_D,locs_D] = findpeaks(FFT_D,f);
[pks_max_D,idx_pks_max_D] = max(pks_D);
locs_max_D = locs_D(idx_pks_max_D);
% results
```

```
f_fft_D = locs_max_D;
a_fft_D = pks_max_D;

%%%%%%%%%%%%%%%%%%%%%%%%%% mD INSPIRE %%%%%%%%%%%%%%%%%%%%%%%%%%%%%%%%%%

y_D_inspire = xD2_noC_inspire;
% Fourier transformation
y_fft_D_inspire = y_D_inspire - mean(y_D_inspire);
FFT_D_inspire = fft(y_fft_D_inspire,nfft_inspire)/nt_sign_inspire;
FFT_D_inspire = 2*abs(FFT_D_inspire(1:nfft_inspire/2+1));
% find maximum amplitude and frequency
[pks_D_inspire,locs_D_inspire] = findpeaks(FFT_D_inspire,f_inspire);
[pks_max_D_inspire,idx_pks_max_D_inspire] = max(pks_D_inspire);
locs_max_D_inspire = locs_D_inspire(idx_pks_max_D_inspire);
% results
f_fft_D_inspire = locs_max_D_inspire;
a_fft_D_inspire = pks_max_D_inspire;

disp(['A_mD_MATLAB/A_mD_INSPIRE = ',num2str(a_fft_D/a_fft_D_inspire)])
disp(['f_mD_MATLAB/f_mD_INSPIRE = ',num2str(f_fft_D/f_fft_D_inspire)])

%%%%%%%%%%%%%%%%%%%%%%%%%%%%%%%%%%%%%%%%%%%%%%%%%%%%%%%%%%%%%%%%%%%%%%%%%%%
%%%%%%%%%%%%%%%%%%%%%%%%%%%%%%%%%%%%%%%%%%%%%%%%%%%%%%%%%%%%%%%%%%%%%%%%%%%
%%%%%%%%%%%%%%%%%%%%%%%%%%%%%%%% COM DVA %%%%%%%%%%%%%%%%%%%%%%%%%%%%%%%%%%
%%%%%%%%%%%%%%%%%%%%%%%%%%%%%%%%%%%%%%%%%%%%%%%%%%%%%%%%%%%%%%%%%%%%%%%%%%%
%%%%%%%%%%%%%%%%%%%%%%%%%%%%%%%%%%%%%%%%%%%%%%%%%%%%%%%%%%%%%%%%%%%%%%%%%%%

% %%%%%%%%%%%%%%%%%%% ADAMS VIEW COM DVA, corpo D %%%%%%%%%%%%%%%%%%%%%%%%%

teste_inspire = xD2_inspire;
% Fourier transformation
teste_fft_D_inspire = teste_inspire - mean(teste_inspire);
testeFFT_D_inspire = fft(teste_fft_D_inspire,nfft_inspire)/nt_sign_inspire;
testeFFT_D_inspire = 2*abs(testeFFT_D_inspire(1:nfft_inspire/2+1));
% find maximum amplitude and frequency
[testepks_D_inspire,testelocs_D_inspire] = findpeaks(testeFFT_D_inspire,f_inspire);
[testepks_max_D_inspire,testeidx_pks_max_D_inspire] = max(testepks_D_inspire);
testelocs_max_D_inspire = testelocs_D_inspire(testeidx_pks_max_D_inspire);
% results
f_fft_D_inspire_teste = testelocs_max_D_inspire;
a_fft_D_inspire_teste = testepks_max_D_inspire;

disp(['A_mD_ADAMS_noDVA/A_mD_ADAMS = ',num2str↙
(a_fft_D_inspire/a_fft_D_inspire_teste)])
disp(['f_mD_ADAMS_noDVA/f_mD_ADAMS = ',num2str↙
(f_fft_D_inspire/f_fft_D_inspire_teste)])

%% Plots
```

```
figure(1)

plot(t,xA2_noC)
hold on
plot(t_inspire,xA2_noC_inspire)
hold on
%plot(t_inspire,xA2_noC_inspire_corr,'-o')
%hold off
title('Displacement x time for mass A','FontSize',16)
legend('MATLAB','Adams View')
xlabel('Time [s]')
ylabel('Displacement [m]')
%xlim([0 0.1091])

figure(2)

plot(t,xB2_noC)
hold on
plot(t_inspire,xB2_noC_inspire,'LineWidth',1)
hold on
%plot(t_inspire,xB2_noC_inspire_corr,'-o')
%hold off
title('Displacement x time for mass B','FontSize',16)
legend('MATLAB','Adams View')
xlabel('Time [s]')
ylabel('Displacement [m]')
%xlim([0 0.1091])

figure(3)

plot(t,xD2_noC)
hold on
% plot(t_inspire,xD2_inspire,'-*')
% hold on
% %plot(t_inspire,xD2_noC_inspire_corr_2,'-d')
% %hold on
plot(t_inspire,xD2_noC_inspire,'LineWidth',1)
hold off
title('Displacement x time for mass D','FontSize',16)
legend('MATLAB','Adams View')
% %'Inspire',strcat('Inspire * ',num2str(corr_factor_D)),'Teste')
xlabel('Time [s]')
ylabel('Displacement [m]')
% %xlim([0 0.1158])

figure(4)

plot(t,u2_noC,'-*','MarkerIndices',1:10:length(u2_noC),'LineWidth',2)
hold on
```

```
plot(t_inspire,force_inspire,'-o','MarkerIndices',25:10:length↙
(force_inspire),'LineWidth',2)
hold off
title('Force x time','FontSize',16)
legend('MATLAB','Adams View')
%'Inspire',strcat('Inspire * ',num2str(corr_factor_D)),'Teste')
xlabel('Time [s]')
ylabel('Force [N]')
%xlim([0 0.1158])

% % figure(5)
% %
% % plot(t,xD2_noC,t_inspire_D,xD2_noC_inspire_corr_2,'-d');
% % title('Displacement x time for mass D when P0 = 4500 N')
% % legend('MATLAB no C','Inspire * corr factor 2 + phase shift')
% % xlabel('Time [s]')
% % ylabel('Displacement [m]')
% % %xlim([0 0.1158])

%% %%%%%%%%%%%%%%%%%%%%%%%%%%%%%%%%%%%%%%%%%%%%%%%%%%%%%%%%%%%%%%%%%%%%%%%%%%%%%%%
%%%%%%%%%%%%%%%%%%%%%% NO PASSIVE BALANCER (MASS "C") %%%%%%%%%%%%%%%%%%%%%%%%%
%%%%%%%%%%%%%%%%%%%%%%%%%%%%%%%%%%%%%%%%%%%%%%%%%%%%%%%%%%%%%%%%%%%%%%%%%%%%%%%

% % ESSA É A SEÇÃO QUE EU RODO PRA DAR OS SUBPLOTS DA DISSERTACAO
%
% % State space
%
% for n = 1:6
%
%     c4 = 200*(n-1);
%
%     A_noC = [0 1 0 0 0 0;...
%         -(k2+k3+k4)/mA -(c2+c3+c4)/mA k3/mA c3/mA (k2+k4)/mA (c2+c4)/mA;...
%         0 0 0 1 0 0;...
%         k3/mB c3/mB -k3/mB -c3/mB 0 0;...
%         0 0 0 0 0 1;...
%         (k2+k4)/mD (c2+c4)/mD 0 0 -(k1+k2+k4)/mD -(c1+c2+c4)/mD];
%
%     B_noC = [0;0;0;1/mB;0;0];
%
%     C_noC = eye(6);
%
%     D_noC = 0;
%
%     % Sys
%
%     sys = ss(A_noC,B_noC,C_noC,D_noC);
%
%     % Time
```

```
%
%     t = 0:1.9e-06:50;
%
%     % Initial condition
%
%     x0_noC = [0;0;xB0;0;0;0];
%
%     % %%%%%%%%%%%%%%% Plotting displacements for one specific omega ↙
%%%%%%%%%%%%%%%%%%
%
%     P0 = 4500; % [N]
%     omega_spec = 376.99; % [rad/s]
%
%     % External excitation
%     %for n = 1:6
%
%
%     %omega_spec = 200*(n-1);
%     %P0 = 10^n;
%     u2_noC = P0*sin(omega_spec*t);
%     %u = 0*t;
%
%     % Simulating a linear system
%     [y2_noC,t,x2_noC] = lsim(sys,u2_noC,t,x0_noC);
%
%     % Plotting results
%     %y_positions = zeros(length(y),length(B)/2);
%     y2_positions_noC = [y2_noC(:,1) y2_noC(:,3) y2_noC(:,5)];
%     xA2_noC = y2_noC(:,1); xB2_noC = y2_noC(:,3); xD2_noC = y2_noC(:,5);
%
%     figure(1)
%
%     subplot(3,2,n);
%     plot(t,xA2_noC,'*',t,xB2_noC,'.',t,xD2_noC,'o');
%     legend('x_A','x_B','x_D','location','northeast')
%     title(['c_4 = ',num2str(c4),' Ns/m'])
%     xlabel('Time [s]')
%     ylabel('Displacement [m]')
%     sgtitle(['Displacement x time for masses A, B, and D when P0 = ',num2str(P0),' ↙
N'])
%
%
%     %title(['Displacement x time for masses A, B, and D when \omega = ',num2str ↙
(omega_spec),' rad/s'])
%     %axis([0 50 -0.2e-5 0.3e-5])
%
% end

%%
```

```
%%%%%%%%%%%%% Plotting displacement by excitation frequency (for loop)%%%%%%%%%%

% omega_i = 285.99;
% omega_step = 91;
% omega_f = 740.99;
% i = 1;
% spec_A_noC = zeros(length(omega_i:omega_step:omega_f),2);
% spec_B_noC = zeros(length(omega_i:omega_step:omega_f),2);
% spec_D_noC = zeros(length(omega_i:omega_step:omega_f),2);
%
% for omega_noC = omega_i:omega_step:omega_f % [rad/s]
%     % External excitation
%     u_noC = P0*sin(omega_noC*t);
%     %u = 0*t;
%
%     % Simulating a linear system
%     [y_noC,t,x_noC] = lsim(sys,u_noC,t,x0_noC);
%
%     % Plotting results
%     %y_positions = zeros(length(y),length(B)/2);
%     y_positions_noC = [y_noC(:,1) y_noC(:,3) y_noC(:,5)];
%     xA_noC = y_noC(:,1); xB_noC = y_noC(:,3); xD_noC = y_noC(:,5);
%
%     figure(2)
%     %if length(omega_i:omega_step:omega_f)/4 > 2
%     subplot(5,4,i);
%     plot(t,y_positions_noC);
%     legend('x_A','x_B','x_D','location','northeast')
%     title(['\omega = ',num2str(omega_noC),' rad/s'])
%     %title(sprintf('Displacement x time for masses A, B, C, and ↙
D\nc1=c2=c3=c4=c5=100 Ns/m, u=10sin(\omega t) N, xB(0) = 0.5, \omega ='))
%     xlabel('Time [s]')
%     ylabel('Displacement [m]')
%     sgtitle('Displacement x time for masses A, B, and D when c1=c2=c3=c4=100 Ns/m, ↙
u=10sin(\omega t) N, xB(0) = 0.5 m')
%
% %     % Spectral analysis
% %     LM_A_noC = islocalmax(xA_noC);
% %     GM_A_noC = max(xA_noC(LM_A_noC));
% %     spec_A_noC(i,1) = omega_noC;
% %     spec_A_noC(i,2) = GM_A_noC;
% %
% %     LM_B_noC = islocalmax(xB_noC);
% %     GM_B_noC = max(xB_noC(LM_B_noC));
% %     spec_B_noC(i,1) = omega_noC;
% %     spec_B_noC(i,2) = GM_B_noC;
% %
% %     LM_D_noC = islocalmax(xD_noC);
% %     GM_D_noC = max(xD_noC(LM_D_noC));
```

```
% %     spec_D_noC(i,1) = omega_noC;
% %     spec_D_noC(i,2) = GM_D_noC;
%
%     i = i + 1;
% end

% % %%%%%%%%%%%%%%%%%%%%%%% Plotting spectral analysis %%%%%%%%%%%%%%%%%%%%%%%%%%%%
%
% figure(3)
% plot(spec_A_noC(:,1),spec_A_noC(:,2),'-*',spec_B_noC(:,1),spec_B_noC(:,2),'-*',...
%     spec_D_noC(:,1),spec_D_noC(:,2),'-*')
% legend('x_A','x_B','x_D','location','east')
% title('Spectral analysis: vibration amplitude global maxima per imposed frequency')
% xlabel('Frequency [rad/s]')
% ylabel('Displacement [m]')

% %% %%%%%%%%%%%%%%%%%%%%%%%%%%%%%%%%%%%%%%%%%%%%%%%%%%%%%%%%%%%%%%%%%%%%%%%%%%%%%%%
% %%%%%%%%%%%%%%%%%%%%%%% WITH PASSIVE BALANCER (MASS "C")%%%%%%%%%%%%%%%%%%%%%%%%
% %%%%%%%%%%%%%%%%%%%%%%%%%%%%%%%%%%%%%%%%%%%%%%%%%%%%%%%%%%%%%%%%%%%%%%%%%%%%%%%
%
% %State space (with mass C)
%
% A = [0 1 0 0 0 0 0 0;...
%     -(k2+k3)/mA -(c2+c3)/mA k3/mA c3/mA 0 0 0 0;...
%     0 0 0 1 0 0 0 0;...
%     k3/mB c3/mB -(k3+k4)/mB -(c3+c4)/mB 0 0 0 0;...
%     0 0 0 0 0 1 0 0;...
%     0 0 0 0 -k5/mC -c5/mC k5/mC c5/mC;...
%     0 0 0 0 0 0 0 1;...
%     k2/mD c2/mD k4/mD c4/mD k5/mD c5/mD -(k1+k2+k4+k5)/mD -(-c1+c2+c4+c5)/mD];
%
% B = [0;0;0;1/mB;0;0;0;0];
%
% C = eye(8);
%
% D = 0;
%
% % Sys
%
% sys = ss(A,B,C,D);
%
% % % % Time
% % %
% % % t = 0:0.01:20;
%
% % Initial condition
%
% x0 = [0;0;0.5;0;0;0;0;0];
%
```

```
% % % Plotting displacements for one specific omega
%
% % % omega_spec = 10;
% %
% % % External excitation
% % u2 = P0*sin(omega*t);
% % %u = 0*t;
% %
% % % Simulating a linear system
% % [y2,t,x2] = lsim(sys,u2,t,x0);
% %
% % % Plotting results
% % %y_positions = zeros(length(y),length(B)/2);
% % y2_positions = [y2(:,1) y2(:,3) y2(:,5) y2(:,7)];
% % xA2 = y2(:,1); xB2 = y2(:,3); xC2 = y2(:,5); xD2 = y2(:,7);
% %
% % figure(4)
% % plot(t,y2_positions);
% % legend('x_A','x_B','x_C','x_D','location','northeast')
% % title(sprintf('Displacement x time for masses A, B, C, and D ↙
when\nk1=k2=k3=k4=k5=1kN/m, c1=c2=c3=c4=c5=10 Ns/m, mA=mB=mC=5 kg,\nmD=15 kg, ↙
u=100sin(10t) N, xB(0) = 0.5 m'))
% % xlabel('Time [s]')
% % ylabel('Displacement [m]')
%
% % Plotting displacement by excitation frequency (for loop)
%
% % omega_i = 600;
% % omega_step = 5;
% % omega_f = 700;
% j = 1;
% spec_A = zeros(length(omega_i:omega_step:omega_f),2);
% spec_B = zeros(length(omega_i:omega_step:omega_f),2);
% spec_C = zeros(length(omega_i:omega_step:omega_f),2);
% spec_D = zeros(length(omega_i:omega_step:omega_f),2);
%
% for omega = omega_i:omega_step:omega_f % [rad/s]
%     % External excitation
%     u = P0*sin(omega*t);
%     %u = 0*t;
%
%     % Simulating a linear system
%     [y,t,x] = lsim(sys,u,t,x0);
%
%     % Plotting results
%     %y_positions = zeros(length(y),length(B)/2);
%     y_positions = [y(:,1) y(:,3) y(:,5) y(:,7)];
%     xA = y(:,1); xB = y(:,3); xC = y(:,5); xD = y(:,7);
%
```

```
%     figure(5)
%     %if length(omega_i:omega_step:omega_f)/4 > 2
%     subplot(5,4,j);
%     plot(t,y_positions);
%     legend('x_A','x_B','x_C','x_D','location','northeast')
%     title(['\omega = ',num2str(omega),' rad/s'])
%     %title(sprintf('Displacement x time for masses A, B, C, and ↙
D\nc1=c2=c3=c4=c5=100 Ns/m, u=10sin(\omega t) N, xB(0) = 0.5, \omega ='))
%     xlabel('Time [s]')
%     ylabel('Displacement [m]')
%     sgtitle('Displacement x time for masses A, B, C, and D when c1=c2=c3=c4=c5=100 ↙
Ns/m, u=10sin(\omega t) N, xB(0) = 0.5 m')
%
%     % Spectral analysis
%     LM_A = islocalmax(xA);
%     GM_A = max(xA(LM_A));
%     spec_A(j,1) = omega;
%     spec_A(j,2) = GM_A;
%
%     LM_B = islocalmax(xB);
%     GM_B = max(xB(LM_B));
%     spec_B(j,1) = omega;
%     spec_B(j,2) = GM_B;
%
%     LM_C = islocalmax(xC);
%     GM_C = max(xC(LM_C));
%     spec_C(j,1) = omega;
%     spec_C(j,2) = GM_C;
%
%     LM_D = islocalmax(xD);
%     GM_D = max(xD(LM_D));
%     spec_D(j,1) = omega;
%     spec_D(j,2) = GM_D;
%
% %     else
% %         subplot(3,3,i);
% %         plot(t,y_positions,'-*');
% %         legend('x_A','x_B','x_C','x_D','location','northeast')
% %         title(['\omega = ',num2str(omega),' rad/s'])
% %         %title(sprintf('Displacement x time for masses A, B, C, and ↙
D\nc1=c2=c3=c4=c5=100 Ns/m, u=10sin(\omega t) N, xB(0) = 0.5, \omega ='))
% %         xlabel('Time [s]')
% %         ylabel('Displacement [m]')
% %     end
%     j = j + 1;
% end
%
% % % Plotting spectral analysis
%
```

```
% % figure(6)
% % plot(spec_A(:,1),spec_A(:,2),'-*',spec_B(:,1),spec_B(:,2),'-*',...
% %     spec_C(:,1),spec_C(:,2),'-*',spec_D(:,1),spec_D(:,2),'-*')
% % legend('x_A','x_B','x_C','x_D','location','east')
% % title('Spectral analysis: vibration amplitude global maxima per imposed ↙
frequency')
% % xlabel('Frequency [rad/s]')
% % ylabel('Displacement [m]')
%
% % % Plotting the global max for a specific omega
%
% % omega1 = 1;
% % u1 = P0*sin(omega1*t);
% % %u = 0*t;
% %
% % % Simulating a linear system
% % [y1,t,x1] = lsim(sys,u1,t,x0);
% %
% % % Plotting results
% % %y_positions = zeros(length(y),length(B)/2);
% % y1_positions = [y1(:,1) y1(:,3) y1(:,5) y1(:,7)];
% % xA1 = y1(:,1); xB1 = y1(:,3); xC1 = y1(:,5); xD1 = y1(:,7);
% % pos_by_time_A1 = [t xA1]; pos_by_time_B1 = [t xB1];
% % pos_by_time_C1 = [t xC1]; pos_by_time_D1 = [t xD1];
% % LM1_A = islocalmax(xA1);
% % GM1_A = max(xA1(LM1_A)); t_LM1_A = pos_by_time_A1((pos_by_time_A1(:,2)==GM1_A), ↙
1);
% % LM1_B = islocalmax(xB1);
% % GM1_B = max(xB1(LM1_B)); t_LM1_B = pos_by_time_B1((pos_by_time_B1(:,2)==GM1_B), ↙
1);
% % LM1_C = islocalmax(xC1);
% % GM1_C = max(xC1(LM1_C)); t_LM1_C = pos_by_time_C1((pos_by_time_C1(:,2)==GM1_C), ↙
1);
% % LM1_D = islocalmax(xD1);
% % GM1_D = max(xD1(LM1_D)); t_LM1_D = pos_by_time_D1((pos_by_time_D1(:,2)==GM1_D), ↙
1);
% %
% % % t_LM = [t t t t];
% %
% % figure(7)
% % plot(t,y1_positions,t_LM1_A,GM1_A,'r*',t_LM1_B,GM1_B,'b*',...
% %     t_LM1_C,GM1_C,'c*',t_LM1_D,GM1_D,'g*');
% % legend('x_A','x_B','x_C','x_D','Global maximum for A',...
% %     'Global maximum for B','Global maximum for C',...
% %     'Global maximum for D','location','northeast')
% % title('Vibration amplitude global maxima for masses A, B, C, and D (\omega = 1 ↙
rad/s)')
% % xlabel('Time [s]')
% % ylabel('Displacement [m]')
```

A.2 State space code with the DVA

The following code plots Figures 53-61.


```
clear all;
close all;
clc;
format long;

%%%%%%%%%%%%%%%%%%%%%%%%%%%%%%%% SI %%%%%%%%%%%%%%%%%%%%%%%%%%%%%%%%%%%%%%%%%%%%%%%%%
% K = [N/m]                                                                        %
% C = [Ns/m]                                                                       %
% m = [kg]                                                                         %
% F = [N]                                                                          %
% omega = [rad/s]                                                                  %
% x = [m]                                                                          %
%%%%%%%%%%%%%%%%%%%%%%%%%%%%%%%%%%%%%%%%%%%%%%%%%%%%%%%%%%%%%%%%%%%%%%%%%%%%%%%%%%%%%%

%% Given

k1 = 9.26*10^(8); k2 = 11.11*10^(6); k3 = 27.99*10^(6); k4 = 2.87*10^(3); % [N/m]
c1 = 11898.47; % [Ns/m]
c2 = 5.44*10^(-7); % [Ns/m]
c3 = 1.83*10^(-6); % [Ns/m]
c4 = 5.33; % [Ns/m]
mA = 0.75949; mB = 0.56614; mD = 4.80253; % [g]
xB0 = 6.65*10^(-3); % [m]
P0 = 45000; % [N]
omega_spec = 376.99; % [rad/s]
t_final = 0.1666666666666;
t_iteration = 6.1e-5; % 1.9e-06;
t = 0:t_iteration:t_final;

%% Adams View import

t_inspire = readtable('adams_time.xlsx');
t_inspire = t_inspire(2:end,1);
t_inspire = table2array(t_inspire);
t_inspire = string(t_inspire);
t_inspire = str2double(t_inspire);

xA2_noC_inspire = readtable('adams_displacer_novo.xlsx');
xA2_noC_inspire = xA2_noC_inspire(2:end,end);
xA2_noC_inspire = table2array(xA2_noC_inspire);
xA2_noC_inspire = string(xA2_noC_inspire);
xA2_noC_inspire = str2double(xA2_noC_inspire);
xA2_noC_inspire = 10^(-3).*xA2_noC_inspire;

xA2_inspire = readtable('adams_displacer_dva.xlsx');
xA2_inspire = xA2_inspire(2:end,end);
xA2_inspire = table2array(xA2_inspire);
xA2_inspire = string(xA2_inspire);
xA2_inspire = str2double(xA2_inspire);
```

```
xA2_inspire = 10^(-3).*xA2_inspire;

xB2_noC_inspire = readtable('adams_piston_novo.xlsx');
xB2_noC_inspire = xB2_noC_inspire(2:end,end);
xB2_noC_inspire = table2array(xB2_noC_inspire);
xB2_noC_inspire = string(xB2_noC_inspire);
xB2_noC_inspire = str2double(xB2_noC_inspire);
xB2_noC_inspire = 10^(-3).*xB2_noC_inspire;

xB2_inspire = readtable('adams_piston_dva.xlsx');
xB2_inspire = xB2_inspire(2:end,end);
xB2_inspire = table2array(xB2_inspire);
xB2_inspire = string(xB2_inspire);
xB2_inspire = str2double(xB2_inspire);
xB2_inspire = 10^(-3).*xB2_inspire;

xD2_noC_inspire = readtable('adams_outershell_0.75k3_tentative3.xlsx');
xD2_noC_inspire = xD2_noC_inspire(2:end,end);
xD2_noC_inspire = table2array(xD2_noC_inspire);
xD2_noC_inspire = string(xD2_noC_inspire);
xD2_noC_inspire = str2double(xD2_noC_inspire);
xD2_noC_inspire = 10^(-3).*xD2_noC_inspire;

xD2_inspire = readtable('adams_outershell_dva_novo.xlsx');
xD2_inspire = xD2_inspire(2:end,end);
xD2_inspire = table2array(xD2_inspire);
xD2_inspire = string(xD2_inspire);
xD2_inspire = str2double(xD2_inspire);
xD2_inspire = 10^(-3).*xD2_inspire;

%% Without C

A_noC = [0 1 0 0 0 0;...
    -(k2+k3+k4)/mA -(c2+c3+c4)/mA k3/mA c3/mA (k2+k4)/mA (c2+c4)/mA; ...
    0 0 0 1 0 0;...
    k3/mB c3/mB -k3/mB -c3/mB 0 0;...
    0 0 0 0 0 1;...
    (k2+k4)/mD (c2+c4)/mD 0 0 -(k1+k2+k4)/mD -(c1+c2+c4)/mD];

%A_noC = [0 1 0 0 0 0;...
%    -(k2+k3+k4)/mA -(c2+c3+c4)/mA k3/mA c3/mA 0 0;...
%    0 0 0 1 0 0;...
%    k3/mB c3/mB -k3/mB -c3/mB 0 0;...
%    0 0 0 0 0 1;...
%    (k2+k4)/mD (c2+c4)/mD 0 0 -(k1+k2+k4)/mD -(c1+c2+c4)/mD];

B_noC = [0;0;0;1/mB;0;0];

C_noC = eye(6);
```

```
D_noC = 0;

% Sys

sys0 = ss(A_noC,B_noC,C_noC,D_noC);

% Initial condition

x0_noC = [0;0;xB0;0;0;0];

% %%%%%%%%%%%%%% Plotting displacements for one specific omega %%%%%%%%%%%%%%%%%%

%omega_spec = 200*(n-1);
%P0 = 10^n;
u2_noC = P0*sin(omega_spec*t);
%u = 0*t;

% Simulating a linear system
[y2_noC,t,x2_noC] = lsim(sys0,u2_noC,t,x0_noC);

% Plotting results
%y_positions = zeros(length(y),length(B)/2);
y2_positions_noC = [y2_noC(:,1) y2_noC(:,3) y2_noC(:,5)];
xA2_noC = y2_noC(:,1); xB2_noC = y2_noC(:,3); xD2_noC = y2_noC(:,5);

%% Without C, FFT

%%%%%%%%%%%%%%%%%%%%%%%%%%%%%%%%%% mA %%%%%%%%%%%%%%%%%%%%%%%%%%%%%%%%%%%%%%%%

dt_sign = t_iteration;
nt_sign = length(t);
y_A_noC = xA2_noC;
% Fourier transformation
y_fft_A_noC = y_A_noC - mean(y_A_noC);
nfft = 2^nextpow2(nt_sign)*2;
FFT_A_noC = fft(y_fft_A_noC,nfft)/nt_sign;
FFT_A_noC = 2*abs(FFT_A_noC(1:nfft/2+1));
fs=1/dt_sign;
f = fs/2*linspace(0,1,nfft/2+1);
% find maximum amplitude and frequency
[pks_A_noC,locs_A_noC] = findpeaks(FFT_A_noC,f);
[pks_max_A_noC,idx_pks_max_A_noC] = max(pks_A_noC);
locs_max_A_noC = locs_A_noC(idx_pks_max_A_noC);
% results
f_fft_A_noC = locs_max_A_noC;
a_fft_A_noC = pks_max_A_noC;

%%%%%%%%%%%%%%%%%%%%%%%%%%%%%% mA INSPIRE %%%%%%%%%%%%%%%%%%%%%%%%%%%%%%%%%%%%%%
```

```
dt_sign_inspire = t_inspire(end)/length(t_inspire);
nt_sign_inspire = length(t_inspire);
y_A_noC_inspire = xA2_noC_inspire;
% Fourier transformation
y_fft_A_noC_inspire = y_A_noC_inspire - mean(y_A_noC_inspire);
nfft_inspire = 2^nextpow2(nt_sign_inspire)*2;
FFT_A_noC_inspire = fft(y_fft_A_noC_inspire,nfft_inspire)/nt_sign_inspire;
FFT_A_noC_inspire = 2*abs(FFT_A_noC_inspire(1:nfft_inspire/2+1));
fs_inspire=1/dt_sign_inspire;
f_inspire = fs_inspire/2*linspace(0,1,nfft_inspire/2+1);
% find maximum amplitude and frequency
[pks_A_noC_inspire,locs_A_noC_inspire] = findpeaks(FFT_A_noC_inspire,f_inspire);
[pks_max_A_noC_inspire,idx_pks_max_A_noC_inspire] = max(pks_A_noC_inspire);
locs_max_A_noC_inspire = locs_A_noC_inspire(idx_pks_max_A_noC_inspire);
% results
f_fft_A_noC_inspire = locs_max_A_noC_inspire;
a_fft_A_noC_inspire = pks_max_A_noC_inspire;

disp(['A_mA_noC_MATLAB/A_mA_noC_INSPIRE = ',num2str↙
(a_fft_A_noC/a_fft_A_noC_inspire)])
disp(['f_mA_noC_MATLAB/f_mA_noC_INSPIRE = ',num2str↙
(f_fft_A_noC/f_fft_A_noC_inspire)])

%%%%%%%%%%%%%%%%%%%%%%%%%%%%%%%% mB %%%%%%%%%%%%%%%%%%%%%%%%%%%%%%%%%%%%%%%%

y_B_noC = xB2_noC;
% Fourier transformation
y_fft_B_noC = y_B_noC - mean(y_B_noC);
FFT_B_noC = fft(y_fft_B_noC,nfft)/nt_sign;
FFT_B_noC = 2*abs(FFT_B_noC(1:nfft/2+1));
% find maximum amplitude and frequency
[pks_B_noC,locs_B_noC] = findpeaks(FFT_B_noC,f);
[pks_max_B_noC,idx_pks_max_B_noC] = max(pks_B_noC);
locs_max_B_noC = locs_B_noC(idx_pks_max_B_noC);
% results
f_fft_B_noC = locs_max_B_noC;
a_fft_B_noC = pks_max_B_noC;

%%%%%%%%%%%%%%%%%%%%%%%%%%%% mB INSPIRE %%%%%%%%%%%%%%%%%%%%%%%%%%%%%%%%%%%%

y_B_noC_inspire = xB2_noC_inspire;
% Fourier transformation
y_fft_B_noC_inspire = y_B_noC_inspire - mean(y_B_noC_inspire);
FFT_B_noC_inspire = fft(y_fft_B_noC_inspire,nfft_inspire)/nt_sign_inspire;
FFT_B_noC_inspire = 2*abs(FFT_B_noC_inspire(1:nfft_inspire/2+1));
% find maximum amplitude and frequency
[pks_B_noC_inspire,locs_B_noC_inspire] = findpeaks(FFT_B_noC_inspire,f_inspire);
[pks_max_B_noC_inspire,idx_pks_max_B_noC_inspire] = max(pks_B_noC_inspire);
```

```
locs_max_B_noC_inspire = locs_B_noC_inspire(idx_pks_max_B_noC_inspire);
% results
f_fft_B_noC_inspire = locs_max_B_noC_inspire;
a_fft_B_noC_inspire = pks_max_B_noC_inspire;

disp(['A_mB_noC_MATLAB/A_mB_noC_INSPIRE = ',num2str↙
(a_fft_B_noC/a_fft_B_noC_inspire)])
disp(['f_mB_noC_MATLAB/f_mB_noC_INSPIRE = ',num2str↙
(f_fft_B_noC/f_fft_B_noC_inspire)])

%%%%%%%%%%%%%%%%%%%%%%%%%%%%%%%% mD %%%%%%%%%%%%%%%%%%%%%%%%%%%%%%%%%%%%%%%%

y_D_noC = xD2_noC;
% Fourier transformation
y_fft_D_noC = y_D_noC - mean(y_D_noC);
FFT_D_noC = fft(y_fft_D_noC,nfft)/nt_sign;
FFT_D_noC = 2*abs(FFT_D_noC(1:nfft/2+1));
% find maximum amplitude and frequency
[pks_D_noC,locs_D_noC] = findpeaks(FFT_D_noC,f);
[pks_max_D_noC,idx_pks_max_D_noC] = max(pks_D_noC);
locs_max_D_noC = locs_D_noC(idx_pks_max_D_noC);
% results
f_fft_D_noC = locs_max_D_noC;
a_fft_D_noC = pks_max_D_noC;

%%%%%%%%%%%%%%%%%%%%%%%%%% mD INSPIRE %%%%%%%%%%%%%%%%%%%%%%%%%%%%%%%%%%%%%%%%

y_D_noC_inspire = xD2_noC_inspire;
% Fourier transformation
y_fft_D_noC_inspire = y_D_noC_inspire - mean(y_D_noC_inspire);
FFT_D_noC_inspire = fft(y_fft_D_noC_inspire,nfft_inspire)/nt_sign_inspire;
FFT_D_noC_inspire = 2*abs(FFT_D_noC_inspire(1:nfft_inspire/2+1));
% find maximum amplitude and frequency
[pks_D_noC_inspire,locs_D_noC_inspire] = findpeaks(FFT_D_noC_inspire,f_inspire);
[pks_max_D_noC_inspire,idx_pks_max_D_noC_inspire] = max(pks_D_noC_inspire);
locs_max_D_noC_inspire = locs_D_noC_inspire(idx_pks_max_D_noC_inspire);
% results
f_fft_D_noC_inspire = locs_max_D_noC_inspire;
a_fft_D_noC_inspire = pks_max_D_noC_inspire;

disp(['A_mD_noC_MATLAB/A_mD_noC_INSPIRE = ',num2str↙
(a_fft_D_noC/a_fft_D_noC_inspire)])
disp(['f_mD_noC_MATLAB/f_mD_noC_INSPIRE = ',num2str↙
(f_fft_D_noC/f_fft_D_noC_inspire)])

%% With C

mu_start_1 = 0.001;
mu_iterations = 0.025;
```

```
mu_final_1 = 0.5;
mu_start_2 = mu_final_1;
mu_final_2 = 0.999999999;

mC_1 = zeros(length(mu_start_1:mu_iterations:mu_final_1),1);
k5_1 = zeros(length(mu_start_1:mu_iterations:mu_final_1),1);
c5_1 = zeros(length(mu_start_1:mu_iterations:mu_final_1),1);
A_1 = zeros(8*length(mu_start_1:mu_iterations:mu_final_1),8);
absvalsums_1 = zeros(length(mu_start_1:mu_iterations:mu_final_1),1);
y_D_1 = zeros(length(t),length(mu_start_1:mu_iterations:mu_final_1));
a_fft_D_array_1 = zeros(length(mu_start_1:mu_iterations:mu_final_1),1);
f_fft_D_array_1 = zeros(length(mu_start_1:mu_iterations:mu_final_1),1);
mC_2 = zeros(length(mu_start_1:mu_iterations:mu_final_1),1);
k5_2 = zeros(length(mu_start_1:mu_iterations:mu_final_1),1);
c5_2 = zeros(length(mu_start_1:mu_iterations:mu_final_1),1);
A_2 = zeros(8*length(mu_start_1:mu_iterations:mu_final_1),8);
absvalsums_2 = zeros(length(mu_start_1:mu_iterations:mu_final_1),1);
y_D_2 = zeros(length(t),length(mu_start_1:mu_iterations:mu_final_1));
a_fft_D_array_2 = zeros(length(mu_start_1:mu_iterations:mu_final_1),1);
f_fft_D_array_2 = zeros(length(mu_start_1:mu_iterations:mu_final_1),1);

i = 1;
j = 1;

for mu_1 = mu_start_1:mu_iterations:mu_final_1

    mC_1(j) = mu_1*mD;
    k5_1(j) = (k1*mu_1*(1-mu_1))/((1+mu_1)^2);
    c5_1(j) = 2*(sqrt(mu_1)/(1-mu_1))*sqrt(k5_1(j)*mC_1(j));

    A_1(i:i+7,:) = [0 1 0 0 0 0 0 0;...
                    -(k2+k3+k4)/mA -(c2+c3+c4)/mA k3/mA c3/mA 0 0 (k2+k4)/mA (c2+c4) ↙
/mA;...
                    0 0 0 1 0 0 0 0;...
                    k3/mB c3/mB -k3/mB -c3/mB 0 0 0 0;...
                    0 0 0 0 0 1 0 0;...
                    0 0 0 0 -k5_1(j)/mC_1(j) -c5_1(j)/mC_1(j) k5_1(j)/mC_1(j) c5_1(j) ↙
/mC_1(j);...
                    0 0 0 0 0 0 0 1;
                    (k2+k4)/mD (c2+c4)/mD 0 0 0 0 -(k1+k2+k4+k5_1(j))/mD - ↙
(c1+c2+c4+c5_1(j))/mD];

    B_1 = [0;0;0;1/mB;0;0;0;0];

    C_1 = eye(8);

    D_1 = 0;

    % Sys %%%%%%%%%%%%%%%%%%%%%%%%%%%%%%%%%%%%%%%%%%%%%%%%%%%%%%%%%%%%%%%%%%%%
```

```
    %%%%%%%%%%%%%%%%%%%%%%%% única parte do código que tá codada manualmente
    %%%%%%%%%%%%%%%%%%%%%%%%%%%%%%%%%%%%%%%%%%%%%%%%%%%%%%%%%%%%%%%%%%%%%%%%

    sys1_1 = ss(A_1(1:8,:),B_1,C_1,D_1); sys2_1 = ss(A_1(9:16,:),B_1,C_1,D_1); sys3_1 ↙
= ss(A_1(17:24,:),B_1,C_1,D_1);
    sys4_1 = ss(A_1(25:32,:),B_1,C_1,D_1); sys5_1 = ss(A_1(33:40,:),B_1,C_1,D_1); ↙
sys6_1 = ss(A_1(41:48,:),B_1,C_1,D_1);
    sys7_1 = ss(A_1(49:56,:),B_1,C_1,D_1); sys8_1 = ss(A_1(57:64,:),B_1,C_1,D_1); ↙
sys9_1 = ss(A_1(65:72,:),B_1,C_1,D_1);
    sys10_1 = ss(A_1(73:80,:),B_1,C_1,D_1); sys11_1 = ss(A_1(81:88,:),B_1,C_1,D_1); ↙
sys12_1 = ss(A_1(89:96,:),B_1,C_1,D_1);
    sys13_1 = ss(A_1(97:104,:),B_1,C_1,D_1); sys14_1 = ss(A_1(105:112,:),B_1,C_1, ↙
D_1); sys15_1 = ss(A_1(113:120,:),B_1,C_1,D_1);
    sys16_1 = ss(A_1(121:128,:),B_1,C_1,D_1); sys17_1 = ss(A_1(129:136,:),B_1,C_1, ↙
D_1); sys18_1 = ss(A_1(137:144,:),B_1,C_1,D_1);
    sys19_1 = ss(A_1(145:152,:),B_1,C_1,D_1); sys20_1 = ss(A_1(153:160,:),B_1,C_1, ↙
D_1);

    % Preallocating y2
    y2_1 = zeros(length(t),8*length(mu_start_1:mu_iterations:mu_final_1));
    % xD2 = zeros(length(t),length(mu_start:mu_iterations:mu_final));

    % Initial condition

    x0_1 = [0;0;xB0;0;0;0;0;0];

    % %%%%%%%%%%%%%%% Plotting displacements for one specific omega ↙
%%%%%%%%%%%%%%%%%%%

    %P0 = 45000; % [N]
    %omega_spec = 376.99; % [rad/s]

    u2_1 = P0*sin(omega_spec*t);

    % Simulating a linear system %%%%%%%%%%%%%%%%%%%%%%%%%%%%%%%%%%%%%%%%%%%%
    %%%%%%%%%%%%%%%%%%%%%%%% única parte do código que tá codada manualmente
    %%%%%%%%%%%%%%%%%%%%%%%%%%%%%%%%%%%%%%%%%%%%%%%%%%%%%%%%%%%%%%%%%%%%%%%%

    [y2_1(:,1:8),t,x2] = lsim(sys1_1,u2_1,t,x0_1); [y2_1(:,9:16),t,x2] = lsim(sys2_1, ↙
u2_1,t,x0_1);
    [y2_1(:,17:24),t,x2] = lsim(sys3_1,u2_1,t,x0_1); [y2_1(:,25:32),t,x2] = lsim ↙
(sys4_1,u2_1,t,x0_1);
    [y2_1(:,33:40),t,x2] = lsim(sys5_1,u2_1,t,x0_1); [y2_1(:,41:48),t,x2] = lsim ↙
(sys6_1,u2_1,t,x0_1);
    [y2_1(:,49:56),t,x2] = lsim(sys7_1,u2_1,t,x0_1); [y2_1(:,57:64),t,x2] = lsim ↙
(sys8_1,u2_1,t,x0_1);
    [y2_1(:,65:72),t,x2] = lsim(sys9_1,u2_1,t,x0_1); [y2_1(:,73:80),t,x2] = lsim ↙
(sys10_1,u2_1,t,x0_1);
    [y2_1(:,81:88),t,x2] = lsim(sys11_1,u2_1,t,x0_1); [y2_1(:,89:96),t,x2] = lsim ↙
```

```
(sys12_1,u2_1,t,x0_1);
    [y2_1(:,97:104),t,x2] = lsim(sys13_1,u2_1,t,x0_1); [y2_1(:,105:112),t,x2] = lsim ↙
(sys14_1,u2_1,t,x0_1);
    [y2_1(:,113:120),t,x2] = lsim(sys15_1,u2_1,t,x0_1); [y2_1(:,121:128),t,x2] = lsim ↙
(sys16_1,u2_1,t,x0_1);
    [y2_1(:,129:136),t,x2] = lsim(sys17_1,u2_1,t,x0_1); [y2_1(:,137:144),t,x2] = lsim ↙
(sys18_1,u2_1,t,x0_1);
    [y2_1(:,145:152),t,x2] = lsim(sys19_1,u2_1,t,x0_1); [y2_1(:,153:160),t,x2] = lsim ↙
(sys20_1,u2_1,t,x0_1);

    xD2_1 = y2_1(:,7:8:end); xA2_1 = y2_1(:,1:8:end); xB2_1 = y2_1(:,3:8:end);

    %%%%%%%%%%%%%%%%%%%%%% RIP SAV 2023-2023 %%%%%%%%%%%%%%%%%%%%%%%%%%%%%

    mu_array_1 = mu_start_1:mu_iterations:mu_final_1;

    %%%%%%%%%%%%%%%%%%%%%%%%%%%%%%%%% mD %%%%%%%%%%%%%%%%%%%%%%%%%%%%%%%%%%%%

    dt_sign_1 = t_iteration;
    nt_sign_1 = length(t);
    nfft_1 = 2^nextpow2(nt_sign_1)*2;
    fs_1=1/dt_sign_1;
    f_1 = fs_1/2*linspace(0,1,nfft_1/2+1);

    y_D_1 = xD2_1(:,j);
    % Fourier transformation
    y_fft_D_1 = y_D_1 - mean(y_D_1);
    FFT_D_1 = fft(y_fft_D_1,nfft_1)/nt_sign_1;
    FFT_D_1 = 2*abs(FFT_D_1(1:nfft_1/2+1));
    % find maximum amplitude and frequency
    [pks_D_1,locs_D_1] = findpeaks(FFT_D_1,f_1);
    [pks_max_D_1,idx_pks_max_D_1] = max(pks_D_1);

    locs_max_D_1 = locs_D_1(idx_pks_max_D_1);


    % results
    f_fft_D_1 = locs_max_D_1;
    a_fft_D_1 = pks_max_D_1;

    a_fft_D_array_1(j) = a_fft_D_1;
    f_fft_D_array_1(j) = f_fft_D_1;



    %%%%%%%%%%%%%%%%%%%%%%%%%%%%%%%%%%%%%%%%%%%%%%%%%%%%%%%%%%%%%%%%%%%%%%%%%%%
    %%%%%%%%%%%%%%%%%%%%%%%%%%%%% PLOTS %%%%%%%%%%%%%%%%%%%%%%%%%%%%%%%%%%%%%%
    %%%%%%%%%%%%%%%%%%%%%%%%%%%%%%%%%%%%%%%%%%%%%%%%%%%%%%%%%%%%%%%%%%%%%%%%%%%
```

```
%     figure(1)
%     subplot(ceil(length(mu_start_1:mu_iterations:mu_final_1)/2),2,j);
%     plot(t,xD2_1(:,j));
%     title(['\mu = ',num2str(mu_1)])
%     xlabel('Time [s]')
%     ylabel('Disp. [m]')
%     sgtitle('Displacement x time for mass D')
%
% %     figure(2)
% %     plot(t,xD2_noC,'-o','MarkerIndices',1:1000:length(xD2_noC),'MarkerSize', ↙
10,...
% %         'MarkerFaceColor',[0.3010 0.7450 0.9330])
% %     hold on
% %     plot(t,xD2_1(:,ColMinAmplitude),'-square','MarkerIndices',5000:1000:length ↙
(xD2_1),...
% %         'MarkerSize',5,'MarkerFaceColor',[0.6350 0.0780 0.1840],'LineWidth',3)
% %     hold off
% %     title('Displacement x time for mass D with vs. without mass C','FontSize',16)
% %     xlabel('Time [s]')
% %     ylabel('Displacement [m]')
% %     legend('Without C','With C, \mu = 0.376')
    i = i+8;
    j = j+1;
end

m = 1; %i
n = 1; %j

for mu_2 = mu_start_2:mu_iterations:mu_final_2

    mC_2(n) = mu_2*mD;
    k5_2(n) = (k1*mu_2*(1-mu_2))/((1+mu_2)^2);
    c5_2(n) = 2*(sqrt(mu_2)/(1-mu_2))*sqrt(k5_2(n)*mC_2(n));

    A_2(m:m+7,:) = [0 1 0 0 0 0 0 0;...
                    -(k2+k3+k4)/mA -(c2+c3+c4)/mA k3/mA c3/mA 0 0 (k2+k4)/mA (c2+c4) ↙
/mA;...
                    0 0 0 1 0 0 0 0;...
                    k3/mB c3/mB -k3/mB -c3/mB 0 0 0 0;...
                    0 0 0 0 0 1 0 0;...
                    0 0 0 0 -k5_2(n)/mC_2(n) -c5_2(n)/mC_2(n) k5_2(n)/mC_2(n) c5_2(n) ↙
/mC_2(n);...
                    0 0 0 0 0 0 0 1;
                    (k2+k4)/mD (c2+c4)/mD 0 0 0 0 -(k1+k2+k4+k5_2(n))/mD - ↙
(c1+c2+c4+c5_2(n))/mD];

    B_2 = [0;0;0;1/mB;0;0;0;0];

    C_2 = eye(8);
```

```
    D_2 = 0;

    % Sys %%%%%%%%%%%%%%%%%%%%%%%%%%%%%%%%%%%%%%%%%%%%%%%%%%%%%%%%%%%%%%%%%%%%
    %%%%%%%%%%%%%%%%%%%%%%% única parte do código que tá codada manualmente
    %%%%%%%%%%%%%%%%%%%%%%%%%%%%%%%%%%%%%%%%%%%%%%%%%%%%%%%%%%%%%%%%%%%%%%%%%%%

    sys1_2 = ss(A_2(1:8,:),B_2,C_2,D_2); sys2_2 = ss(A_2(9:16,:),B_2,C_2,D_2); sys3_2 ↙
= ss(A_2(17:24,:),B_2,C_2,D_2);
    sys4_2 = ss(A_2(25:32,:),B_2,C_2,D_2); sys5_2 = ss(A_2(33:40,:),B_2,C_2,D_2); ↙
sys6_2 = ss(A_2(41:48,:),B_2,C_2,D_2);
    sys7_2 = ss(A_2(49:56,:),B_2,C_2,D_2); sys8_2 = ss(A_2(57:64,:),B_2,C_2,D_2); ↙
sys9_2 = ss(A_2(65:72,:),B_2,C_2,D_2);
    sys10_2 = ss(A_2(73:80,:),B_2,C_2,D_2); sys11_2 = ss(A_2(81:88,:),B_2,C_2,D_2); ↙
sys12_2 = ss(A_2(89:96,:),B_2,C_2,D_2);
    sys13_2 = ss(A_2(97:104,:),B_2,C_2,D_2); sys14_2 = ss(A_2(105:112,:),B_2,C_2, ↙
D_2); sys15_2 = ss(A_2(113:120,:),B_2,C_2,D_2);
    sys16_2 = ss(A_2(121:128,:),B_2,C_2,D_2); sys17_2 = ss(A_2(129:136,:),B_2,C_2, ↙
D_2); sys18_2 = ss(A_2(137:144,:),B_2,C_2,D_2);
    sys19_2 = ss(A_2(145:152,:),B_2,C_2,D_2); sys20_2 = ss(A_2(153:160,:),B_2,C_2, ↙
D_2);

    % Preallocating y2
    y2_2 = zeros(length(t),8*length(mu_start_2:mu_iterations:mu_final_2));
    % xD2 = zeros(length(t),length(mu_start:mu_iterations:mu_final));

    % Simulating a linear system %%%%%%%%%%%%%%%%%%%%%%%%%%%%%%%%%%%%%%%%%%%%
    %%%%%%%%%%%%%%%%%%%%%%% única parte do código que tá codada manualmente
    %%%%%%%%%%%%%%%%%%%%%%%%%%%%%%%%%%%%%%%%%%%%%%%%%%%%%%%%%%%%%%%%%%%%%%%%%%%

    [y2_2(:,1:8),t,x2] = lsim(sys1_2,u2_1,t,x0_1); [y2_2(:,9:16),t,x2] = lsim(sys2_2, ↙
u2_1,t,x0_1);
    [y2_2(:,17:24),t,x2] = lsim(sys3_2,u2_1,t,x0_1); [y2_2(:,25:32),t,x2] = lsim ↙
(sys4_2,u2_1,t,x0_1);
    [y2_2(:,33:40),t,x2] = lsim(sys5_2,u2_1,t,x0_1); [y2_2(:,41:48),t,x2] = lsim ↙
(sys6_2,u2_1,t,x0_1);
    [y2_2(:,49:56),t,x2] = lsim(sys7_2,u2_1,t,x0_1); [y2_2(:,57:64),t,x2] = lsim ↙
(sys8_2,u2_1,t,x0_1);
    [y2_2(:,65:72),t,x2] = lsim(sys9_2,u2_1,t,x0_1); [y2_2(:,73:80),t,x2] = lsim ↙
(sys10_2,u2_1,t,x0_1);
    [y2_2(:,81:88),t,x2] = lsim(sys11_2,u2_1,t,x0_1); [y2_2(:,89:96),t,x2] = lsim ↙
(sys12_2,u2_1,t,x0_1);
    [y2_2(:,97:104),t,x2] = lsim(sys13_2,u2_1,t,x0_1); [y2_2(:,105:112),t,x2] = lsim ↙
(sys14_2,u2_1,t,x0_1);
    [y2_2(:,113:120),t,x2] = lsim(sys15_2,u2_1,t,x0_1); [y2_2(:,121:128),t,x2] = lsim ↙
(sys16_2,u2_1,t,x0_1);
    [y2_2(:,129:136),t,x2] = lsim(sys17_2,u2_1,t,x0_1); [y2_2(:,137:144),t,x2] = lsim ↙
(sys18_2,u2_1,t,x0_1);
    [y2_2(:,145:152),t,x2] = lsim(sys19_2,u2_1,t,x0_1); [y2_2(:,153:160),t,x2] = lsim ↙
```

```
(sys20_2,u2_1,t,x0_1);

    xD2_2 = y2_2(:,7:8:end); xA2_2 = y2_2(:,1:8:end); xB2_2 = y2_2(:,3:8:end);

    %%%%%%%%%%%%%%%%%%%%%%% RIP SAV 2023-2023 %%%%%%%%%%%%%%%%%%%%%%%%%%%%

     mu_array_2 = mu_start_2:mu_iterations:mu_final_2;

    %%%%%%%%%%%%%%%%%%%%%%%%%%%%%%%% mD %%%%%%%%%%%%%%%%%%%%%%%%%%%%%%%%%%%%

    dt_sign_2 = t_iteration;
    nt_sign_2 = length(t);
    nfft_2 = 2^nextpow2(nt_sign_2)*2;
    fs_2=1/dt_sign_2;
    f_2 = fs_2/2*linspace(0,1,nfft_2/2+1);

    y_D_2 = xD2_2(:,n);
    % Fourier transformation
    y_fft_D_2 = y_D_2   mean(y_D_2);
    FFT_D_2 = fft(y_fft_D_2,nfft_2)/nt_sign_2;
    FFT_D_2 = 2*abs(FFT_D_2(1:nfft_2/2+1));
    % find maximum amplitude and frequency
    [pks_D_2,locs_D_2] = findpeaks(FFT_D_2,f_2);
    [pks_max_D_2,idx_pks_max_D_2] = max(pks_D_2);

    locs_max_D_2 = locs_D_2(idx_pks_max_D_2);


    % results
    f_fft_D_2 = locs_max_D_2;
    a_fft_D_2 = pks_max_D_2;

    a_fft_D_array_2(n) = a_fft_D_2;
    f_fft_D_array_2(n) = f_fft_D_2;

    %%%%%%%%%%%%%%%%%%%%%%%%%%%%%%%%%%%%%%%%%%%%%%%%%%%%%%%%%%%%%%%%%%%%%%%
    %%%%%%%%%%%%%%%%%%%%%%%%%%%% PLOTS %%%%%%%%%%%%%%%%%%%%%%%%%%%%%%%%%%%%
    %%%%%%%%%%%%%%%%%%%%%%%%%%%%%%%%%%%%%%%%%%%%%%%%%%%%%%%%%%%%%%%%%%%%%%%

%     figure(3)
%     subplot(ceil(length(mu_start_2:mu_iterations:mu_final_2)/2),2,n);
%     plot(t,xD2_2(:,n));
%     title(['\mu = ',num2str(mu_2)])
%     xlabel('Time [s]')
%     ylabel('Disp. [m]')
%     sgtitle('Displacement x time for mass D')
%
% %     figure(4)
% %     plot(t,xD2_noC,'-o','MarkerIndices',1:1000:length(xD2_noC),'MarkerSize', ↙
```

```
10,...
% %         'MarkerFaceColor',[0.3010 0.7450 0.9330])
% %     hold on
% %     plot(t,xD2(:,ColMinAmplitude),'-square','MarkerIndices',5000:1000:length ↙
(xD2),...
% %         'MarkerSize',5,'MarkerFaceColor',[0.6350 0.0780 0.1840],'LineWidth',3)
% %     hold off
% %     title('Displacement x time for mass D with vs. without mass C','FontSize',16)
% %     xlabel('Time [s]')
% %     ylabel('Displacement [m]')
% %     legend('Without C','With C, \mu = 0.376')
    m = m+8;
    n = n+1;
end

%% Consolidating for loop arrays
a_fft_D_array = [a_fft_D_array_1;a_fft_D_array_2];
f_fft_D_array = [f_fft_D_array_1;f_fft_D_array_2];

mu_array = [mu_array_1 mu_array_2]';

minFFT = min(a_fft_D_array);
colminFFT = find(a_fft_D_array == minFFT);
mu_lowest_FFT = mu_array(colminFFT);

%% [Finding out \mu] Amplitude reduction

disp(['The lowest outer shell amplitude obtained through FFT is ',num2str(minFFT),'↙
and occurs at mu = ',num2str(mu_lowest_FFT)])

%% [DVA vs. no DVA] Amplitude reduction

% FFT_noC_MATLAB = 4.95582132165818e-05; FFT_noC_ADAMSVIEW = 4.95901432097639e-05; % ↙
[m]

ampreduc_FFT_MATLAB = (((a_fft_D_noC-a_fft_D_array(colminFFT)))/a_fft_D_noC)*100;
ampreduc_FFT_ADAMSVIEW = (((a_fft_D_noC_inspire-a_fft_D_array(colminFFT))) ↙
/a_fft_D_noC_inspire)*100;
disp(['FFT for the outer shell without C is ',num2str(a_fft_D_noC),' through↙
MATLAB'])
disp(['FFT for the outer shell without C is ',num2str(a_fft_D_noC_inspire),' through↙
Adams View'])
disp(['Amplitude reduction obtained through FFT  for the outer shell, MATLAB curve: ↙
',num2str(ampreduc_FFT_MATLAB),' %'])
disp(['Amplitude reduction obtained through FFT  for the outer shell, Adams View ↙
curve: ',num2str(ampreduc_FFT_ADAMSVIEW),' %'])


%% Plot mu x Amp
```

```
% figure(5)
% plot(mu_array,a_fft_D_array,'-*') %,mu_array,absvalsums/2000,'-o'
% hold on
% plot(mu_array(colminFFT),a_fft_D_array(colminFFT),'o','LineWidth',3)
% hold off
% xlabel('\mu')
% ylabel('Amplitude (m)')
% title('\mu (or "mu") vs. amplitude of motion of body D')
% legend('FFT results for different \mu s',sprintf('mu = %.3f, amp. = %0.3e', ↙
mu_lowest_FFT,minFFT));

%% Amplitude plot for mu that minimizes amplitude - now plotted with "plot fft vs. ↙
sumabsvals"

xA2 = [xA2_1 xA2_2]; xB2 = [xB2_1 xB2_2];
xD2 = [xD2_1 xD2_2];
disp_minFFT = xD2(:,colminFFT);
xA2min = xA2(:,colminFFT);
xB2min = xB2(:,colminFFT);
xD2_maxmu = xD2(:,1);

figure(6)
plot(t,xD2_noC)
hold on
plot(t,disp_minFFT,'LineWidth',3)
% hold on
% plot(t,disp_minSAV,'LineWidth',3)
hold off
title('Displacement x time for mass D with vs. without DVA','FontSize',16)
xlabel('Time [s]')
ylabel('Displacement [m]')
legend('Without DVA',sprintf('With DVA, mu = %.3f',mu_lowest_FFT)) %,'With C, \mu =↙
0.975'

%% Plot juxtaposing 3 \mu s

figure(7)
plot(t,xD2_maxmu)
hold on
plot(t,disp_minFFT,'LineWidth',2)
hold off
title('Displacement x time for mass D with DVA for varying values of \mu','FontSize',↙
16)
xlabel('Time [s]')
ylabel('Displacement [m]')
legend(sprintf('mu = %.3f',mu_array(1)),sprintf('mu = %.3f',mu_array(colminFFT)))

%% THE ULTIMATE MF PLOT HELL YEA LIGHTWEIGHT BABYYYY
```

```
figure(8)
plot(t,xD2_noC)
hold on
plot(t,disp_minFFT,'LineWidth',1)
hold on
plot(t_inspire,xD2_noC_inspire,'LineWidth',1)
hold on
plot(t_inspire,xD2_inspire,'LineWidth',1)
hold off
title('Displacement x time for cryocooler outer shell with vs. without ↙
DVA','FontSize',16)
xlabel('Time [s]')
ylabel('Displacement [m]')
legend('Without DVA, MATLAB simulation','With DVA, MATLAB simulation',...
    'Without DVA, Adams View simulation','With DVA, Adams View simulation')

axes('position',[.65 .175 .25 .25])
box on % put box around new pair of axes
indexOfInterest = (t < 0.1056) & (t > 0.1027); % range of t near perturbation
plot(t(indexOfInterest),xD2_noC(indexOfInterest)) % plot on new axes
hold on
plot(t(indexOfInterest),disp_minFFT(indexOfInterest))
hold on
plot(t(indexOfInterest),xD2_noC_inspire(indexOfInterest))
hold on
plot(t(indexOfInterest),xD2_inspire(indexOfInterest))
hold off
axis tight

%% With C, FFT (bodies A and B)

%%%%%%%%%%%%%%%%%%%%%%%%%%%%%% A MATLAB %%%%%%%%%%%%%%%%%%%%%%%%%%%%%%%%%%%%

y_A = xA2(:,colminFFT);
% Fourier transformation
y_fft_A = y_A - mean(y_A);
FFT_A = fft(y_fft_A,nfft_1)/nt_sign_1;
FFT_A = 2*abs(FFT_A(1:nfft_1/2+1));
% find maximum amplitude and frequency
[pks_A,locs_A] = findpeaks(FFT_A,f_1);
[pks_max_A,idx_pks_max_A] = max(pks_A);

locs_max_A = locs_A(idx_pks_max_A);


% results
f_fft_A = locs_max_A;
a_fft_A = pks_max_A;
```

```
%%%%%%%%%%%%%%%%%%%%%%%%%%%%%%%% A INSPIRE %%%%%%%%%%%%%%%%%%%%%%%%%%%%%%%%%%%%

y_A_inspire = xA2_inspire;
% Fourier transformation
y_fft_A_inspire = y_A_inspire - mean(y_A_inspire);
FFT_A_inspire = fft(y_fft_A_inspire,nfft_1)/nt_sign_1;
FFT_A_inspire = 2*abs(FFT_A_inspire(1:nfft_1/2+1));
% find maximum amplitude and frequency
[pks_A_inspire,locs_A_inspire] = findpeaks(FFT_A_inspire,f_1);
[pks_max_A_inspire,idx_pks_max_A_inspire] = max(pks_A_inspire);

locs_max_A_inspire = locs_A_inspire(idx_pks_max_A_inspire);


% results
f_fft_A_inspire = locs_max_A_inspire;
a_fft_A_inspire = pks_max_A_inspire;

disp(['A_mA_MATLAB/A_mA_INSPIRE = ',num2str(a_fft_A/a_fft_A_inspire)])
disp(['f_mA_MATLAB/f_mA_INSPIRE = ',num2str(f_fft_A/f_fft_A_inspire)])

%%%%%%%%%%%%%%%%%%%%%%%%%%%%%%%% B MATLAB %%%%%%%%%%%%%%%%%%%%%%%%%%%%%%%%%%%%

y_B = xB2(:,colminFFT);
% Fourier transformation
y_fft_B = y_B - mean(y_B);
FFT_B = fft(y_fft_B,nfft_1)/nt_sign_1;
FFT_B = 2*abs(FFT_B(1:nfft_1/2+1));
% find maximum amplitude and frequency
[pks_B,locs_B] = findpeaks(FFT_B,f_1);
[pks_max_B,idx_pks_max_B] = max(pks_B);

locs_max_B = locs_B(idx_pks_max_B);


% results
f_fft_B = locs_max_B;
a_fft_B = pks_max_B;

%%%%%%%%%%%%%%%%%%%%%%%%%%%%%%%% B INSPIRE %%%%%%%%%%%%%%%%%%%%%%%%%%%%%%%%%%%%

y_B_inspire = xB2_inspire;
% Fourier transformation
y_fft_B_inspire = y_B_inspire - mean(y_B_inspire);
FFT_B_inspire = fft(y_fft_B_inspire,nfft_1)/nt_sign_1;
FFT_B_inspire = 2*abs(FFT_B_inspire(1:nfft_1/2+1));
% find maximum amplitude and frequency
[pks_B_inspire,locs_B_inspire] = findpeaks(FFT_B_inspire,f_1);
```

```
[pks_max_B_inspire,idx_pks_max_B_inspire] = max(pks_B_inspire);

locs_max_B_inspire = locs_B_inspire(idx_pks_max_B_inspire);


% results
f_fft_B_inspire = locs_max_B_inspire;
a_fft_B_inspire = pks_max_B_inspire;

disp(['A_mB_MATLAB/A_mB_INSPIRE = ',num2str(a_fft_B/a_fft_B_inspire)])
disp(['f_mB_MATLAB/f_mB_INSPIRE = ',num2str(f_fft_B/f_fft_B_inspire)])

%%%%%%%%%%%%%%%%%%%%%%%%%%%%%% D INSPIRE %%%%%%%%%%%%%%%%%%%%%%%%%%%%%%%%

y_D_inspire = xD2_inspire;
% Fourier transformation
y_fft_D_inspire = y_D_inspire - mean(y_D_inspire);
FFT_D_inspire = fft(y_fft_D_inspire,nfft_1)/nt_sign_1;
FFT_D_inspire = 2*abs(FFT_D_inspire(1:nfft_1/2+1));
% find maximum amplitude and frequency
[pks_D_inspire,locs_D_inspire] = findpeaks(FFT_D_inspire,f_1);
[pks_max_D_inspire,idx_pks_max_D_inspire] = max(pks_D_inspire);

locs_max_D_inspire = locs_D_inspire(idx_pks_max_D_inspire);


% results
f_fft_D_inspire = locs_max_D_inspire;
a_fft_D_inspire = pks_max_D_inspire;

disp(['A_mD_MATLAB/A_mD_INSPIRE = ',num2str(a_fft_D_array(colminFFT)↙
/a_fft_D_inspire)])
disp(['f_mD_MATLAB/f_mD_INSPIRE = ',num2str(f_fft_D_array(colminFFT)↙
/f_fft_D_inspire)])

%% Plots A and B

figure(9)
plot(t,xA2_noC)
hold on
plot(t,xA2min)
hold on
plot(t_inspire,xA2_noC_inspire)
hold on
plot(t_inspire,xA2_inspire)
hold off
title('Displacement x time for cryocooler piston with vs. without DVA','FontSize',16)
xlabel('Time [s]')
ylabel('Displacement [m]')
```

```
legend('Without DVA, MATLAB simulation','With DVA, MATLAB simulation',...
    'Without DVA, Adams View simulation','With DVA, Adams View simulation')
axes('position',[.65 .175 .25 .25])
box on % put box around new pair of axes
indexOfInterest = (t < 0.1056) & (t > 0.1027); % range of t near perturbation
plot(t(indexOfInterest),xA2_noC(indexOfInterest)) % plot on new axes
hold on
plot(t(indexOfInterest),xA2min(indexOfInterest))
hold on
plot(t(indexOfInterest),xA2_noC_inspire(indexOfInterest))
hold on
plot(t(indexOfInterest),xA2_inspire(indexOfInterest))
hold off
axis tight

figure(10)
plot(t,xB2_noC)
hold on
plot(t,xB2min)
hold on
plot(t_inspire,xB2_noC_inspire)
hold on
plot(t_inspire,xB2_inspire)
hold off
title('Displacement x time for cryocooler displacer with vs. without DVA','FontSize',↙
16)
xlabel('Time [s]')
ylabel('Displacement [m]')
legend('Without DVA, MATLAB simulation','With DVA, MATLAB simulation',...
    'Without DVA, Adams View simulation','With DVA, Adams View simulation')
axes('position',[.65 .175 .25 .25])
box on % put box around new pair of axes
indexOfInterest = (t < 0.1056) & (t > 0.1027); % range of t near perturbation
plot(t(indexOfInterest),xB2_noC(indexOfInterest)) % plot on new axes
hold on
plot(t(indexOfInterest),xB2min(indexOfInterest))
hold on
plot(t(indexOfInterest),xB2_noC_inspire(indexOfInterest))
hold on
plot(t(indexOfInterest),xB2_inspire(indexOfInterest))
hold off
axis tight

disp(['Amplitude reduction for the displacer (matlab): ',num2str(((a_fft_A_noC-↙
a_fft_A)/a_fft_A_noC)*100),' %'])
disp(['Amplitude reduction for the piston (matlab): ',num2str(((a_fft_B_noC-a_fft_B)↙
/a_fft_B_noC)*100),' %'])
disp(['Amplitude reduction for the outer shell (matlab): ',num2str(((a_fft_D_noC-↙
a_fft_D_array(colminFFT))/a_fft_D_noC)*100),' %'])
```

```
disp(['Amplitude reduction for the displacer (av): ',num2str(((a_fft_A_noC_inspire-
a_fft_A_inspire)/a_fft_A_noC_inspire)*100),' %'])
disp(['Amplitude reduction for the piston (av): ',num2str(((a_fft_B_noC_inspire-
a_fft_B_inspire)/a_fft_B_noC_inspire)*100),' %'])
disp(['Amplitude reduction for the outer shell (av): ',num2str(((a_fft_D_noC_inspire-
a_fft_D_inspire)/a_fft_D_noC_inspire)*100),' %'])
```

A.3 Code for plotting displacements with varying P0

The following code plots Figure 45.


```
clear all;
close all;
clc;
%pkg load control;

%%%%%%%%%%%%%%%%%%%%%%%%%%%%%% SI %%%%%%%%%%%%%%%%%%%%%%%%%%%%%%%%%%%%%%%%%%%%%%%%
% K - [N/m]                                                                     %
% C = [Ns/m]                                                                    %
% m = [kg]                                                                      %
% F = [N]                                                                      %
% omega = [rad/s]                                                               %
% x = [m]                                                                       %
%%%%%%%%%%%%%%%%%%%%%%%%%%%%%%%%%%%%%%%%%%%%%%%%%%%%%%%%%%%%%%%%%%%%%%%%%%%%%%%%%

%% Given

%k1 = 1000; k2 = 1000; k3 = 1000; k4 = 1000;
k1 = 9.26*10^(8); k2 = 11.11*10^(6); k3 = 27.99*10^(6); k4 = 2.87*10^(3); % [N/m]
c1 = 11898.47; % [Ns/m]
c2 = 5.44*10^(-7); % [Ns/m]
c3 = 1.83*10^(-6); % [Ns/m]
c4 = 5.33; % [Ns/m]
%c1 = 1000; c2 = 1000; c3 = 1000; c4 = 1000;
mA = 0.75949; mB = 0.56614; mD = 4.80253; % [g]
%P0 = 10^2; % [N]
xB0 = 6.65*10^(-3); % [m]


% Time

t_final = 0.1666666666666;
t_iteration = 6.1e-5; % 1.9e-06;
t = 0:t_iteration:t_final;

% For C
%mC = 5; k5 = 1000; c5 = 10;

%% %%%%%%%%%%%%%%%%%%%% STRAIGHTFORWARD FEA %%%%%%%%%%%%%%%%%%%%%%%%%%%%%%

A_noC = [0 1 0 0 0 0;...
    -(k2+k3+k4)/mA -(c2+c3+c4)/mA k3/mA c3/mA (k2+k4)/mA (c2+c4)/mA; ...
    0 0 0 1 0 0;...
    k3/mB c3/mB -k3/mB -c3/mB 0 0;...
    0 0 0 0 0 1;...
    (k2+k4)/mD (c2+c4)/mD 0 0 -(k1+k2+k4)/mD -(c1+c2+c4)/mD];

B_noC = [0;0;0;1/mB;0;0];

C_noC = eye(6);
```

```
D_noC = 0;

% Sys

sys = ss(A_noC,B_noC,C_noC,D_noC);

% Initial condition

x0_noC = [0;0;xB0;0;0;0];
omega_spec = 376.99; % [rad/s]

% %%%%%%%%%%%%%% Plotting displacements for one specific omega %%%%%%%%%%%%%%%%%%

for i = 1:6
    P0 = 10^i; % [N]

    u2_noC = P0*sin(omega_spec*t);

    % Simulating a linear system
    [y2_noC,t,x2_noC] = lsim(sys,u2_noC,t,x0_noC);

    y2_positions_noC = [y2_noC(:,1) y2_noC(:,3) y2_noC(:,5)];
    xA2_noC = y2_noC(:,1); xB2_noC = y2_noC(:,3); xD2_noC = y2_noC(:,5);

    %% Plot

    figure(1)
    subplot(3,2,i)
    plot(t,xA2_noC,'*',t,xB2_noC,'.',t,xD2_noC,'o')
    title(['P0 = ',num2str(P0),' N'])
    sgtitle('Displacement x time for masses A, B, and D','FontSize',16)
    legend('xA','xB','xD','location','northeast')
    %'Inspire',strcat('Inspire * ',num2str(corr_factor_D)),'Teste')
    xlabel('Time [s]')
    ylabel('Displacement [m]')
    %xlim([0 0.1158])
end
```

A.4 Code for plotting the spectral analysis

The following code plots Figure 62.


```
clear all;
close all;
clc;
format long;

%%%%%%%%%%%%%%%%%%%%%%%%%%%%%% SI %%%%%%%%%%%%%%%%%%%%%%%%%%%%%%%%%%%%%%%%%%%%%%%%%%
% K = [N/m]                                                                     %
% C = [Ns/m]                                                                    %
% m = [kg]                                                                      %
% F = [N]                                                                       %
% omega = [rad/s]                                                               %
% x = [m]                                                                       %
%%%%%%%%%%%%%%%%%%%%%%%%%%%%%%%%%%%%%%%%%%%%%%%%%%%%%%%%%%%%%%%%%%%%%%%%%%%%%%%%%%

%% Given

k1 = 9.26*10^(8); k2 = 11.11*10^(6); k3 = 27.99*10^(6); k4 = 2.87*10^(3); % [N/m]
c1 = 11898.47; % [Ns/m]
c2 = 5.44*10^( 7); % [Ns/m]
c3 = 1.83*10^(-6); % [Ns/m]
c4 = 5.33; % [Ns/m]
mA = 0.75949; mB = 0.56614; mD = 4.80253; % [g]
xB0 = 6.65*10^(-3); % [m]
P0 = 45000; % [N]
% omega_spec = 376.99; % [rad/s]
t_final = 0.1666666666666;
t_iteration = 6.1e-5; % 1.9e-06;
t = 0:t_iteration:t_final;

%% Without C

A_noC = [0 1 0 0 0 0;...
    -(k2+k3+k4)/mA -(c2+c3+c4)/mA k3/mA c3/mA (k2+k4)/mA (c2+c4)/mA; ...
    0 0 0 1 0 0;...
    k3/mB c3/mB -k3/mB -c3/mB 0 0;...
    0 0 0 0 0 1;...
    (k2+k4)/mD (c2+c4)/mD 0 0 -(k1+k2+k4)/mD -(c1+c2+c4)/mD];

B_noC = [0;0;0;1/mB;0;0];

C_noC = eye(6);

D_noC = 0;

% Sys

sys0 = ss(A_noC,B_noC,C_noC,D_noC);

% Initial condition
```

```
x0_noC = [0;0;xB0;0;0;0];

g = 1;
%u2_noC_array = zeros(21,1);
omega_array_noC = zeros(21,1);
a_fft_D_noC_array = zeros(21,1);
for omega_noC = 0:37.699:2*376.99
    u2_noC = P0*sin(omega_noC*t);

    % Simulating a linear system
    [y2_noC,t,x2_noC] = lsim(sys0,u2_noC,t,x0_noC);

    % Plotting results
    y2_positions_noC = [y2_noC(:,1) y2_noC(:,3) y2_noC(:,5)];
    xD2_noC = y2_noC(:,5);

    dt_sign = t_iteration;
    nt_sign = length(t);
    nfft = 2^nextpow2(nt_sign)*2;
    y_D_noC = xD2_noC;
    fs=1/dt_sign;
    f = fs/2*linspace(0,1,nfft/2+1);
    % Fourier transformation
    y_fft_D_noC = y_D_noC - mean(y_D_noC);
    FFT_D_noC = fft(y_fft_D_noC,nfft)/nt_sign;
    FFT_D_noC = 2*abs(FFT_D_noC(1:nfft/2+1));
    % find maximum amplitude and frequency
    [pks_D_noC,locs_D_noC] = findpeaks(FFT_D_noC,f);
    [pks_max_D_noC,idx_pks_max_D_noC] = max(pks_D_noC);
    locs_max_D_noC = locs_D_noC(idx_pks_max_D_noC);
    % results
    f_fft_D_noC = locs_max_D_noC;
    a_fft_D_noC = pks_max_D_noC;

    %u2_noC_array(g) = u2_noC;
    omega_array_noC(g) = omega_noC;
    a_fft_D_noC_array(g) = a_fft_D_noC;
    g = g+1;
end

%% With C

mu = 0.326;
mC = mu*mD;
k5 = (k1*mu*(1-mu))/((1+mu)^2);
c5 = 2*(sqrt(mu)/(1-mu))*sqrt(k5*mC);

A = [0 1 0 0 0 0 0 0;...
```

```
    -(k2+k3+k4)/mA -(c2+c3+c4)/mA k3/mA c3/mA 0 0 (k2+k4)/mA (c2+c4)/mA; ...
    0 0 0 1 0 0 0 0;...
    k3/mB c3/mB -k3/mB -c3/mB 0 0 0 0;...
    0 0 0 0 0 1 0 0;...
    0 0 0 0 -k5/mC -c5/mC k5/mC c5/mC;...
    0 0 0 0 0 0 0 1;
    (k2+k4)/mD (c2+c4)/mD 0 0 0 0 -(k1+k2+k4+k5)/mD -(c1+c2+c4+c5)/mD];

B = [0;0;0;1/mB;0;0;0;0];

C = eye(8);

D = 0;

% Sys

sys1 = ss(A,B,C,D);

% Initial condition

x0 = [0;0;xB0;0;0;0;0;0];

h = 1;
%u2_noC_array = zeros(21,1);
omega_array = zeros(21,1);
a_fft_D_array = zeros(21,1);
for omega = 0:37.699:2*376.99
    u2 = P0*sin(omega*t);

    % Simulating a linear system
    [y2,t,x2] = lsim(sys1,u2,t,x0);

    % Plotting results
    y2_positions = [y2(:,1) y2(:,3) y2(:,5)];
    xD2 = y2(:,5);

    dt_sign = t_iteration;
    nt_sign = length(t);
    nfft = 2^nextpow2(nt_sign)*2;
    y_D = xD2;
    fs=1/dt_sign;
    f = fs/2*linspace(0,1,nfft/2+1);
    % Fourier transformation
    y_fft_D = y_D - mean(y_D);
    FFT_D = fft(y_fft_D,nfft)/nt_sign;
    FFT_D = 2*abs(FFT_D(1:nfft/2+1));
    % find maximum amplitude and frequency
    [pks_D,locs_D] = findpeaks(FFT_D,f);
    [pks_max_D,idx_pks_max_D] = max(pks_D);
```

```
    locs_max_D = locs_D(idx_pks_max_D);
    % results
    f_fft_D = locs_max_D;
    a_fft_D = pks_max_D;

    %u2_noC_array(g) = u2_noC;
    omega_array(h) = omega;
    a_fft_D_array(h) = a_fft_D;
    h = h+1;
end

%% Plot

figure(1)
plot(omega_array_noC,a_fft_D_noC_array,'-*',omega_array_noC(11),a_fft_D_noC_array↙
(11),'o',...
    omega_array,a_fft_D_array,'-*',omega_array(11),a_fft_D_array(11),'o')
legend('No DVA','\omega = 376.99 rad/s','With DVA','\omega = 376.99 rad/s',...
    'Location','SouthEast')
xlabel('Angular frequency of vibration of the cryocooler \omega [rad/s]')
ylabel('Amplitude of vibration the Outer Shell [m]')
title('Spectral analysis of the Outer Shell')
```